الجمهورية الجزائرية الديمقراطية الشعبية
People's Democratic Republic of Algeria
وزارة التعليم العالي والبحث العلمي
Ministry of Higher Education and Scientific Research

Mohamed Khider University – Biskra
جامعة محمد خيضر - بسكرة

Faculty of Science and Technology
كلية العلوم والتكنولوجيا

Department of Electrical Engineering
قسم الهندسة الكهربائية

Ref :……..
المرجع :……..

Thesis presented with a view to obtaining
the diploma of :

LMD Doctorate in Electrical Engineering

Specialty: Automatic

Option: Modeling and Control of Dynamics systems

Entitled:

“Study and control of an intelligent autonomous hybrid vehicle using on-board sources”

“Etude et contrôle d’un véhicule hybride autonome intelligent utilisant des sources embarquées”

Presented by:

BACHA Sofiane

Publicly defended on:

In front of the jury composed of:

President:	**Dr. Hammoudi Mohamed-Yacine**	**MCA**	**University of Biskra**
Supervisor:	**Dr. Saadi Ramzi**	**MCA**	**University of Biskra**
Ex-supervisor:	**Pr. Aboubou Abdennacer**	**Prof**	**University of Biskra**
Co-supervisor:	**Dr. Ayad Mohamed-Yacine**	**MCA**	**R&D in the industry**
Examiner:	**Pr. Zellouma Laid**	**Prof**	**University of Eloued**
Examiner:	**Pr. Guettaf Abderrazak**	**Prof**	**University of Biskra**

DEDICATION

To my beloved family, this thesis is dedicated to you with profound gratitude and immeasurable love. Your unwavering support, encouragement, and sacrifices have been the foundation upon which my academic journey has flourished.

To my parents, your boundless faith in my potential has been a guiding light in my pursuit of knowledge. You instilled in me a thirst for learning, a curiosity that knows no bounds. Your sacrifices, both seen and unseen, have allowed me to pursue this doctorate and for that, I am eternally grateful.

To my siblings, your unwavering belief in my abilities has served as a constant source of inspiration. Your relentless enthusiasm and unwavering support have given me the strength to overcome challenges and strive for excellence. Your presence in my life has made this journey all the more fulfilling.

To my friends and mentors, your guidance and wisdom have been invaluable. Your intellectual prowess, insightful feedback, and unwavering encouragement have pushed me to surpass my limits and reach new heights. Your faith in my abilities has fueled my determination and motivated me to excel.

Lastly, to all those who have supported me, directly or indirectly, in this academic endeavor, your contributions have not gone unnoticed. Your words of encouragement, acts of kindness, and belief in my capabilities have been the wind beneath my wings.

ACKNOWLEDGEMENTS

First and foremost, I express my deepest gratitude to Allah, the Most Merciful and Compassionate, for granting me the strength, guidance, and wisdom throughout my doctoral years.

I would like to extend my sincere appreciation to my supervisor, **Dr. SAADI RAMZI**, for their unwavering support, invaluable guidance, and endless patience. Their expertise, dedication, and encouragement have been instrumental in shaping my research and academic growth.

I would also like to acknowledge my ex-supervisor, **Pr. ABOUBOU ABDENNACER**, for their initial guidance and valuable insights that laid the foundation of my research. I am grateful for the lessons I have learned under their guidance.

I extend my heartfelt gratitude to my co-supervisor, **Dr. AYAD MOHAMED YACINE**, for their continuous support, valuable feedback, and collaborative spirit. I am thankful for their mentorship and the opportunity to work alongside them.

I would like to express my gratitude to the esteemed jury members for their time, expertise, and critical evaluation of my thesis:

- **1 Dr. Hammoudi Mohamed-Yacine**
- **2 Pr. Zellouma Laid**
- **3 Pr. Guettaf Abderrazak**

I am deeply indebted to the director of the Laboratory LGEB **Pr. ZOUZOU SALAHEDDINE** for providing me with the necessary resources, facilities, and a conducive research environment. Their guidance and vision have played a pivotal role in shaping my research.

I extend my heartfelt gratitude to my dear friend **DR. THABET SEDDIK** for his unwavering support and assistance. His guidance has been instrumental in shaping the success of this endeavor.

My heartfelt appreciation goes out to the entire team of laboratories **LMSE** and **LGEB**. Their collaboration, support, and collective efforts have fostered an intellectually stimulating environment that has contributed to my growth as a researcher.

Finally, I want to express my deepest gratitude to my parents, who have been a constant source of love, encouragement, and support. Their unwavering belief in my abilities and sacrifices have been the driving force behind my achievements.

ABSTRACT

Autonomous electric vehicles have emerged as an innovative and groundbreaking solution in the field of transportation. The development of autonomous electric vehicle control has been swiftly progressing, fueled by the constant advancement of sophisticated control techniques. This progress has led to an expansion of the potential of autonomous electric vehicle technology. However, despite these impressive advancements, the field still confronts a wide array of challenges that demand attention and solutions to unlock its full capabilities.

This thesis delves into the realm of autonomous electrical vehicle control, focusing on three essential aspects: lateral control strategy, longitudinal control strategy, and traction system emulation. The first aspect introduces a dynamic model tailored for autonomous vehicles, with a primary focus on the lateral control strategy. To achieve precise lateral motion along a predefined trajectory, an advanced super-twisting control technique is employed. This technique ensures exceptional accuracy, responsiveness, and stability throughout the vehicle's lateral movement. The second aspect centers around optimizing the longitudinal control strategy through the development of a sophisticated speed planning algorithm. This algorithm takes various factors into account to intelligently generate a suitable speed profile. By considering these crucial elements, the algorithm ensures safe and secure motion within predefined boundaries. The third aspect focuses on emulating the behavior of the traction system. A meticulously designed back-stepping technique is employed with the aim of controlling the speed of an induction motor to mimic the desired performance of the traction system.

The results of the mentioned aspects of this thesis are obtained through numerical simulation using the Matlab/Simulink software. Additionally, real-time implementation is conducted in the electrical engineering laboratory of Biskra (LGEB), equipped with dSpace 1104. By addressing the lateral control strategy, longitudinal control strategy, and traction system emulation, this thesis makes significant contributions to the field of autonomous electrical vehicle control.

Keywords: Autonomous electric vehicle, Vehicle modeling, Trajectory tracking, Sliding mode control, Speed planning algorithm, Back-stepping control.

RÉSUMÉ

Les véhicules électriques autonomes se sont imposés comme une solution innovante et révolutionnaire dans le domaine des transports. Le développement du contrôle autonome des véhicules électriques progresse rapidement, alimenté par les progrès de techniques de contrôle sophistiquées. Ces progrès ont conduit à une expansion du potentiel de la technologie des véhicules électriques autonomes. Cependant, malgré ces avancées impressionnantes, le domaine est toujours confronté à un large éventail de défis qui exigent une attention pour libérer toutes ses capacités.

Cette thèse plonge dans le domaine du contrôle autonome des véhicules électriques, en se concentrant sur trois aspects essentiels : la stratégie de contrôle latéral, la stratégie de contrôle longitudinal et l'émulation du système de traction. Le premier aspect introduit un modèle dynamique adapté aux véhicules autonomes, avec un accent principal sur la stratégie de contrôle latéral. Pour obtenir un mouvement latéral précis le long d'une trajectoire prédéfinie, une technique de contrôle de super-twisting avancée est utilisée. Cette technique assure une précision, une réactivité et une stabilité exceptionnelles tout au long du mouvement latéral du véhicule. Le deuxième aspect est centré sur l'optimisation de la stratégie de contrôle longitudinal par le développement d'un algorithme sophistiqué de planification de la vitesse. Cet algorithme prend en compte différents facteurs pour générer intelligemment un profil de vitesse adapté. En tenant compte de ces éléments cruciaux, l'algorithme garantit un mouvement sûr et sécurisé dans des limites prédéfinies. Le troisième aspect se concentre sur l'émulation du comportement du système de traction. Une technique de back-stepping conçue est utilisée dans le but de contrôler la vitesse d'un moteur asynchrone pour imiter les performances souhaitées du système de traction.

Les résultats des aspects mentionnés de cette thèse sont obtenus par simulation numérique à l'aide du logiciel Matlab/Simulink. De plus, la mise en œuvre en temps réel est menée dans le laboratoire de génie électrique de Biskra (LGEB), équipé du dSpace 1104. En abordant la stratégie de contrôle latéral, contrôle longitudinal et l'émulation du système de traction, cette thèse apporte des contributions significatives au domaine de commande de véhicule électrique autonome.

Mots-clés : Véhicule électrique autonome, Modélisation du véhicule, Suivi de trajectoire, Contrôle en mode glissant, Algorithme de planification de la vitesse, Contrôle en back-stepping.

ملخص

ظهرت السيارات الكهربائية المستقلة كحل مبتكر ورائد في مجال النقل. يتقدم تطوير التحكم في السيارة الكهربائية المستقلة بسرعة، مدعومًا بالتقدم المستمر في تقنيات التحكم المتطورة. أدى هذا التقدم إلى توسيع إمكانات تكنولوجيا المركبات الكهربائية المستقلة. مع ذلك، على الرغم من هذه التطورات المثيرة للإعجاب، لا يزال المجال يواجه مجموعة واسعة من التحديات التي تتطلب اهتماما وحلولا لإطلاق العنان لقدراته الكاملة.

تتعمق هذه الأطروحة في مجال التحكم الذاتي في السيارة الكهربائية، مع التركيز على ثلاثة جوانب أساسية: استراتيجية التحكم الجانبي، واستراتيجية التحكم الطولي، ومحاكاة نظام الجر. يقدم الجانب الأول نموذجًا ديناميكيًا مصممًا للمركبات ذاتية القيادة، مع التركيز بشكل أساسي على استراتيجية التحكم الجانبي. لتحقيق حركة جانبية دقيقة على طول مسار محدد مسبقًا، يتم استخدام تقنية تحكم متقدمة في الالتواء الفائق. تضمن هذه التقنية دقة استثنائية واستجابة واستقرارًا خلال الحركة الجانبية للسيارة. يتمحور الجانب الثاني حول تحسين استراتيجية التحكم الطولي من خلال تطوير خوارزمية متطورة لتخطيط السرعة. تأخذ هذه الخوارزمية في الاعتبار العديد من العوامل لإنشاء ملف تعريف سرعة مناسب بذكاء. من خلال النظر في هذه العناصر الحاسمة، تضمن الخوارزمية حركة آمنة داخل حدود محددة مسبقًا. يركز الجانب الثالث على محاكاة سلوك نظام الجر. يتم استخدام تقنية التحكم ذو النمط الخلفي المصممة بدقة بهدف التحكم في سرعة المحرك الغير متزامن لتقليد الأداء المطلوب لنظام الجر.

يتم الحصول على نتائج الجوانب المذكورة من هذه الرسالة من خلال المحاكاة العددية باستخدام برنامج MATLAB/Simulink. بالإضافة إلى ذلك، يتم تنفيذ تطبيق تجريبي في مختبر الهندسة الكهربائية ببسكرة (LGEB) المجهز بـ dSpace 1104 . من خلال معالجة استراتيجية التحكم الجانبي ، واستراتيجية التحكم الطولي ، ومحاكاة نظام الجر ، تقدم هذه الأطروحة مساهمات كبيرة في مجال الحكم الذاتي التحكم في السيارة الكهربائية.

الكلمات الرئيسية: السيارة الكهربائية المستقلة، نمذجة المركبات، تتبع المسار، تحكم ذو نمط انزلاقي، خوارزمية تخطيط السرعة، تحكم ذو نمط خلفي.

LISTE OF FIGURES

LISTE OF TABLES

LISTE OF ACRONYMS

AASHTO	American Association of State Highway and Transportation Officials.
AC	Alternative Current.
ACC	Adaptive Cruise Control.
ACO	Ant Colony Optimization.
AEV	Autonomous Electric Vehicle.
BLDC	Brushless Direct Current Motor.
DBQ	Driver Behaviour Questionnaire.
DC	Direct Current.
DFOC	Direct Field Orientation Control.
DTC	Direct Torque Control.
EV	Electric Vehicle.
FOC	Field-Oriented Control.
FOSC	First Order Sliding Control.
HOSC	Higher Order Sliding Control techniques.
IFOC	Indirect Field Orientation Control.
IGBT	Insulated Gate Bipolar Transistor.
IM	Induction Motor.
IP	Intersection Point.
GM	General Motors.
GSA	Gravitational Search Algorithm.
LKA	Lane Keeping Assistance.
LPV	Linear Parameter-Varying.
LQ	Linear Quadratic.
LQG	Linear Quadratic Gaussian.
MPC	Model Predictive Control.
PC	Point of Curvature.
PD	Proportional Derivative.
PI	Proportional Integral.

PID	Proportional Integral Derivative.
PMSM	Permanent Magnet Synchronous Motor.
PSO	Particle Swarm Optimization.
PT	Point of Tangency.
PWM	Pulse Width Modulation.
SMC	Sliding Mode Control.
STC	Super Twisting Control.
SRM	Switched Reluctance Motor.
SVM	Space Vector Modulation.
VFD	Variable Frequency Drive.

LISTE OF SYMBOLS

L_v	Vehicle wheelbase.
W_v	Vehicle width.
F_v	Point at the center of the front axle of the vehicle.
R_v	Point at the center of the rear axle of the vehicle.
δ_1, δ_2	Equivalent steering angles of the front wheels of the vehicle.
F_x	Longitudinal force.
F_y	Lateral force.
F_z	Vertical force.
T_x	Reversal torque.
T_y	Rolling resistance torque.
T_z	Auto-alignment torque.
T_m	Motor torque.
T_b	Braking resistive torque.
C_w	Center of the wheel.
O_g	Center of the $(x - y - z)$ coordinate of the wheel at the ground.
β	Sliding for the lateral dynamic.
λ	Sliding for the longitudinal dynamic.
C_λ	Longitudinal stiffness.
C_β	Lateral stiffness.
x_f, y_f	Global coordinates of the front wheel.
x_r, y_r	Global coordinates of the rear wheel.
δ	Steering angle of the front wheel.
ψ	Orientation of the vehicle.
v	Forward speed of the vehicle.
G_v	Vehicle center of gravity.
L_f, L_r	Geometric distance $\overline{GF}$ and $\overline{GR}$.
v_g	Vehicle velocity at the center of gravity.

v_x , v_y	Longitudinal and lateral velocities at the center of gravity.
β_f, β_r	Sliding angles of the front and rear wheels.
F_{xf}, F_{yf}	Longitudinal and lateral forces applied on the front wheel.
F_{xr}, F_{yr}	Longitudinal and lateral forces applied on the rear wheel.
M_z	Dynamic moment of the vehicle.
m	Vehicle mass at the center of gravity.
I_z	Vehicle inertia at the center of gravity.
a_x, a_y	Total lateral and longitudinal accelerations.
V_{ab}, V_{ab}, V_{ab}	Phase to phase voltages $(a-b-c)$.
V_{an}, V_{an}, V_{an}	Phases voltages $(a-b-c)$.
S_1, S_2, S_3	Switches 1,2,3 of the inverter.
V_{DC}	DC bus voltage.
θ	Position of the rotor phase in relation to that of the stator phase.
ω	Electrical speed of the induction motor.
S_a, S_b, S_c	Stator phases $(a-b-c)$.
R_a, R_b, R_c	Rotor phases $(a-b-c)$.
V_{sa}, V_{sb}, V_{sc}	Voltage of the stator phases in $(a-b-c)$ frame.
V_{ra}, V_{rb}, V_{rc}	Voltage of the rotor phases in $(a-b-c)$ frame.
I_{sa}, I_{sb}, I_{sc}	Current of the stator phases in $(a-b-c)$ frame.
I_{ra}, I_{rb}, I_{rc}	Current of the rotor phases in $(a-b-c)$ frame.
$\phi_{sa}, \phi_{sb}, \phi_{sc}$	Flux of the stator phases in $(a-b-c)$ frame.
$\phi_{ra}, \phi_{rb}, \phi_{rc}$	Flux of the rotor phases in $(a-b-c)$ frame.
R_s	Resistance of the stator.
R_r	Resistance of the rotor.
L_s	Inductance of the stator.
L_r	Inductance of the rotor.
L_m	Mutual inductance.
T	Transformation matrix from $(a-b-c)$ reference to $(d-q)$ reference.
k	Constant of the transformation matrix.

V_{sd}, V_{sq}	Voltage of the stator phases in $(d-q)$ frame.
V_{rd}, V_{rq}	Voltage of the rotor phases in $(d-q)$ frame.
I_{sd}, I_{sq}	Current of the stator phases in $(d-q)$ frame.
I_{rd}, I_{rq}	Current of the rotor phases in $(d-q)$ frame.
ϕ_{sd}, ϕ_{sq}	Flux of the stator phases in $(d-q)$ frame.
ϕ_{rd}, ϕ_{rq}	Flux of the rotor phases in $(d-q)$ frame.
$V_{s\alpha}, V_{s\beta}$	Voltage of the stator phases in $(\alpha-\beta)$ frame.
$V_{r\alpha}, V_{r\beta}$	Voltage of the rotor phases in $(\alpha-\beta)$ frame.
$I_{s\alpha}, I_{s\beta}$	Current of the stator phases in $(\alpha-\beta)$ frame.
$I_{r\alpha}, I_{r\beta}$	Current of the rotor phases in $(\alpha-\beta)$ frame.
$\phi_{s\alpha}, \phi_{s\beta}$	Flux of the stator phases in $(\alpha-\beta)$ frame.
$\phi_{r\alpha}, \phi_{r\beta}$	Flux of the rotor phases in $(\alpha-\beta)$ frame.
θ_s	Angles between the stator phase a and the direct axis d.
θ_r	Angles between the rotor phase a and the direct axis d.
T_e	Electromagnetic Torque.
T_L	Load torque.
Ω	Motor mechanical speed.
J	Motor inertia.
f	Viscous damping coefficient.
s	Sliding surface.
x	State variable.
$A(x), B(x)$	General nonlinear functions.
e	General error.
λ_s	Sliding surface coefficient.
V	General Lyapunov function.
u	General control law.
n	Relative degree of the system.
u_{dis}	Sliding mode discontinious control.

k_s	Discontinious control constant.
u_{eq}	Sliding mode equivalent control.
S_M	Upper bound of sliding surface.
Γ_M	Upper bound of the signal Γ.
Γ_m	Lower bound of the signal Γ.
Φ_M	Upper bound of the signal Φ.
U_M	The lower bound of the signal Φ.
u_1	Super twisting mode control law first part.
u_2	Super twisting mode control law second part.
α_s, β_s	Super twisting coefficients.
ρ	Super twisting constructive factor.
C_f, C_r	Drift stiffness of the front and rear tires.
μ	Coefficient of adhesion.
e_{ST}	Error of the designed super twisting control.
κ	Path curvature.
δ_{ST}	Designed super twisting control law.
δ_{SM}	Designed second order sliding mode control.
V_{SM}	Lyapunov function of the designed second order sliding mode control.
α	Bearing angle.
ι	Intersection angle.
R_c	Curve Radius.
L_c	Curve Length.
C_c	Curve Length Chord.
O_c	Curve Center.
ϑ	Central angle.
φ	Banked angle.
F_c	Centrifugal force.
N	Normal force.
f_r	Friction force.

w	Weight force.
g	Gravity acceleration.
ξ	Super-elevation.
d	Appropriate distance required to reach the desired speed.
d_r	Required distance.
d_a	Actual traveled distance.
d_c	Distance to next speed.
d_m	Distance to maximum speed.
v_c	Optimal speed of the curve.
v_a	Actual speed.
v_d	Desired speed.
v_m	Maximum speed.
a	Acceleration value.
a_p	Acceleration.
a_n	Deceleration.
δ_d	Desired steering angle.
x_d	Desired position in X coordinate.
y_d	Desired position in Y coordinate.
ψ_d	Desired vehicle orientation.
ψ_r	Real vehicle orientation.
e_1, e_2	Back-stepping control outer loops errors.
k_1, k_2	Back-stepping control outer loops coefficients.
C_1, C_2	Back-stepping control outer loops outcomes.
V_{B1}	Back-stepping control outer loops Lyapunov function.
e_3, e_4	Back-stepping control inner loops errors.
k_3, k_4	Back-stepping control inner loops coefficients.
$V_{s\alpha}, V_{s\beta}$	Back-stepping control laws.
V_{B2}	Back-stepping control inner loops Lyapunov function.
e_5	Back-stepping observer error.

V_{B3}	Back-stepping observer Lyapunov function.
T_z	Sampling time.
T_1, T_2, T_3	Reference voltages vectors corresponding durations.
T_a, T_b, T_c	Switching durations.
p	Number of pair poles.
F	Induction motor frequency.
P	Induction motor power.
F_{roll}	Rolling force.
F_{aero}	Aerodynamic force.
F_{grad}	Gradient force.
F_{res}	Resistive force.
c_d	Gradient coefficient.
ρ_a	Density of the air.
A_a	Frontal vehicle area.

TABLE OF CONTENTS

Contents **Page**

CHAPTER 1

GENERAL INTRODUCTION

Contents **Page**

1.1. Overview

An autonomous electric vehicle, commonly referred to as an AEV, is a revolutionary form of transportation that combines the advantages of electric power and autonomous driving technology. With ongoing technological advancements and increasing interest from automotive manufacturers and tech companies, AEVs are poised to play a pivotal role in the future of transportation, paving the way for sustainable and efficient mobility solutions.

Autonomous driving technology forms the cornerstone of autonomous electric vehicles, ushering in a transformative era for transportation. AEVs are equipped with a remarkable array of state-of-the-art sensors, such as radars, lidars, and cameras, enabling them to perceive and analyze their surroundings with exceptional precision. Through the utilization of advanced algorithms, these vehicles swiftly process extensive data in real-time, allowing for intelligent decision-making regarding acceleration, braking, and steering. The primary objective is to create a driving experience that places utmost importance on safety and efficiency, mitigating the potential for human errors and significantly enhancing overall road safety. As AEVs continue to advance, the vision of a future with self-driving cars becomes increasingly tangible, reshaping the way we travel and setting new standards for transportation technology.

Electric vehicles (EVs) have emerged as an innovative alternative to conventional internal combustion engine vehicles, utilizing electric motors and rechargeable batteries. This shift brings numerous benefits that promote the transition to a more environmentally friendly future. EVs offer a remarkable decrease in greenhouse gas emissions, contributing to cleaner and more sustainable transportation. Moreover, these vehicles have lower operational costs due to reduced maintenance needs and the expanding availability of charging infrastructure. In addition to their economic and environmental advantages, EVs provide an unmatched driving experience characterized by quiet propulsion and smooth acceleration.

The quick growth and global impact of AEVs are powered by various companies and research institutions at the forefront of innovation. Established car manufacturers, major technology firms, and emerging startups are actively investing in enhancing self-driving technology and electric vehicles. Concurrently, governments and regulatory organizations collaborate to establish specific standards and regulations. These measures are crucial to ensure the safe and responsible use of

AEVs on public roads. The collaborative efforts of these diverse groups are driving the advancement and adoption of AEVs, ultimately leading us to a future with safer, environmentally friendly, and more efficient transportation.

Despite the existing challenges in areas like regulatory frameworks, cybersecurity, and public acceptance, the relentless progress in autonomous driving and electric vehicle technologies is incessantly pushing the boundaries of what autonomous electric vehicles can achieve. This ongoing innovation holds immense promise for transforming the landscape of transportation. As we look ahead, the future of AEVs is teeming with possibilities, poised to revolutionize how we commute and shape the future of transportation for the better.

1.2. Problematic

This thesis is devoted to the proficient design of an autonomous electric vehicle capable of smoothly navigating along a predetermined trajectory. To ensure the vehicle's exceptional performance throughout its operation, the research problem is meticulously divided into three fundamental aspects. Each aspect focuses on crucial factors essential for optimizing the vehicle's overall efficiency and effectiveness. By delving into these key areas, this thesis aims to address and overcome the challenges associated with achieving superior performance in autonomous electric vehicle navigation.

From a control perspective, the precise determination of the lateral control law is of utmost importance to ensure the vehicle's motion remains within secure boundaries. While existing solutions offer control laws built upon the assumption of possessing perfect knowledge of the route, the reality of real-world scenarios introduces a multitude of evolving constraints that make the system vulnerable to changes. This lack of robustness poses the primary challenge that this thesis aims to conquer.

In order to guarantee the secure and comfortable travel of autonomous electric vehicles, meticulous attention must be devoted to the precise management of their speed, especially when traversing dangerous curves. Failing to acknowledge the significance of speed control within an autonomous vehicle system can lead to serious consequences, including compromised safety, low performance, violations of traffic regulations, a diminished experience for passengers, and limited

adaptability in dynamic environments. Therefore, the integration of robust speed planning functionality into the autonomous vehicle system emerges as an indispensable problem that this thesis aims to tackle head-on.

For the longitudinal control of the autonomous electric vehicle, the development of a sophisticated technique is essential to regulate the vehicle's speed and enable it to follow a desired speed profile accurately. To accurately emulate the efficient behavior of an electric vehicle, the desired speed profile extends beyond controlling the vehicle's speed to encompass controlling the vehicle's drive speed. Therefore, the thesis should focus on developing a robust control technique capable of handling uncertainties and external disturbances to ensure precise control of the vehicle's drive.

From a broader perspective, this thesis should contribute to the development of an optimal and robust control strategy for the navigation of autonomous electric vehicles along predetermined trajectories. The vehicle should effectively examine the speed factor by following a desired speed profile that is generated through a carefully designed speed planning algorithm. Lastly, the thesis should consider the development of a robust control technique to govern the vehicle's drive, guaranteeing seamless synchronization with the desired speed profile throughout the entire navigation process.

1.3. Objectives and contributions

The main goal of this thesis is to significantly contribute to the advancement of an efficient and reliable control strategy for guiding autonomous electric vehicles along predetermined paths with varying speeds. This innovative research includes three fundamental objectives, each addressing a critical aspect of autonomous vehicle control. Firstly, it aims to propose a comprehensive mathematical model that accurately determines the lateral control law, enabling precise vehicle trajectory tracking while ensuring a paramount level of safety. By introducing this model, the thesis seeks to enhance the vehicle's ability to navigate along the desired path with utmost accuracy and robustness. Secondly, this research focuses on the integration of a robust speed planning feature into the autonomous vehicle system. By incorporating advanced algorithms and methodologies, the thesis aims to optimize the vehicle speed profile, taking into account many

factors such as passenger comfort and road conditions. The ultimate goal is to provide passengers with a smooth and comfortable travel experience while maintaining efficient and adaptive control over the vehicle's velocity. Lastly, the thesis aims to develop a robust control technique to govern the vehicle's propulsion. By utilizing advanced control algorithms and strategies, the research endeavors to ensure seamless synchronization between the vehicle's propulsion system and the desired speed profile throughout the entire navigation process. This will enable the vehicle to respond swiftly and accurately to changes in speed, guaranteeing a high degree of control and stability during operation.

To achieve the mentioned objectives, a set of robust control techniques has been developed. These control techniques have been carefully designed and improved to be very accurate and effective. By analyzing the desired objectives, we have built a powerful set of control methods that can easily adjust to complicated and ever-changing situations. These robust techniques have been customized to handle the specific challenges and requirements of our objectives, ensuring the best possible performance and results. In fact, these control techniques will be described as follows:

- For the lateral control strategy, a dynamic model for the autonomous vehicle is introduced. Then, a specifically designed super-twisting control technique is used to ensure precise lateral motion of the autonomous vehicle through the trajectory. By leveraging this advanced control technique, we can guarantee that the vehicle maintains exceptional accuracy, responsiveness, and stability throughout its lateral movement, enabling it to navigate the trajectory with unparalleled precision.
- To optimize the longitudinal control strategy, a speed planning algorithm has been developed. This algorithm is intelligently designed, taking into account various factors such as path geometry and trajectory curvature. By considering these crucial elements, the algorithm generates a suitable speed profile that ensures safe and secure motion within the predefined boundaries. This innovative approach allows for the precise adjustment of the vehicle's speed, enabling it to navigate the designated path with utmost safety and efficiency.
- To imitate the way the traction part works, we have used a carefully created back-stepping control method. This method is designed to closely match how we want the traction system

to perform. To make sure this method works well, we have done lots of testing and experiments on an induction motor. Through this rigorous evaluation, we have confirmed that the motor can smoothly follow the speed profile taken from the speed planning algorithm. This testing process makes sure that the traction system and the planned speed profile work together smoothly, ensuring the vehicle moves in a controlled and dependable manner.

1.4. Thesis structure

Following a comprehensive introductory chapter that offers a well-defined overview of the fundamental aspects to be examined in this thesis regarding the control of autonomous electric vehicles, the subsequent chapters of the thesis are meticulously structured in the following manner:

The second chapter will introduce the state of the art of the longitudinal and lateral control techniques and the advancements in speed planning used in autonomous electric fields. Then, an overview of the electrical drives used in electric vehicles and a review of the control technique implemented on the induction motor as a traction drive will be given.

The third chapter will address the explicit mathematical modeling of the studied system, including the autonomous vehicle, voltage inverter, and electrical motor, which in fact makes it possible to extract the appropriate control laws.

The fourth chapter will be devoted to the design of a lateral control law based on the autonomous vehicle dynamic model and super-twisting control technique to ensure high tracking performance through the desired trajectory.

The fifth chapter will describe the detailed design of a speed planning algorithm based on path geometry and trajectory curvatures to generate an adequate speed profile for vehicle navigation with variable velocity.

The sixth chapter will present a meticulous implementation of a designed back-stepping approach to control the induction motor to follow the extracted speed profile from the speed planning algorithm.

The last chapter will provide a summary of our work and outline our future goals and aspirations.

CHAPTER 2

STATE OF THE ART

Contents **Page**

2.1. Introduction

Autonomous electric vehicle control represents the marriage of two groundbreaking technologies, autonomous driving and electric power, to revolutionize the way vehicles are operated. This innovative combination promises to reshape the future of transportation, offering enhanced safety, efficiency, and sustainability. The autonomous aspect of AEV control allows vehicles to perform complex tasks such as lane keeping, adaptive cruise control, and object detection. These capabilities are achieved through sophisticated algorithms that analyze sensor data, create a detailed understanding of the vehicle's environment, and execute appropriate actions based on pre-programmed rules or machine learning models. Furthermore, electric power provides numerous advantages to AEV control. Electric motors, driven by high-capacity batteries, offer instant torque and smooth acceleration, ensuring responsive and efficient vehicle control. Electric propulsion also eliminates the need for traditional transmission systems, simplifying the overall control architecture and reducing mechanical complexity. The remarkable journey of autonomous vehicles traces back to the pioneering efforts of Carnegie Mellon University in the 1980s [1, 2], where their successful implementations laid the foundation for future advancements. In recent times, the automotive industry has experienced a surge of research and technological breakthroughs, resulting in a noteworthy collective endeavor by diverse automotive companies to materialize the vision of intelligent autonomous vehicles [3].

This chapter offers a comprehensive exploration of the autonomous vehicle system, encompassing its different levels of autonomy and the key stages and modules that constitute it. A particular emphasis is placed on the examination of control strategies employed for trajectory tracking and path following in autonomous vehicles. The review delves into the control phase of the autonomous vehicle system, focusing specifically on trajectory tracking and the underlying vehicle model. Extensive research in this field is incorporated into the discussion, shedding light on the latest advancements and findings. Furthermore, the chapter delves into the traction aspect of autonomous electric vehicles, providing insights into the diverse electric drives utilized and the sophisticated control techniques developed to effectively regulate their speed. This comprehensive analysis aims to provide a deeper understanding of the autonomous vehicle system and its critical components, paving the way for further advancements in the field.

2.2. Autonomy levels and development challenges in automated vehicles

Within the realm of automated vehicle systems, the classification of autonomy spans six distinct levels, as set forth by the guidelines established under SAE-J3016 [4]. These levels delineate the varying degrees of autonomous capabilities exhibited by vehicles, providing a comprehensive framework for understanding their functional autonomy:

- **Level 0:** At this level, the vehicle is under the complete control of the human operator, although the automated system may issue warnings or alerts.
- **Level 1:** The system provides several automated assistances, such as Adaptive Cruise Control (ACC), Parking Assistance with automated steering, and Lane Keeping Assistance (LKA).
- **Level 2:** The automated vehicle system assumes responsibility for functions like acceleration, braking, and steering, with the driver able to regain control immediately if necessary.
- **Level 3:** Within predefined, limited environments like freeways, the automated vehicle can perform auto-pilot functions.
- **Level 4:** The automated vehicle system is capable of controlling the vehicle in all directions, with a few exceptions for specific environments like severe weather. The driver must activate the automated system only when it is safe, and once engaged, the driver's attention is not required.
- **Level 5:** The pinnacle of autonomy is achieved at this level, where the automated vehicle system operates without any human intervention. It can navigate itself to any location permitted by law, demonstrating full autonomy.

Developing a successful autonomous ground vehicle involves addressing various challenges. According to [5], the development process should tackle three fundamental questions:

- Where is the vehicle currently located?
- What is the desired destination?
- How can the vehicle safely reach its destination?

Considering these criteria, it becomes evident that the autonomous system should encompass multiple modules and tasks, as illustrated in Figure 2.1. The system consists of three key stages:

- **Sensing and Perception:** This module collects real-time data to determine the vehicle's location and its surrounding environment. The gathered data is then processed into a suitable format for further analysis.
- **Planning:** Using the data acquired from Sensing and Perception, this module determines a safe and feasible path for the vehicle to follow.
- **Control:** This module integrates control strategies to guide the vehicle along the desired path, including actuator control for each subsystem.

Each of these modules plays a crucial role, and numerous publications have offered comprehensive overviews on related topics. These encompass an examination of the overall construction of autonomous vehicles [6], path planning methods and strategies in autonomous vehicles [7], motion planning for highway autonomous driving [8], as well as trajectory planning and tracking for autonomous overtaking [9].

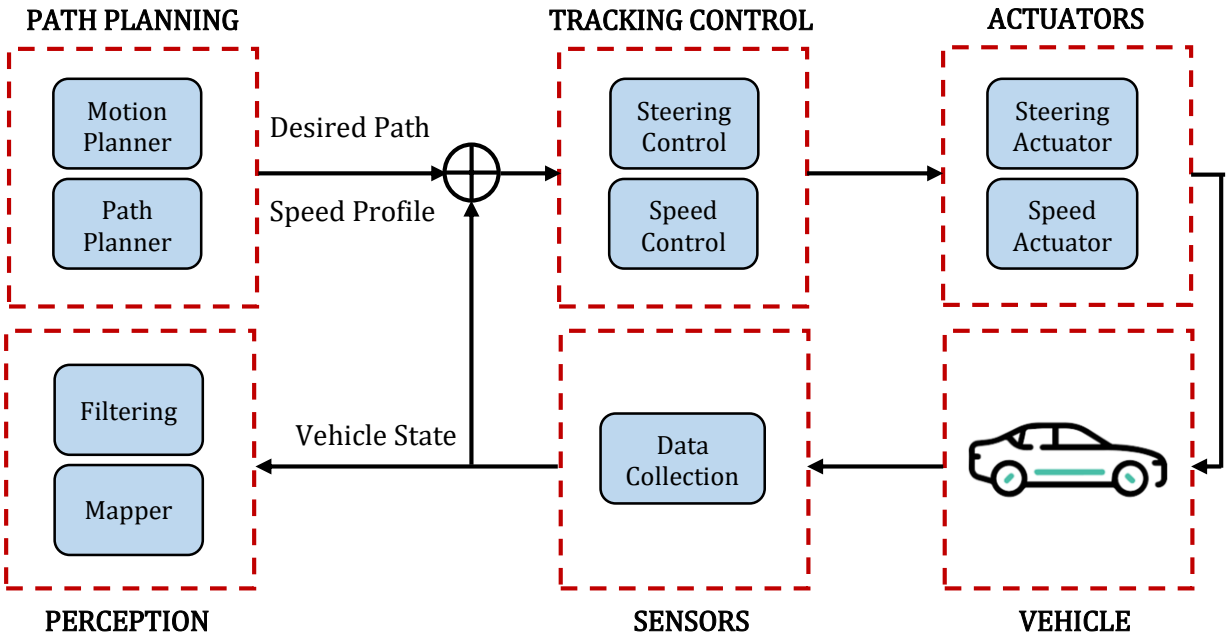

Figure 2.1. Autonomous vehicle system.

2.3. Control of autonomous vehicle

The literature encompasses a wide array of strategies for vehicle dynamics control, offering numerous approaches to tackle this area. In practice, it is common to utilize a combination of two distinct controllers to effectively govern the longitudinal and lateral dynamics of a vehicle. The lateral control component comes into play during lane keeping or lane change maneuvers, whereas the longitudinal control aspect finds its application in cruise control, adaptive cruise control, and platooning tasks. It is worth emphasizing that the vehicle dynamics in both longitudinal and lateral directions are intricately intertwined. This means that we should consider them as one system when dealing with them. By looking at the whole system, we can make sure the vehicle handles well and, most importantly, keeps everyone safe, especially in challenging driving situations.

2.3.1. Lateral control

The primary objective in the realm of lateral control for autonomous vehicles revolves around the precise guidance of vehicles along predetermined reference trajectories, achieved through the adjustment of steering angles. However, the inherent nonlinearity of the system, coupled with uncertainties in parameters and the potential for encountering disturbances during real-world automotive applications, poses a considered challenge. Overcoming this challenge necessitates the development of a robust controller that can effectively accommodate and mitigate these factors. The efficacy of such a controller is gauged by its ability to consistently deliver reliable performance in the face of disturbances, parametric uncertainties, wind effects, variations in road grip, and other pertinent variables. In the following, we will delve into an exploration of existing control laws that specifically address the management of lateral dynamics in autonomous vehicles.

Proportional Integral Derivative (PID) controller has been used in this study [10], where two cascaded PID controllers have been suggested for controlling the lateral movement of a vehicle. The internal loop ensures that the vehicle maintains the desired yaw rate, even in the presence of constant disturbances and uncertainties in the vehicle's parameters. The external loop generates the reference yaw rate based on the error in the lateral position, aiming to minimize this error. To account for uncertainties in the vehicle's parameters, a robust stability analysis is performed, considering the longitudinal velocity as a variable. The optimization process deduces

the values of the seven control parameters and the desired distance. By regulating the lateral position at a distance ahead of the vehicle rather than at its center of gravity, this well-established approach compensates for inherent delays and enhances robustness, especially at high speeds [11,12]. In a similar fashion, Amer et al. [13] employ the same cascaded PID structure for lateral control of a military vehicle, optimizing the gains using a particle swarm algorithm. In contrast, Ping et al. [14] use an adaptive fuzzy controller in the inner loop (yaw rate control) along with a PID controller in the outer loop. Another study [15] presents a PID controller specifically designed for monitoring the steering wheel angle set-point. This set-point is determined through a trajectory planning module, which assumes the vehicle follows a circular path and incorporates a sighting distance. Additionally, the system compensates for the dead zone of the steering and adjusts the setpoint obtained from trajectory planning.

Linear Quadratic (LQ) control was used in [16] for a robotic vehicle equipped with four independent steering wheels. The LQ control synchronized the steering angles of the front and rear wheels, independently, to enhance overall handling performance. In a comparative study by Mouri and Furusho [17], a Proportional-Derivative (PD) controller and an LQ controller were evaluated. The LQ controller demonstrated an advantage by decoupling the yaw control of the vehicle from its lateral position, eliminating the need for a cascade structure as required by the PD controller. In [18], a technique called model-based Linear Quadratic Gaussian (LQG) Control with adaptive Q-matrix is introduced. This method aims to design a path tracking controller for a desired vehicle by efficiently and systematically addressing challenges related to noise and errors caused by localization and path planning algorithms. Notably, the controller is automatically designed without requiring extra adjustments for different speeds, simplifying the tuning process. Hsiao and Tomizuka [19] proposed a two-step procedure to overcome this limitation, while Son et al. [20] suggested using an observer to estimate unmeasured states in the control system.

Neural network technique based on learning by imitation has been utilized in the field of autonomous vehicles to replicate driver behavior, aiming to provide control that closely aligns with driver expectations. One of the early applications of neural networks in autonomous vehicles is proposed in the work by Pomerleau [21]. To accurately capture driver behavior on highways, the authors of [22] propose learning by imitation of trajectory generation module parameters. To achieve this, a cost function is computed based on dynamic data generated by the driver's actions,

including lane position, relative position to nearby and preceding vehicles, speeds, accelerations, and jerks. Subsequently, the trajectory generation module is capable of generating trajectories that imitate the driver's behavior.

Fuzzy logic is employed in various studies to achieve lateral control of vehicles. In a study conducted by Hessburg and Tomizuka [23], three fuzzy logic modules are utilized. The first module determines the gains for state feedback, while the second module anticipates the road curvature to adjust the control action. The last module adjusts the control based on the vehicle's longitudinal speed. The rules for these modules are manually defined, drawing upon the expertise of the authors. In another investigation by Cai et al. [24], two parallel fuzzy PD controllers are proposed to independently control the vehicle's lateral deviation and yaw angle. The parameters of these controllers are optimized using a genetic algorithm, facilitating their adjustment. Pérez et al. [25] adopt a cascade architecture in their approach, where a low-level discrete PID controller receives inputs from a high-level fuzzy controller. Real-world tests conducted across different longitudinal speeds validate the effectiveness and performance of this architecture. The low-level controller plays a crucial role in ensuring comfort by filtering the outputs of the high-level controller to prevent undesired oscillations. Onieva et al. [26] introduce a fuzzy controller with automatically adjusted parameters. They use an iterative genetic algorithm that utilizes data collected during an initial driving phase to provide three distinct autonomous control modes (eco, comfort, sport), tailored to the driver preferences and driving style.

Sliding Mode Control (SMC) has been successfully implemented in many papers for the lateral control of vehicles or mobile robots. In most of these studies, the sliding variable used is the lateral deviation. In [27], the inherent reluctance issue in this type of control is addressed using a saturation function, while Guo et al. [28] propose an algorithm based on neural networks to overcome this challenge. Hingwe and Tomizuka [29] introduce a sliding mode controller for generating a flying speed command, and they implement an integrator filter to reduce controller oscillations. In [30], the authors combine the measurement of lateral deviation and yaw angle into a single slip variable, ensuring the convergence of these two states. The Super-Twisting Control (STC), which was suggested in references [31-33], is helpful in reducing the resistance effect and it remains strong even when there are uncertainties about the values of certain parameters, external disturbances, and variations in the system.

The back-stepping technique was used in [34] to develop an integrated control approach for a lightweight road vehicle operating at low speeds (below 50 km/h) on a known and highly secure route. Another study by Norouzi et al. [35] introduced a novel Lyapunov-based robust controller for the lateral control of an autonomous vehicle. This controller was designed using a meta-heuristic optimization algorithm and focused on a double lane change maneuver. The path planning involved designing a fifth-degree polynomial function with dynamic constraints, while a lane changing path planning method was utilized. To address position and orientation errors based on a two-degree-of-freedom vehicle bicycle model, a combination of sliding mode and back-stepping controllers was employed for steering control in this research. Furthermore, Jiang and Astolfi [36] investigated the problem of asymptotic stabilization for a specific class of nonlinear systems and proposed a solution. This solution, along with back-stepping and forwarding control design methods, was applied to control the nonlinear lateral dynamics of a vehicle.

Adaptive control techniques are employed in various studies to address challenges in the lateral control of vehicles. In the article by Netto et al. [37], a self-adapting controller is implemented to handle external disturbances like wind and road curvature, as well as parametric uncertainties. Although these aspects are considered unknown, they are assumed to belong to a compact set. Simulation results on a nonlinear model demonstrate the robustness of this control strategy. In [38], an inverse tire model is proposed to handle variations in tire stiffness, and an adaptive law is employed to estimate the unknown mass and inertia matrix of the vehicle. Stability of the control structure and convergence of the estimated parameters are ensured through the use of a Lyapunov function. Hima et al. [39] adopt an adaptive back-stepping approach to compensate for parametric uncertainties and nonlinearities. Furthermore, Shirazi and Rad [40] introduce an adaptive control method based on the $\mathcal{L}_1$ command [41], which offers robustness guarantees and quick adaptation settings.

Model Predictive Control (MPC) has been implemented by the authors of the paper [42] for the lateral control of a vehicle. They compared the performance and complexity of nonlinear MPC with linear MPC, which involved successive linearization of the model. The evaluation demonstrated satisfactory performance, even on low grip roads, indicating the robustness of the introduced approach in different challenging conditions. To enable online implementation, the use of lightweight optimization algorithms become essential. In another study by Merabti et al. [43],

three metaheuristic optimization algorithms were compared for trajectory tracking of a mobile robot. Particle Swarm Optimization (PSO) proved to be the most efficient in terms of convergence time towards the optimal solution compared to ant colony algorithms (Ant Colony Optimization or ACO) and the gravitational search (Gravitational Search Algorithm or GSA). Furthermore, the application of MPC control can be extended to Linear Parameter-Varying (LPV) systems, eliminating the need for nonlinear models and resolving complex and expensive associated problems [44].

2.3.2. Longitudinal control

Precise speed tracking assumes a paramount significance in the domain of fully automated driving, where longitudinal control strives to flawlessly synchronize with a predetermined speed profile originated from a higher-level module. This pivotal task encompasses a diverse array of invaluable applications that contribute to the seamless operation of automated vehicles.

Proportional Integral Derivative controllers are widely used in cruise control systems for their simplicity and effectiveness, not requiring precise vehicle model identification. Kim et al. [45] demonstrates successful implementation of a PID controller for longitudinal dynamics regulation, leveraging the vehicle powertrain model's inverse dynamics for accurate control. The work of Hoffmann et al. [46] employs a Proportional Integral (PI) controller to govern longitudinal dynamics, emphasizing its versatility and effectiveness. Hima et al. [47] further validates the PID controller's efficacy, solidifying its position as a reliable choice for precise and adaptive cruise control. These studies collectively highlight the importance of PID and PI controllers in developing efficient control strategies for cruise control applications.

Linear Quadratic control, as investigated in the study conducted by Shakouri et al. [48], emerges as a prominent control strategy that undergoes meticulous comparison with an adjustable gain Proportional Integral controller. Through an exhaustive analysis, the authors meticulously uncover a multitude of advantageous characteristics exhibited by both controllers, culminating in remarkably similar performance on a global scale. This comprehensive exploration not only highlights the inherent versatility and efficacy of LQ control but also showcases its potential as a powerful control strategy that extends to a wide range of applications. Moreover, the researchers emphasize the value of the adjustable gain PI controller, which exhibits commendable

performance and effectively tackles dynamic control challenges.

Machine learning serves as the foundation for the research presented in [49], offering a data-driven solution aimed at estimating stochastic driver models by analyzing their behavior traces. Introducing the Bayesian Autonomous Driver Mixture-of-Behaviors (BAD-MoB) model, specifically tailored for the longitudinal control of human drivers in inner-city traffic scenarios, the researchers strive to replicate and comprehend human driver behavior. Moreover, they propose utilizing this model to prototype intelligent assistance systems capable of emulating human-like behavior. This novel machine learning approach opens up a promising path towards comprehending the intricacies of human driving behavior, ultimately laying the groundwork for the development of advanced assistance systems that respond in a more natural manner.

Fuzzy logic, a widely embraced control methodology for regulating longitudinal speed in vehicles, plays a pivotal role in the field. The study conducted in [50] represents a significant contribution as researchers meticulously develop an adaptive cruise controller that harnesses the power of fuzzy logic. To validate its efficacy, the controller undergoes rigorous testing in real-world conditions using an instrumented automatic driving system. The obtained experimental results showcase the controller's exceptional performance, demonstrating its remarkable adaptability across a diverse range of speeds and its ability to select safe inter-vehicle gaps with precision. Furthermore, [51] extends the application of fuzzy logic by designing a coordinated throttle and brake fuzzy controller, accentuating the versatility of fuzzy logic in enabling effective control strategies that address both acceleration and deceleration dynamics.

Sliding mode control takes center stage in the study presented in [52], as researchers propose a groundbreaking design for a cruise controller. This innovative controller harnesses the power of sliding mode techniques and undergoes rigorous validation through experimentation. Its primary focus lies in facilitating precise longitudinal control of vehicles operating at low speeds, with the ultimate goal of optimizing traffic capacity while simultaneously enhancing safety and comfort levels. Furthermore, Ferrara and Vecchio [53] introduce a distinctive approach in which second-order sliding mode control is employed for vehicles engaged in platooning tasks. This advanced control strategy showcases the versatility of sliding mode control methodologies and highlights their potential in addressing complex operational scenarios, thus contributing to the advancement of intelligent transportation systems.

2.3.3. Summary control strategies

In the preceding sections, we have examined the various methods employed to manage the longitudinal and lateral motions of a vehicle. Each of these strategies offers its own set of strengths and weaknesses, either inherent to their nature or due to practical implementation considerations. Therefore, when choosing a control strategy, one must consider the requirements of the system, available measurements, and the computing capabilities onboard. Table 2.1 provides a summary of these diverse strategies.

Table 2.1. Summary of the different control strategies.

Control strategy	Advantages	Disdvantages
PID	Simple and widely used control technique.	Limited ability to handle complex systems or nonlinearities.
Linear Quadratic	Provides optimal control for linear time-invariant systems.	Limited to linear systems.
Neural Network	Nonlinear system modeling.	Training complexity. Black-box nature.
Fuzzy Logic	Ability to handle uncertainty and imprecise information.	Design and tuning of fuzzy control systems can be complex.
Sliding Mode	Robustness to uncertainties and disturbances.	Chattering phenomenon causes wear on mechanical systems.
Back − Stepping	Good reference signals tracking and disturbances rejecting.	Requires a detailed model of the system dynamics.
Adaptive Control	Ability to handle uncertainties and adapt to changing system dynamics.	Complexity in design and tuning. It may require a priori knowledge of the system dynamics.
MPC	Can handle complex systems with constraints and time-varying dynamics.	Solving an optimization problem at each sampling time can be computationally demanding.

2.3.4. Advancements in speed planning

In the realm of autonomous vehicle systems, speed planning holds immense significance. It refers to the process of determining and adjusting the appropriate speed at which an autonomous vehicle should operate in various driving scenarios. Effective speed planning plays a critical role in ensuring the safety, efficiency, and comfort of autonomous vehicles and their occupants.

Curve speed warning systems represent a category of semi-autonomous solutions designed to effectively inform drivers about the optimal speed through the utilization of auditory or visual indicators [54, 55]. An exemplification of such an innovation is the system proposed by Varhelyi [56], which surpasses the mere consideration of curves by factoring in additional variables like road conditions (such as wet surfaces) and visibility parameters (like darkness) to accurately compute the most suitable speed for drivers. This advanced system then proceeds to notify the driver through a combination of visual and auditory alerts, ensuring enhanced situational awareness. Huth et al. [57] innovatively presented a curve warning system tailored specifically for motorcyclists, employing either a force feedback throttle or a haptic glove to promptly and effectively deliver the warning signals, thus significantly enhancing safety on the road.

The study in [58] aims to solve the important problem of creating really smooth paths with very little change in speed and direction. To overcome this challenge, the researchers suggest a new method that includes careful planning of the speed at different times. This planning is important because it helps create sequences of times that can be used by the planners to accurately connect the points on the path. By carefully adjusting the speed for straight and turning movements, the resulting paths are designed to prioritize the most important thing, which is the comfort of humans.

The paper [59] proposes an innovative and cooperative strategy for connected vehicles, aiming to foster seamless coordination between autonomous and nearby vehicles. This is achieved through the integration of multiple components, including vehicle velocity prediction, robust fuzzy path-following control, and motion planning. By incorporating these elements, the approach effectively addresses the inherent uncertainties in the system, enhancing the overall cooperation among vehicles. To accurately anticipate the behavior of nearby vehicles, a state-of-the-art recurrent neural network is utilized, leveraging the rich driving information obtained from the connected vehicles technology. Furthermore, a meticulously designed motion planner generates a reliable

reference trajectory, ensuring adaptability to potential errors in the velocity predictions. Through this comprehensive framework, the study contributes to advancing the collaborative potential of connected vehicles, ultimately leading to safer and more efficient transportation systems.

The research presented in [60] suggests an alternative method for estimating the safe speed for turning by combining static drive safety evaluation with dynamic vehicle speed calculation. Initially, the safety of the driving situation is assessed, taking into account the interaction between the driver, vehicle, road, and environment. This comprehensive evaluation is achieved by combining the analytic hierarchy process and entropy weight analysis method. Subsequently, a critical speed for turning is determined by considering the vehicle's driving dynamics, taking into account both sideslip and rollover factors. To estimate the safe speed for turning, the critical speed is adjusted using a safety correction factor derived from the evaluation of the driving safety state.

The research described in [61] introduces a factor that accounts for the influence of driver behavior on driving styles, in contrast to a theoretical curve speed model that only considers the interaction between the vehicle and the road. This factor is determined by comparing the actual speed selected by drivers to the theoretical curve speed. To obtain this factor for different driving styles, the researchers employed the 28-item Chinese version of the Driver Behaviour Questionnaire (DBQ). By conducting a correlation analysis between the DBQ subscales and the factor, it was found that drivers with higher violation scores are more likely to drive at higher speeds when negotiating curves.

Numerous research studies have embraced the concept of road shape estimation as a fundamental approach for computing curve speed in both semi-autonomous and autonomous systems. The analysis of road geometry entails the crucial task of differentiating between curved and straight segments, a task that has been accomplished through two distinct methods. Firstly, some researchers have opted to examine the movement patterns of preceding vehicles to identify these segments [62, 63]. Alternatively, physical parameters like curve radius, length, and angle have been harnessed in conjunction with GPS and GIS data to achieve the same objective [64-66]. Once the curved segments are successfully identified, the next step involves calculating the appropriate speeds for these curves, a process that factors in crucial elements such as road friction and super-elevation angles [15, 54, 67]. By considering these influential factors, the computed curve speeds can be fine-tuned to optimize safety and performance in driving scenarios.

2.4. Traction part control

The traction system plays a critical role in the functioning of electric vehicles, and the selection of appropriate electric motor types is essential to ensure efficient vehicle operation and superior performance. Therefore, a comprehensive understanding of different electric motor types and their key characteristics is necessary to achieve optimal traction system performance. This knowledge enables electric vehicle manufacturers to make informed choices suitable for their applications.

2.4.1. Electric drives for autonomous electrical vehicle

The electric motor technology used in autonomous electric vehicles has undergone significant advancements to meet the growing demand for high-performance and efficient propulsion systems. Electric vehicles use different types of electric motors, depending on various factors such as vehicle size, performance requirements, and cost considerations. The most common types of electric motors used in EVs are:

Induction Motors (IMs) are commonly used in electric vehicles due to their durability, cost-effectiveness, and regenerative braking capabilities. These motors provide high torque at low speeds, making them ideal for start-stop driving and efficient acceleration. While induction motors may have lower efficiency at light loads and limitations in achieving high speeds, they offer a practical solution without relying on expensive rare-earth magnets. Overall, induction motors remain a popular choice for electric vehicles, particularly when cost-effectiveness, durability, and regenerative braking are prioritized [68, 69].

Permanent Magnet Synchronous Motors (PMSMs) are highly efficient and compact motors favored for electric vehicles. They offer advantages like high efficiency across various conditions, extended driving range, and excellent acceleration. With a high power-to-weight ratio, PMSMs enable lightweight designs, reducing vehicle weight and improving efficiency. However, PMSMs can be costlier due to rare-earth magnets, require cooling systems, and have limited regenerative braking compared to induction motors. Nonetheless, PMSMs remain popular for electric vehicles due to their efficiency, power density, and controllability [70, 71].

Switched Reluctance Motors (SRMs) are emerging as a promising option for electric vehicles due to their unique characteristics and main advantages. They are cost-effective, robust,

and offer high torque density and a wide speed range. SRMs provide efficient acceleration and improved vehicle performance. Despite their inherent fault tolerance, controlling SRMs can be complex and may require advanced algorithms and power electronics. Although SRMs have limited commercial adoption, ongoing research aims to optimize their performance. With further advancements, SRMs have the potential to become a significant player in the electric vehicle market offering cost-effective and robust propulsion solutions. [72].

Brushless Direct Current Motors (BLDC) originally designed for small electric vehicles and hybrids, BLDC motors have demonstrated their versatility by successfully being employed in larger electric vehicles as well. These motors leverage a powerful combination of permanent magnets on the rotor and stator windings, allowing them to achieve exceptional efficiency and precise control over rotation. With their remarkable efficiency, robust torque output, and compact form factor, BLDC motors have become an increasingly attractive choice for electric vehicle propulsion systems. Their ability to deliver efficient and precise power makes them a key component in driving the future of electric transportation [73, 74].

Among the previously mentioned options, the IM has emerged as the preferred choice for several reasons [68, 69, 75, 76]. Firstly, its simple design with fewer components translates to easy maintenance and cost-effective repairs. Secondly, IMs have demonstrated robustness and reliability, which are crucial in the demanding context of electric vehicles that require high efficiency. Furthermore, IMs can operate across a wide range of speeds, making them adaptable to diverse driving conditions. Additionally, IMs are highly efficient and do not rely on rare-earth metals. As a result, IMs are extensively used in electric vehicles like Tesla cars and are anticipated to maintain their dominance in the market for the foreseeable future [77-81].

2.4.2. Induction motor control background

In the past, induction motors were typically operated directly from the electrical grid at a fixed speed and frequency (50Hz/60Hz). However, advancements in power electronic converters have revolutionized their usage by enabling variable frequency operation through the integration of a converter between the motor and the grid. This technological breakthrough allows for the achievement of an adjustable speed motor, providing greater flexibility and control.

The introduction of Variable Frequency Drives (VFDs) has further enhanced the capabilities

of induction motors. These drives offer smoother speed adjustment and significantly improved motor control. Over time, a range of control strategies has been developed to effectively regulate the speed, torque, and position of induction motors. These strategies can be broadly classified into two main principles: scalar control and vector control methods. Scalar control is based on the steady-state model of the machine, enabling manipulation of the magnitude and frequency of voltage, current, and flux [82]. However, it does not operate on the space vector position during transient states. In contrast, vector control is designed for dynamic states, enabling precise control of the instantaneous positions of voltage, current, and flux, in addition to their magnitudes [83].

One highly recognized vector control method is Field-Oriented Control (FOC), originally proposed by Hasse and Blaschke in the early 1970s [84, 85]. Another influential method, known as Direct Torque Control (DTC), was introduced by Takahashi and Depenbrock in the mid-1980s [86, 87]. To provide a visual representation, Figure 2.2 illustrates the different classifications of control strategies for variable frequency drives. This comprehensive categorization enables engineers to choose the most suitable control approach for their specific IM applications.

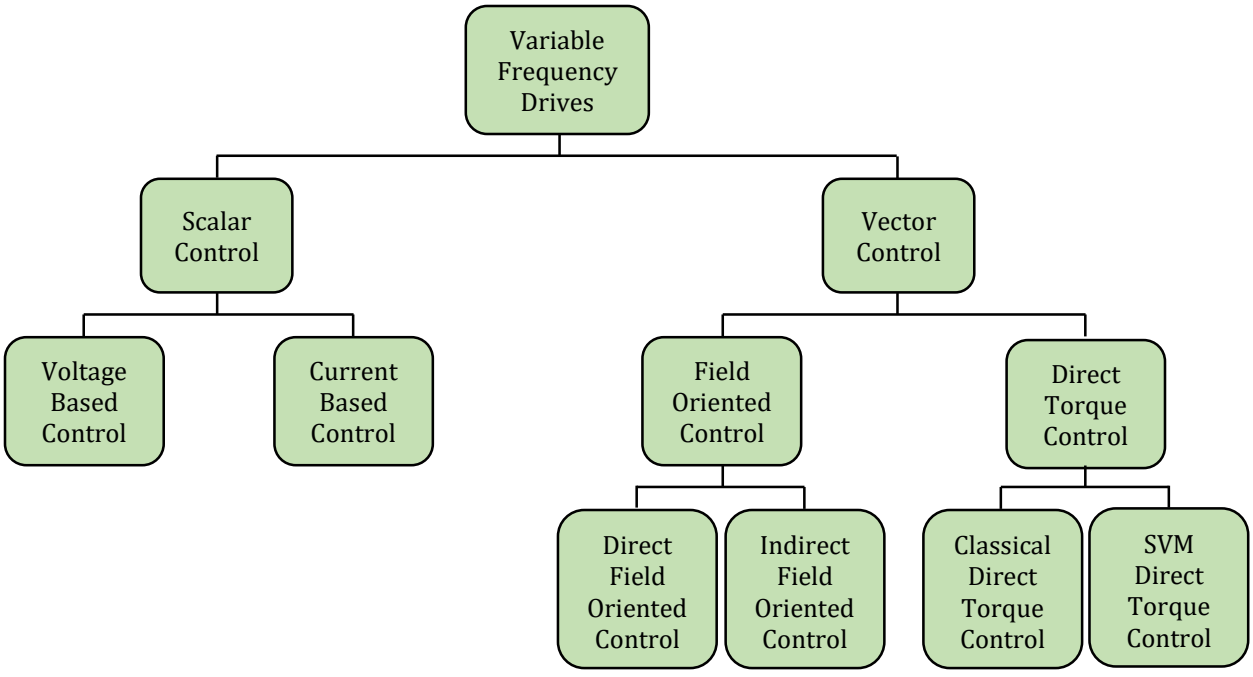

Figure 2.2. Categorization of control strategies for variable frequency induction motor.

2.4.2.1. Scalar control

The Scalar control, known as Volt/Hertz (V/f) control, is a straightforward method used for regulating the speed of induction motors. Its core principle is to keep a constant ratio between the stator voltage and frequency, ensuring a consistent maximum torque output. To achieve speed control within a closed-loop system, a proportional integral controller is employed. The PI controller maintains the desired speed and enhances its accuracy by adjusting the motor's slip speed. The controller receives the speed tracking error, which represents the difference between the desired reference speed (Ω_{ref}) and the actual speed (Ω) [88], as depicted in Figure 2.3.

The primary disadvantages of this technique are the unsatisfied speed accuracy and the sluggish dynamic response that results in a delayed torque response. Since the control design is limited to steady-state conditions, it does not effectively control the magnitude of the stator flux during transients, leading to slow torque response

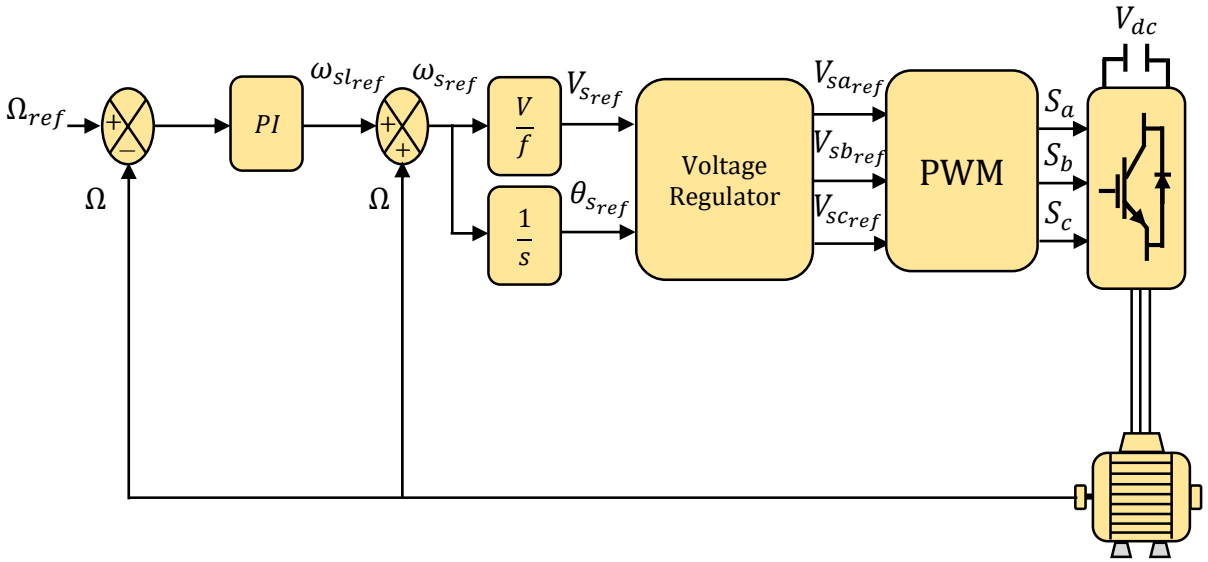

Figure 2.3. Scalar control with closed-loop for variable frequency induction motor.

2.4.2.2. Field oriented control

The control of induction machines currently relies on field-oriented control, which is based on the dynamic model of the machine and applicable in both steady and transient states. This approach treats induction machines as separate excitation Direct Current (DC) machines, providing a natural decoupling effects. By converting variables to a rotating synchronous frame (d, q), all quantities

appear as DC values, achieving comparable results. The principle of rotor flux orientation maintains a constant magnitude by aligning the flux vector with the d-axis of the synchronous frame. Electromagnetic torque is controlled using the quadratic component of the stator current (i_{sq}), while the magnitude of the rotor flux is regulated by its direct component (i_{sd}) [89]. Depending on the required flux information and position, the control of rotor field orientation is classified as Direct Field Orientation Control (DFOC) or Indirect Field Orientation Control (IFOC)

In direct field-oriented control, the control of the rotor flux is achieved directly. This means that the rotor angle or control vector is obtained by directly utilizing the terminal voltages and currents through the use of flux estimators as shown in Figure 2.4. By employing these estimators, the system can accurately determine and control the rotor angle or vector based on the measured voltage and current values [90].

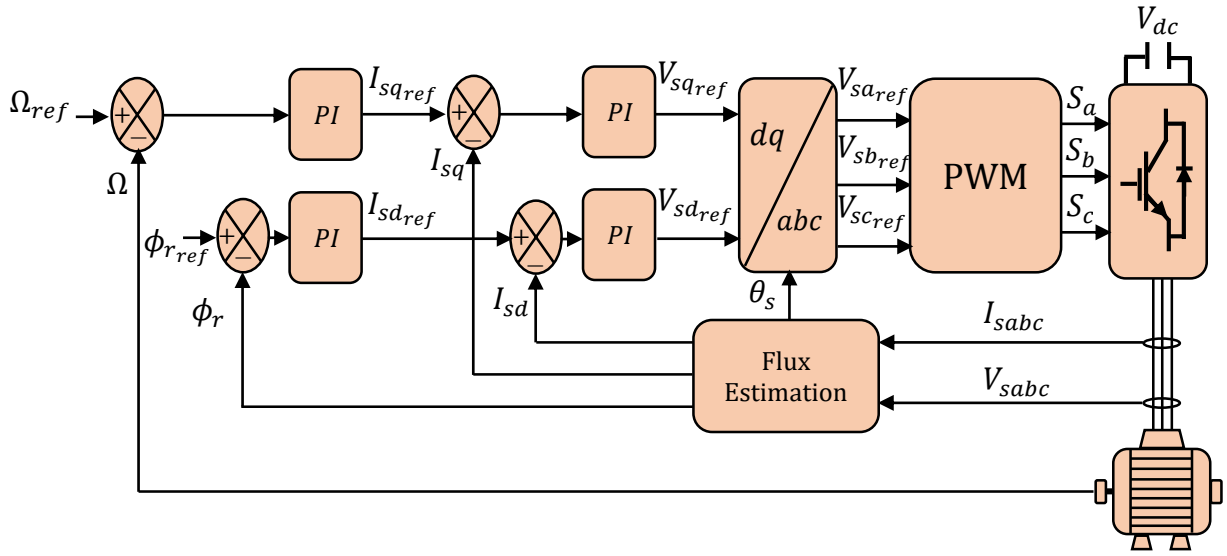

Figure 2.4. Direct field oriented control (DFOC) for variable frequency induction motor.

In indirect field-oriented control, the control of the rotor flux is achieved through an indirect method. Instead of directly manipulating the flux, the rotor angle is determined through the utilization of rotor position measurement and estimation of machine parameters as depicted in Figure 2.5. By accurately measuring the rotor position and estimating the relevant machine parameters, the control system can effectively regulate the rotor angle, thereby indirectly controlling the rotor flux [91].

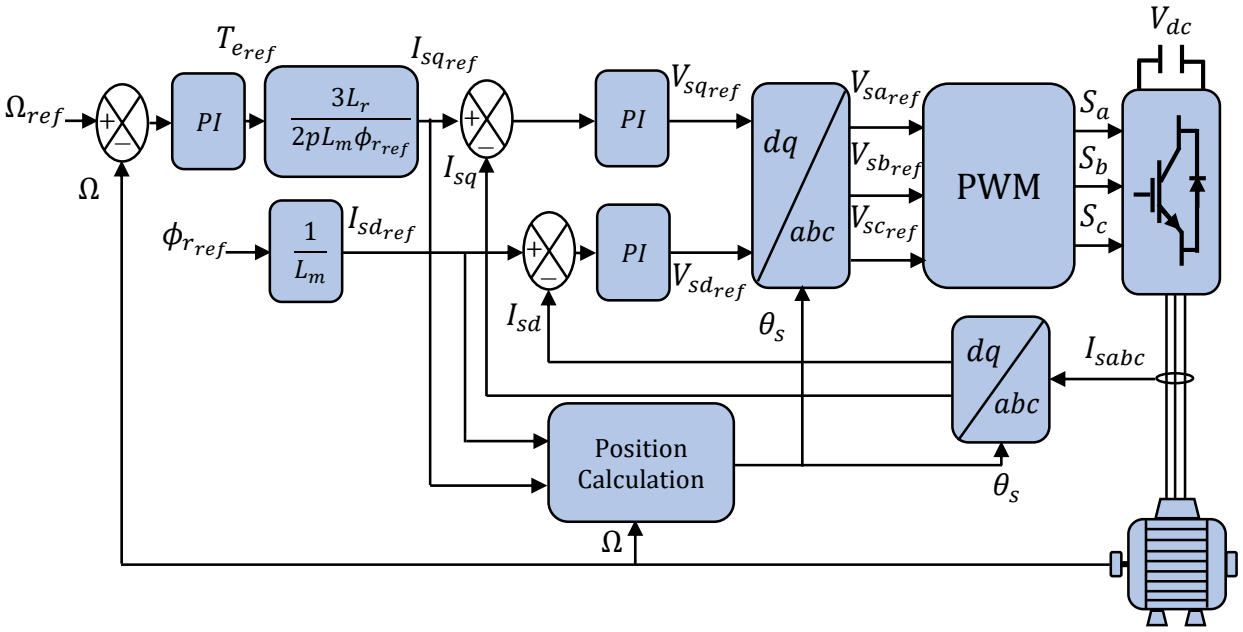

Figure 2.5. Indirect field oriented control (IFOC) for variable frequency induction motor.

2.4.2.3. Direct torque control

In the 1980s, Takahashi made a significant advance in the field of induction motor drives by introducing the concept of direct torque control. This control technique has empowered engineers to exercise meticulous control over the motor's voltage inverter by enabling precise selection of the voltage vector. The selection process is intelligently guided by continuously monitoring the instantaneous errors of both the stator flux and electromagnetic torque, facilitating optimal control and unlocking enhanced motor performance [89]. Over time, DTC has evolved into two main classifications: classical DTC and Space Vector Modulation (SVM) DTC, each offering distinct advantages and tailored solutions to cater to different application requirements.

The primary concept of direct torque control, initially known as classical DTC, was first introduced by Takahashi, setting the foundation for further advancements in this field. In this classical variant, hysteresis controllers take charge of precisely regulating the motor's torque and flux [92, 93]. These controllers provide crucial inputs for selecting the optimal voltage vector from a lookup switching table, which is aligned with the estimated position of the flux vector. To visualize Takahashi's proposed DTC structure, refer to Figure 2.6 [86], which showcases the switching table-based approach.

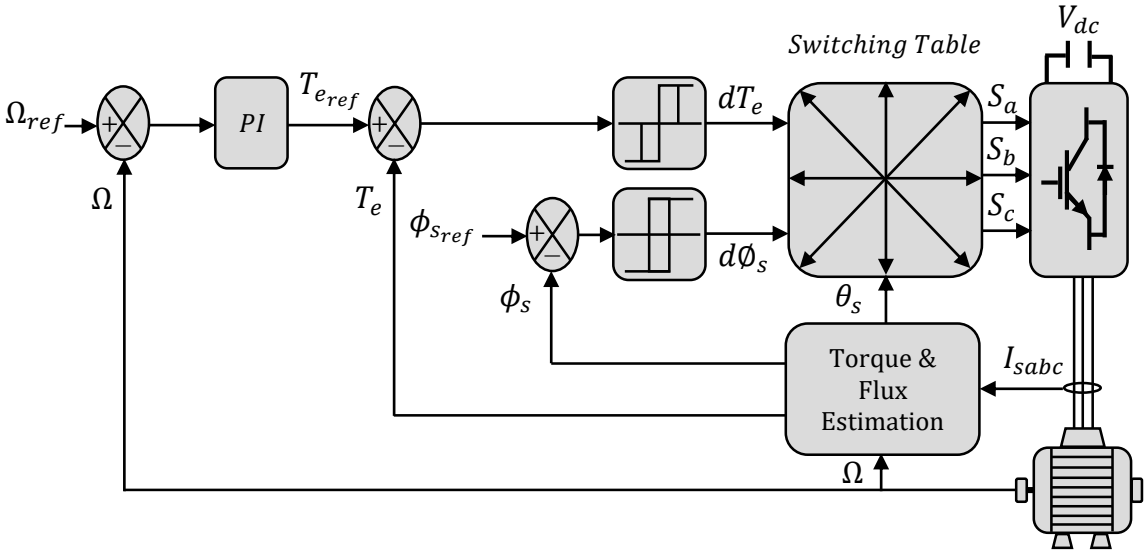

Figure 2.6. Classical direct torque control for variable frequency induction motor.

SVM-DTC, as an alternative to the lookup switching table and hysteresis comparators, utilizes the space vector modulation unit and PI controllers for voltage vector control in the motor. The goal is to minimize torque and flux ripple by generating voltage vectors aligned with predefined voltage vector planes [94, 95]. SVM-DTC offers enhanced efficiency and smoother operation in comparison to classical DTC. Figure 2.7 portrays a general diagram of the control algorithm for SVM-DTC.

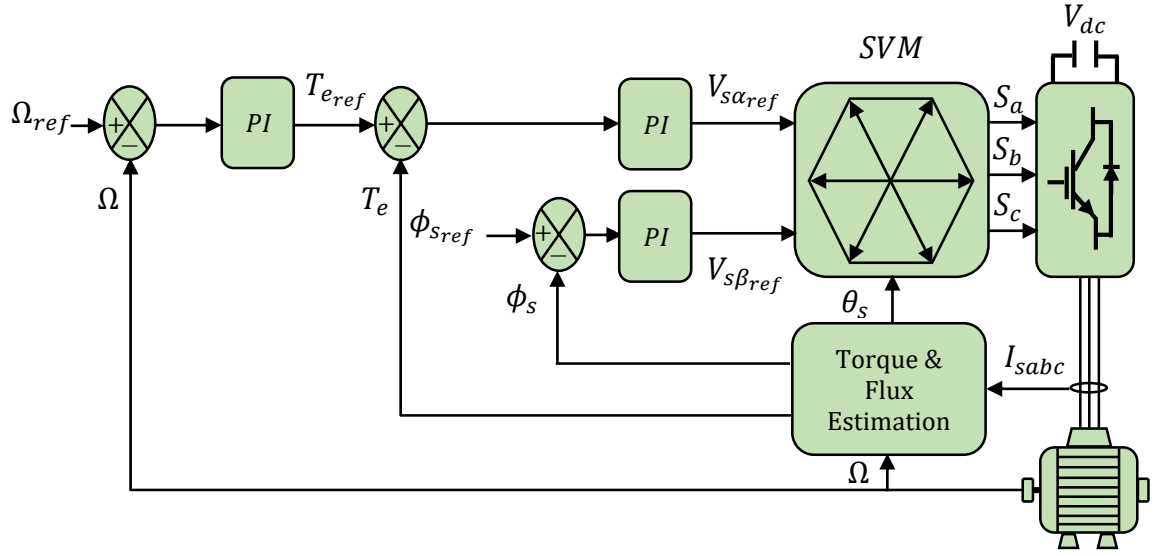

Figure 2.7. SVM direct torque control for variable frequency induction motor.

A summary of the advantages and disadvantages of the mentioned control technique is given in Table 2.2.

Table 2.2. Summary of induction motor control background.

Control strategy	Advantages	Disdvantages
Scalar control	-Simple and easy to implement. -Cost-effective.	-Limited dynamic response. -Less precise control.
Field oriented control	-High torque and speed control accuracy. -Improved control in transient conditions. -Reduced torque ripple.	-More complex implementation. -Sensitive to parameter variation. -Increased computational requirements.
Direct torque control	-High dynamic response. -Fast torque and flux control response. -Less sensitive to parameter variation. -Better efficiency at low speeds.	-More complex implementation. -Higher computational requirements. -Potential increase in audible noise.

2.4.3. Induction motor nonlinear control

Conventional methods, like utilizing proportional-integral-differential controller, may prove insufficient when trying to comprehend the intricacies of induction motor behavior. Discrepancies between the real system and the mathematical model established during the early stages of control design can be significant. As a result, there has been a growing focus on nonlinear control theory as a means to address this issue [96].

Intelligent algorithms have gained widespread use in the field of induction motor control due to their notable advantages, including fast response, high efficiency, and resilience to parameter variations. Among these algorithms, neural network and fuzzy logic control have emerged as leading contenders [97, 98]. However, despite their remarkable benefits, these two techniques have

certain limitations. Their complex structures and reliance on prior knowledge and expertise make them less suitable for applications that require a straightforward and user-friendly approach.

In the electric drive and power electronics fields, model predictive control has garnered attention as a promising technique. It enhances current quality, reduces torque ripples, and improves disturbance rejection by generating an optimal switching state within a sampling period to minimize the cost function [89, 99, 100]. Nevertheless, model predictive control also has its drawbacks. One of the main limitations is the high computational requirements needed for accurate prediction of system behavior. Additionally, accurate models of the system are crucial, which can pose challenges in applications affected by parameter variations.

In contrast to the complexity and knowledge-dependence of intelligent algorithms, researchers have explored robust nonlinear control techniques that offer exceptional performance while maintaining a simpler calculation process. Sliding mode control, super-twisting control, input-output feedback linearization, and back-stepping control [101-104] are among the most promising methods in this regard. These techniques provide an alternative approach to induction motor control, addressing the limitations of traditional methods. They are gaining significant attention due to their impressive performance in challenging environments.

2.5. Driving into the future: “The autonomous electric vehicle era”

As a result of the advancement in the autonomous electric vehicle field, the development of accurate, consistent, and resilient commands to combat sensor failures and environmental disruptions has been accomplished. Furthermore, this progress has led to a reduction in computational costs. Consequently, manufacturers are actively revealing their ambitious intentions to develop and launch their own fully autonomous vehicles in the imminent future. Within the array of announced systems, one particularly captivating innovation garners attention for its remarkable technological advancement and extensive media coverage. This groundbreaking creation is none other than the renowned Google Car, an autonomous vehicle meticulously crafted by the company bearing the same name [105]. The cutting-edge iteration of this revolutionary car can be observed in the visually striking Figure 2.8. This visionary solution represents a paradigm shift in automotive design, envisioning a vehicle that operates seamlessly and independently. Meticulously engineered with autonomy as the primary focus, this transformative vehicle breaks

Figure 2.8. Google car.

free from traditional automotive norms by boldly eliminating conventional elements like the cockpit, including the steering wheel and pedals. This audacious departure from convention reflects a visionary approach to redefining the future of transportation.

On the other side, Tesla, the pioneering automotive company, has captured widespread attention with its groundbreaking electric vehicles and their advanced autonomous capabilities [106]. Among the most remarkable and extensively discussed innovations is the Tesla Model S, showcased in the visually striking Figure 2.9.

Figure 2.9. Tesla car model S.

Tesla's approach to autonomous driving goes beyond incremental advancements, aiming for full self-driving capabilities. The model S embodies the transformative vision, purposefully designed from the ground up with autonomous driving as a central tenet. Tesla's cutting-edge technology, including its Autopilot system, enables the vehicle to navigate roads, change lanes, and park autonomously. This audacious pursuit of a fully autonomous future sets Tesla apart as the company pushes the boundaries of what is possible in the realm of automotive innovation. With their commitment to electric mobility and innovative autonomous features, Tesla continues to shape the trajectory of the automotive industry and redefine the way we envision transportation.

Apart from Tesla and Google car, traditional car manufacturers have ventured into the development of autonomous and electric vehicles. Here are some notable examples:

- **General Motors (GM):** GM introduced the Chevrolet Bolt EV, an all-electric compact car with an impressive range. The company has also been investing in autonomous vehicle technology through its subsidiary, Cruise, which has been testing self-driving cars in various cities.
- **Ford:** Ford has been actively involved in the development of electric vehicles, including the Mustang Mach-E, an all-electric SUV, and the Ford F-150 Lightning, an all-electric version of their popular pickup truck. They have also invested in autonomous vehicle technology and partnered with Argo AI for self-driving vehicle development.
- **Nissan:** Nissan has made significant strides in electric vehicle technology with its Nissan Leaf, one of the world's best-selling electric cars. They continue to innovate in the EV space and have recently introduced the Ariya, an all-electric crossover SUV.
- **BMW:** BMW has released several electric models, including the BMW i3 and BMW i8. The company has been actively exploring autonomous driving technologies and has partnered with other companies for research and development in this field.
- **Audi:** Audi has been developing electric vehicles such as the Audi e-tron, an all-electric SUV, and the Audi e-tron GT. They have also been investing in autonomous driving technology and have showcased autonomous vehicle prototypes.
- **Mercedes-Benz:** Mercedes-Benz has been expanding its electric vehicle offerings with models like the Mercedes-Benz EQC, an all-electric SUV. They have also been investing

in autonomous driving technology and have showcased concept vehicles with advanced autonomous features.

These companies, along with many others, are actively contributing to the advancement of electric and autonomous vehicle technology, aiming to provide sustainable and innovative solutions for future transportation needs.

2.6. Conclusion

In this chapter, we have conducted an extensive bibliographic study on the control of autonomous electric vehicles, providing a comprehensive analysis of both the autonomous vehicle system as a whole and the specific aspects related to the control of the traction part in electric vehicles. By delving into the existing literature, we have gained valuable insights into the various control methodologies, techniques, and advancements in this rapidly evolving field.

Researchers have made significant advancements in lateral control, developing advanced algorithms for accurate path tracking and navigation in complex traffic scenarios. However, challenges in real-time decision-making and handling uncertain environments remain active areas of research. Longitudinal control has also witnessed remarkable progress with technologies like adaptive cruise control and autonomous emergency braking, enabling vehicles to maintain safe distances and react swiftly to obstacles. Further research focuses on enhancing energy efficiency and coordination in mixed traffic scenarios. Speed planning, crucial for safe and efficient autonomous driving, utilizes predictive models, optimization algorithms, and real-time data to generate adaptable speed trajectories.

The selection of an appropriate electrical drive system is crucial for achieving optimal performance and efficiency in autonomous EVs. Induction motors have emerged as a popular choice due to their robustness, reliability, and cost-effectiveness. Various control techniques have been developed to ensure efficient and precise control of induction motors in autonomous EVs. These control techniques include scalar control, field oriented control, direct torque control, and other nonlinear techniques that have gained significant attention due to their ability to operate at varying speeds and torque levels, making them well-suited for the diverse requirements of autonomous vehicles

CHAPTER 3

SYSTEM ANALYTICAL MODELING

Contents **Page**

3.1. Introduction

An autonomous electric vehicle is a non-holonomic system for transporting people and goods. The interest in this type of vehicles has known considerable attention due to the different fields in which these vehicles are used. The development of such applications requires modeling that is sufficiently representative of the vehicle. Modeling a vehicle means, among other things, establishing the differential equations that characterize the evolution of its parameters and variables over time. To describe its behavior, different models are proposed with more or less important simplifications, made according to the need of the embedded application to be designed. The appropriate model depends on the objectives and the application you plan to achieve.

System modeling is a great tool to help understand the phenomena. The first reason for this is that, in order to develop new concepts into prototypes and ultimately into products, system modeling is really necessary. At the concept stage, low order models are required to understand the interactive dynamics of complex systems and, as development progresses in prototyping and manufacturing, more complex models of component size, fatigue determination may be necessary. Second, in order to achieve its objective, namely the simulation of a given phenomenon, the modeler is led to ask questions a little different from those posed by scientists in the field who usually study it. This helps to complete the paradigm used to address the phenomenon in question. Once modeled in the form of a mathematical model, it allows testing hypotheses. Faced with a phenomenon that is misunderstood, a hypothesis can be made about how this phenomenon works. A modeler can then translate this assumption into a model which can then be implemented. Using the resulting software, simulations can be performed. If they conform to certain aspects of the phenomenon, it can be concluded that the hypothesis formulated is not completely unrealistic.

In this chapter, we will first present the most commonly encountered autonomous vehicle models in the literature and used in autonomous driving along a trajectory. Then, a particular model will be selected in this work due to an acceptable compromise between representativeness and simplicity in order to design a lateral control law that makes the autonomous vehicle navigate through a predefined trajectory. After that, we will present a mathematical description of part of the traction system, including the voltage inverter and induction motor used to control the autonomous electric vehicle speed.

3.2. Representation of autonomous vehicle

The autonomous vehicle considered in this study is a vehicle with four drive wheels and one steering gear; only the front wheels are steerable. Their geometric parameters consist of the dimensions given by their wheelbase L_v and their width W_v, and it is assumed that the structure of each vehicle is symmetrical with respect to its sagittal plane. This symmetry assumption is a classic assumption in the context of mobile robotics [108]. This part starts by introducing the different representations used for autonomous vehicle modeling before presenting the modeling technique used for autonomous vehicle driving. The modeling of the vehicle depends mainly on "four-wheel" vehicle representation or bicycle representation.

3.2.1. Four-wheel vehicle representation

The four-wheel vehicle representation bases itself on considering all four wheels of the vehicle to construct a mathematical model that describes the vehicle's motion and behavior under different kinds of situations, as shown in Figure 3.1.

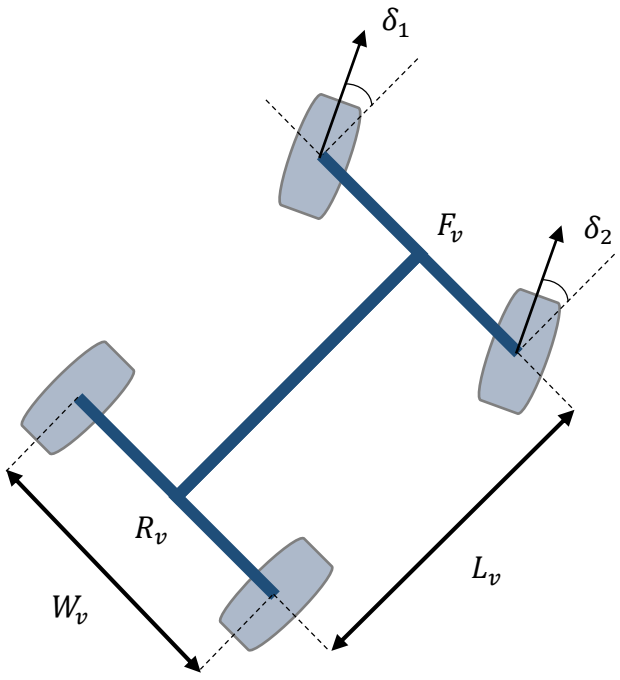

Figure 3.1. Four-wheel vehicle representation.

The notations used in Figure 3.1 and thereafter are as follows:

- L_v: The vehicle wheelbase.
- W_v: The vehicle width.
- F_v: The point at the center of the front axle of the vehicle.
- R_v: The point at the center of the rear axle of the vehicle.
- δ_1 and δ_2: The equivalent steering angles of the front wheels of the vehicle. They are related to actual steering angles.

This representation can be used to simulate the vehicle's dynamics and performance under different circumstances by using different approaches to create a mathematical model of a four-wheel vehicle, such as using differential equations, multibody dynamics, or simplified models based on empirical data. This can include modeling of the vehicle's suspension, steering, powertrain, friction, and aerodynamics.

In general, 4-wheel type representation is very useful when the vehicle is restricted in areas of nonlinear behavior to model the dynamic behavior of the vehicle, but it is rarely used in autonomous driving design due to its complexity.

3.2.2. Bicycle representation

The bicycle representation, which, as the name implies, reduces the four-wheel vehicle representation to only two wheels, similar to a bicycle. To realize this simplification, the vehicle's front wheels are simplified by a virtual wheel at the center of the front axle, and the rear wheels are simplified by a virtual wheel at the center of the rear axle, as shown in Figure 3.2, where the steering angle is consistent with the steering angle of the front wheel.

By using this representation, the number of parameters required to describe the evolution of the vehicle can be kept to a minimum. This simplifies the modeling and, therefore, the development of the control laws for vehicle control while preserving adequate modeling accuracy for the description of motion. This particular bicycle representation is by far the most popular nowadays in autonomous vehicle field. It accurately emulates the real behavior of the vehicle under normal driving circumstances [109].

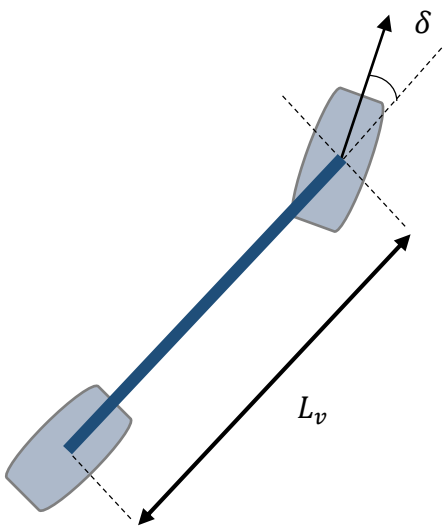

Figure 3.2. Bicycle representation.

In the remainder of this thesis, this simplified representation of the vehicle will be considered. The expressions of the set-points calculated subsequently for the control law of the vehicle will therefore be values of the speed and the steering angle of the virtual wheel of the bicycle.

3.3. Modeling of tire-ground interaction

If the entire vehicle can be considered a non-deformable solid, then the tires motion is evolving under the assumption of rolling without sliding. This assumption is highly sufficient to develop a vehicle model under the condition of operating in an urban environment with good contact on the ground [110,111]. The consideration of sliding in tire-ground contact, however, becomes crucial for studies on the placement of vehicles in natural environments. Since the tire is the only link between the vehicle and the ground, it is a matter of studying the efforts generated between the tire and the surface of the ground.

Having a correct model of the tires in the dynamics of a vehicle is essential since it will make it possible to establish a more efficient control architecture. It is therefore the purpose of this section to introduce the existing models describing the phenomena of friction between the tire and the ground in order to build a model allowing the efforts related to tire-ground contact to be extracted, the first step in the construction of a global model of the vehicle.

3.3.1. Tire-ground contact efforts

A tire is a viscoelastic toroid. It is the only interface between the vehicle and the ground. It mainly makes it possible to support the vertical load of the vehicle, to develop the longitudinal forces in the event of acceleration or braking, and to develop the lateral forces in a bend. Figure 3.3 illustrates the forces and moments generated in the contact zone between the tire and the ground.

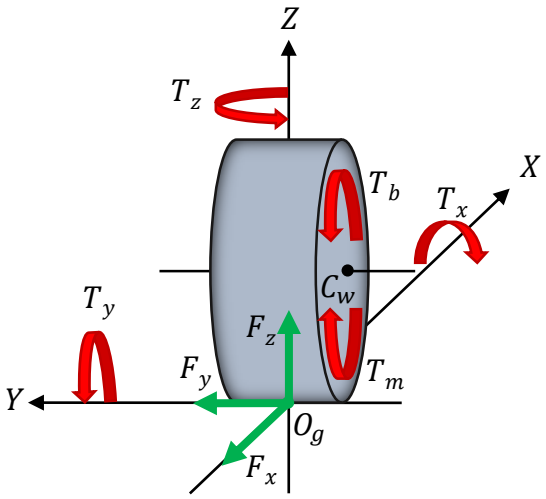

Figure 3.3. Representation of efforts at tire-ground contact.

The sum of the forces applied to the tire by the ground is assumed to be applied at the center of the contact patch and can be divided into three axes:

- F_x: The longitudinal force transmitted by the tire to the ground at the point O_g and defined linearly in the direction of the wheel. It is the main force allowing the vehicle to move forward.
- F_y: The lateral force transmitted by the tire to the ground at the point O_g and defined perpendicularly in the direction of the wheel. It is the main force allowing the vehicle to modify the direction of navigation.
- F_z: The vertical force applied by the tire to the ground at the point O_g. It is mainly due to the mass of the vehicle and varies according to the load transfers during a turn, and the adjustment of the suspension.

By the same way, the torques that the tire receives from the ground can also be divided into three axes:

- T_x: The reversal torque applied at the point O_g is present when the reaction of the ground on the tire pointing upward is not aligned with the vertical force pointing downward.
- T_y: The rolling resistance torque applied at the point O_g which tends to slow down the rotation of the wheel
- T_z: The auto-alignment torque applied at the point O_g which appears in agreement with the lateral force and tends to bring the wheel back to a zero steering angle.
- T_m: The motor torque applied at the point C_w which is transmitted to the wheel either by the motor of the vehicle or by friction from the bearings for the non-driven wheels.
- T_b: The braking resistive torque applied at the point C_w which tends to slow the rotation of the wheel by the effect of the braking unit.

From the perspective of vehicle yaw dynamics, the longitudinal F_x and lateral F_y forces are the most important components as they describe the vehicle's ability to accelerate and brake (longitudinal force) and to turn (lateral force). The result of the forces that the tire transmits in the contact ground could be described as follows:

$$F = \sqrt{{F_x}^2 + {F_y}^2} \tag{3.1}$$

Their value depends on the contact parameters, which are the vertical force, the nature of the ground, and the geometry of the tire. The separation of longitudinal and lateral forces allows for the separation and study of their effects on tire evolution.

3.3.2. Tire-ground contact models

The forces acting on the vehicle and the sliding that occurs in the area where the tires make contact with the ground are what cause this vehicle to move. The performance of the vehicle is significantly influenced by the tire-ground contact force model. Therefore, the choice of an adequate model is a crucial first step in modeling vehicle dynamics.

Modeling tire-ground contact amounts to determining the relationship linking the contact forces to the longitudinal sliding λ and the lateral sliding β. The values of these two parameters may depend on several factors:

- The properties of the tire: the geometry, the composition (stiffness, materials, etc.), and the condition of the tire (pressure, wear, etc.) have an impact on the sliding parameters.
- The type of ground (asphalt, earth, etc.) as well as its properties (dry, wet, etc.) can drastically changes the adhesion conditions.
- The properties of the vehicle: the geometry of the vehicle and the stiffness of the suspensions can influence the load transfer during the change of direction or acceleration.

The modeling of the tire-ground contact forces is quite complex. Many models have been developed [112], we can cite: Brown model [113], Dugoff model [114], Gim model [115,116], Kiencke and Nielsen model [117], Dahl model [118], LuGre Model [119], Pacejka model [120], linear model [121]. All tire evolution models can be categorized into three zone:

- Linear zone: in this zone, the force is proportional to the sliding, both in the longitudinal and lateral planes. This zone, defined by low slippage, corresponds to the elastic deformation of the tire.
- Transition zone: this zone appears when the sliding increases. In this zone, the relation between the slips and the forces transmitted is no longer linear; the slips increase more quickly than the forces, which end up saturating and reaching a maximum value.
- Saturation zone: this zone corresponds to a stall situation of the tire; when the slip value increases, the force transmitted is constant, or even decreases.

The sliding intervals $\beta \in [-5°, 5°]$ for the lateral dynamic and $\lambda \in [-0.1,0.1]$ for the longitudinal dynamic generally limit the linear zone. The forces in this zone can be linked to the sliding by the following relations that express the linear model:

$$\begin{cases} F_x = C_\lambda \cdot \lambda \\ F_y = C_\beta \cdot \beta \end{cases} \tag{3.2}$$

where C_λ and C_β denote the longitudinal and lateral stiffness respectively.

This simplified relationship is used in the automotive field where, when riding on asphalt, the adhesion is high and the riding conditions rarely leave this area.

3.4. Modeling of autonomous vehicle

Autonomous vehicle modeling involves creating mathematical models that simulate the behavior of autonomous vehicles. These models can be used to test and evaluate the performance of the vehicle's control systems, predict how the vehicle will respond in different driving scenarios, and optimize the vehicle's navigation and decision-making algorithms. The vehicle modeling can be represented with different levels of precision and complexity, and the choice depends on the objectives to be achieved [122,123].

3.4.1. Kinematic model

It is a typical approximation for autonomous vehicle motion, for a basic vehicle analysis, and for determining intuitive control laws to model the vehicle system with a kinematic bicycle model. A kinematic model of a vehicle is a mathematical representation of the motion of the vehicle, without taking into account the forces that cause the motion (such as friction or aerodynamics). It typically includes equations of motion for the position, velocity, and acceleration of the vehicle, as well as any constraints on the motion such as steering angle.

In an absolute coordinate system $(X-Y)$, the location of the vehicle is described by the position of the center point R_v of the rear wheel characterized by its abscissa x and its ordinate y, and by the orientation ψ of the vehicle axis with respect to the horizontal axis. These notations are represented in Figure 3.4, where v is the forward speed of the vehicle.

The kinematic model of a vehicle can be described using a set of nonlinear equations. These equations describe the relationship between the inputs (such as steering and desired speed) and the outputs (such as position, velocity, and acceleration) of the vehicle. For the front and rear wheels, the non-holonomic constraint equations are:

$$\begin{cases} \dot{x}_f \cdot sin(\psi+\delta) - \dot{y}_f \cdot cos(\psi+\delta) = 0 \\ \dot{x}_r \cdot sin(\psi) - \dot{y}_r \cdot cos(\psi) = 0 \end{cases} \tag{3.3}$$

where (x_f, y_f) and (x_r, y_r) are the global coordinates of the front and rear wheels, respectively.

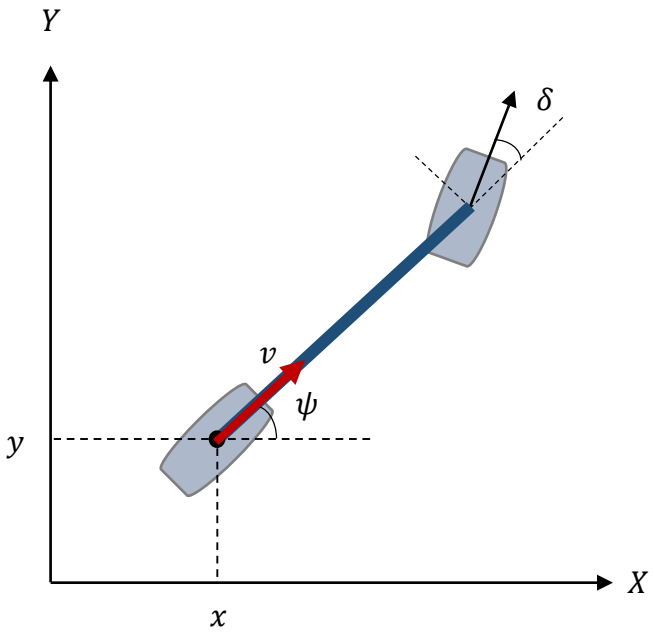

Figure 3.4. Kinematic model based on bicycle representation.

The non-holonomic constraint on the rear wheel in the Equations (3.3), is satisfied by:

$$\begin{cases} \dot{x}_r = cos(\psi) \\ \dot{y}_r = sin(\psi) \end{cases} \tag{3.4}$$

Additionally, any of their scalar multiples can satisfy it. This scalar is equivalent to the longitudinal velocity v:

$$\begin{cases} \dot{x}_r = v \cdot cos(\psi) \\ \dot{y}_r = v \cdot sin(\psi) \end{cases} \tag{3.5}$$

Given that the front wheel is separated by a distance L_v from the rear wheel along the vehicle's orientation, the expression for (x_f, y_f) can be written as follows:

$$\begin{cases} x_f = x_r + L_v \cdot \cos(\psi) \\ y_f = y_r + L_v \cdot \sin(\psi) \end{cases} \tag{3.6}$$

By using the Equations (3.5) and (3.6) in the expression of the front wheel in the equations (3.3), the front wheel equation gives a solution for $\dot{\psi}$ as:

$$\dot{\psi} = \frac{v}{L_v}\tan(\delta) \tag{3.7}$$

Finally, the kinematic model based on the bicycle representation, expressed with respect to the rear wheel, is described by the following system of equations [109]:

$$\begin{cases} \dot{x}_r = v \cdot \cos(\psi) \\ \dot{y}_r = v \cdot \sin(\psi) \\ \dot{\psi} = \frac{v}{L_v}\tan(\delta) \end{cases} \tag{3.8}$$

The three states of this system are (x_r, y_r, ψ) and the two commands are the steering angle δ and the speed v, such as (δ, v). This model is defined at any point in the state space, as long as:

$$\delta \neq \frac{\pi}{2}\ mod(\pi)$$

due to the domain of existence of the tangent function. In practice, the vehicle steering angles never reach $\frac{\pi}{2}\ rad$, they are limited to a maximum deflection depending on the physical structure of the vehicles.

This type of nonlinear model is simple and only requires knowledge of the wheelbase. However, it is only valid for slow variations in trajectory curvature due to low speed [124]. Despite this limitation, the kinematic model is the most commonly used model for generating trajectories and developing control laws for vehicle control [109]. It is sufficiently representative to be commonly used during numerous autonomous vehicle control applications operating in an urban or industrial environment. For example, the autonomous vehicle that won the 2005 DARPA Grand Challenge uses this model for the design of the lateral controller [125].

3.4.2. Dynamic model

A dynamic model of an autonomous vehicle is a more detailed mathematical representation of the vehicle's movement and behavior. It includes factors such as velocity, acceleration, and steering angle, as well as the vehicle's dynamics, such as tire forces and gravity. Dynamic models take into account the vehicle's interactions with the environment and the forces that act on it, which can affect its behavior. This model can be used to predict how the vehicle will behave in different

scenarios, such as when accelerating or turning, and to simulate the effects of different control inputs.

Using an adapted linear model, the wheels are considered deformable solids. It is therefore now possible to explain the overall movement of the vehicle by integrating the phenomena resulting from the wheel-ground interaction. The tire-ground contact model adopted makes it possible to characterize the forces transmitted to the contact in both longitudinal and lateral directions. The dynamic equations then describe the evolution of the vehicle according to these forces. The representation of dynamic model is illustrated in Figure 3.5.

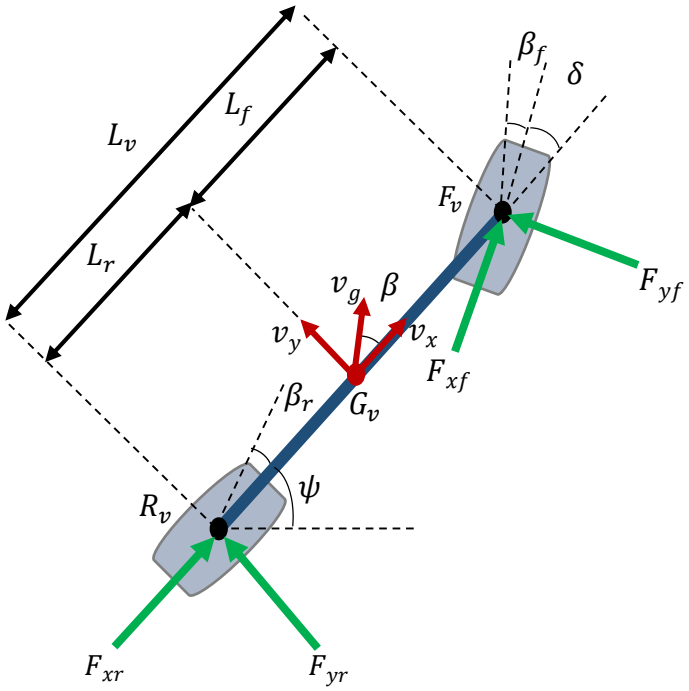

Figure 3.5. Dynamic model based on bicycle representation.

The notations used in this model are as follows:

- G_v: The vehicle center of gravity.
- L_f and L_r: The geometric distance $\overline{GF}$ and $\overline{GR}$, respectively.
- v_g: The vehicle velocity at the center of gravity.

- v_x and v_y: The longitudinal and lateral velocities at the center of gravity, respectively
- β: The overall sliding angle at the center of gravity
- β_f and β_r: The sliding angles of the front and rear wheels, respectively.
- F_{xf} and F_{yf}: The longitudinal and lateral forces applied on the front wheel, respectively.
- F_{xr} and F_{yr}: The longitudinal and lateral forces applied on the rear wheel, respectively.

The establishment of the dynamic model equations is based on two principles: the first concerns the balance of the external forces acting on the vehicle in both the longitudinal direction F_x and the lateral direction F_y, and the second concerns the balance of the dynamic moment M_z of the vehicle with respect to the external moments:

$$\begin{cases} \sum F_x = m \cdot a_x \\ \sum F_y = m \cdot a_y \\ \sum M_z = I_z \cdot \ddot{\psi} \end{cases} \tag{3.9}$$

with m and I_z are the vehicle mass and inertia at the center of gravity, respectively.

The total lateral and longitudinal accelerations, a_x and a_y, used in Equations (3.9) respectively, can be expressed as follows [126]:

$$\begin{cases} a_x = \dot{v_x} - \dot{\psi} \cdot v_y \\ a_y = \dot{v_y} + \dot{\psi} \cdot v_x \end{cases} \tag{3.10}$$

Therefore, the total applied forces in the longitudinal and lateral directions could be expressed as follows:

$$\begin{cases} m\left(\dot{v_g} \cdot \cos\beta - v_g \cdot \dot{\beta} \cdot \sin\beta - v_g \cdot \dot{\psi} \cdot \sin\beta\right) = F_{xf} \cdot \cos\delta - F_{yf} \cdot \sin\delta + F_{xr} \\ m\left(\dot{v_g} \cdot \sin\beta + v_g \cdot \dot{\beta} \cdot \cos\beta + v_g \cdot \dot{\psi} \cdot \cos\beta\right) = F_{xf} \cdot \sin\delta + F_{yf} \cdot \cos\delta + F_{yr} \end{cases} \tag{3.11}$$

Moreover, the equation of the moments around the vertical axis gives the expression of the rotational acceleration:

$$I_z \cdot \ddot{\psi} = L_f\left(F_{xf} \cdot \sin\delta + F_{yf} \cdot \cos\delta\right) - L_r \cdot F_{yr} \tag{3.12}$$

The expressions for the front and rear wheel sliding angles are provided by [109]:

$$\begin{cases} \beta_f = \tan^{-1}\left(\tan\beta + \frac{L_f \cdot \dot{\psi}}{v_g \cdot \cos\beta}\right) - \delta \\ \beta_r = \tan^{-1}\left(\tan\beta - \frac{L_r \cdot \dot{\psi}}{v_g \cdot \cos\beta}\right) \end{cases} \tag{3.13}$$

The evolutions of the linear velocity $\dot{v}_g$, rotational velocity $\ddot{\psi}$, and the drift angle $\dot{\beta}$ at the center of gravity are calculated using Equations (3.11) and (3.12). These relations, along with the front and rear wheel sliding angles define the dynamic evolution of the vehicle [127]:

$$\begin{cases} \dot{v}_g = \frac{1}{m}\left[F_{xf} \cdot \cos(\delta - \beta) - F_{yf} \cdot \sin(\delta - \beta) + F_{xr} \cdot \cos(\beta) + F_{yr} \cdot \sin(\beta)\right] \\ \ddot{\psi} = \frac{1}{I_z}\left[L_f\left(F_{xf} \cdot \sin\delta + F_{yf} \cdot \cos\delta\right) - L_r \cdot F_{yr}\right] \\ \dot{\beta} = \frac{1}{m \cdot v_g}\left[F_{xf} \cdot \sin(\delta - \beta) + F_{yf} \cdot \cos(\delta - \beta) - F_{xr} \cdot \sin(\beta) + F_{yr} \cdot \cos(\beta)\right] - \dot{\psi} \\ \beta_f = \tan^{-1}\left(\tan\beta + \frac{L_f \cdot \dot{\psi}}{v_g \cdot \cos\beta}\right) - \delta \\ \beta_r = \tan^{-1}\left(\tan\beta - \frac{L_r \cdot \dot{\psi}}{v_g \cdot \cos\beta}\right) \end{cases} \tag{3.14}$$

Dynamic model is more accurate than kinematic model, as it takes into account the forces acting on the vehicle, but it is also more complex and computationally intensive. However, it can provide a number of advantages for autonomous vehicles.

3.4.3. Extended kinematic model

The kinematic model for an autonomous vehicle presented previously is a mathematical model that describes the motion of the vehicle without considering the forces that cause the motion. It describes the position, velocity, and acceleration of the vehicle in terms of its components, such as wheels and steering. In the case where the vehicle must evolve in a natural environment, the hypothesis of rolling without sliding is no longer valid and the tires slip on the ground more or less intensely depending on various factors (longitudinal acceleration, lateral acceleration, load, coefficient ground friction etc.).

Another approach, namely extended kinematic model, consists of taking into account the effects of the contact forces, namely the sliding, and considering them as additional movements of

the vehicle [128]. The extended kinematic model for autonomous vehicle is a mathematical model that describes the motion and behavior of the vehicle in a more detailed and complex way than a basic kinematic model. It typically includes additional variables and equations that take into account factors such as tire forces and steering dynamics.

As illustrated in Figure 3.6 that show a representation of the extended kinematic model, the actual direction of the velocity vector differing from its theoretical direction but shifted by angles β_f or β_r which are called sliding angles. These angles are produced by the tire's deformation as well as its sliding motion on the ground, respectively. It is an important variable used to describe the lateral component of the interaction force at the tire's point of contact with the ground.

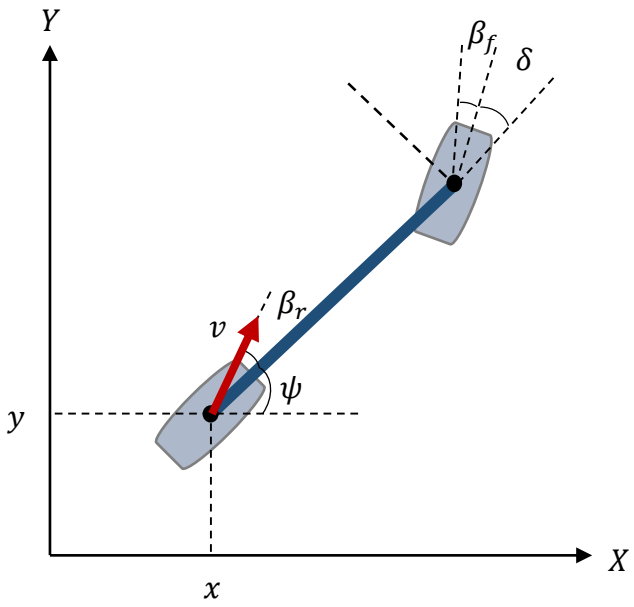

Figure 3.6. Extended kinematic model based on bicycle representation.

To take these drift angles into account, the kinematic model must therefore be based on the real direction of the speed vectors and not on the tires direction. This model, called the extended kinematic model is derived based on the kinematic model in absolute coordinates as [129]:

$$\begin{cases} \dot{x} = v \cdot \cos(\psi + \beta_r) \\ \dot{y} = v \cdot \sin(\psi + \beta_r) \\ \dot{\psi} = v \cdot \cos(\beta_r) \frac{\tan(\delta+\beta_f) - \tan(\beta_r)}{L_v} \end{cases} \tag{3.15}$$

The conditions of existence of this model are:

$$\begin{cases} \delta + \beta_f \neq \frac{\pi}{2}\ mod(\pi) \\ \beta_r \neq \frac{\pi}{2}\ mod(\pi) \end{cases}$$

due to the domain of existence of the tangent function. In real situations, the sliding angles values are small, while the limited value of steering angle allows us to ensure that this situation will never be approached during navigation.

Similarly, to the kinematic model, the three states of this system are (x, y, ψ) and the two commands are the steering angle δ and the speed v, such as (δ, v). However, two additional variables, β_f and β_r, reflecting the sliding are introduced. All the parameters of the model can thus be measured directly or easily deduced from the measurements, with the exception of the sliding angles, which impose additional difficulty. These angles depend on many parameters, such as the speed of the vehicle, the tires, the curvature of the trajectory, or the grip conditions. If these measurements are not possible, we can estimate the sliding angles using an observer [130].

3.5. Modeling of the traction part

In electric vehicles, the traction system is responsible for providing power to the wheels and allowing the vehicle to move. It consists of the electric motor, power electronics, transmission, and forces affecting the vehicle motion. The electric motor receives electricity from energy sources like batteries, super capacitors, and fuel cells and converts it into mechanical energy to propel the vehicle. Power electronics, such as the voltage inverter, control the flow of electricity from the energy sources to the motor. The transmission, also known as the gearbox, manages the transfer of power from the motor to the wheels. This combination of components makes up the electric drivetrain of an electric vehicle.

3.5.1. Voltage inverter model

An inverter in an electric circuit is a device that converts direct current into alternating current. A three-phase two-level inverter will be used in this research to convert a direct current voltage into a three-phase alternating current voltage with different amplitude and frequency. The circuit

of this type of inverter typically consists of three legs with two power switching devices in each leg; each switching device contains an Insulated Gate Bipolar Transistor (IGBT) and a diode mounted from head to tail. The six-pulse converter configuration is another name for this converter (Figure 3.7). In this circuit, the switches in one leg are alternately switched with a brief dead period to prevent both from conducting at the same time. Therefore, to operate both switches in a leg, one switching function is required [131].

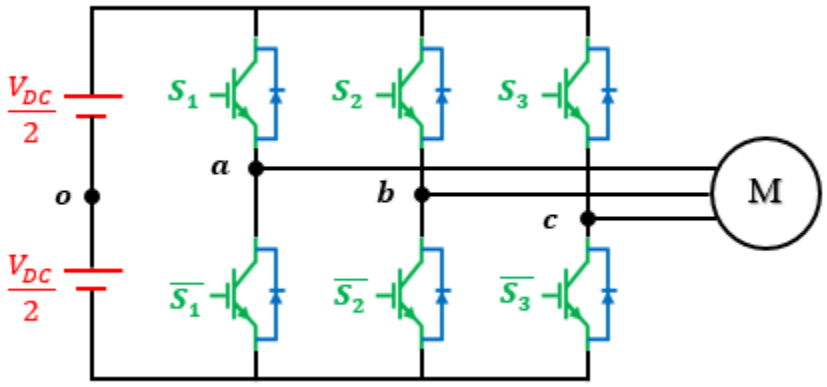

Figure 3.7. Two level voltage inverter.

For the phase-to-phase voltages V_{ab}, V_{bc}, and V_{ca}, we have:

$$\begin{cases} V_{ab} = V_{ao} + V_{ob} = V_{ao} - V_{bo} \\ V_{bc} = V_{bo} + V_{oc} = V_{bo} - V_{co} \\ V_{ca} = V_{co} + V_{oa} = V_{co} - V_{ao} \end{cases} \tag{3.16}$$

These voltages can be expressed in functions of the switches S_1, S_2, and S_3 as follows:

$$\begin{cases} V_{ab} = V_{DC}(S_1 - S_2) \\ V_{bc} = V_{DC}(S_2 - S_3) \\ V_{ca} = V_{DC}(S_3 - S_1) \end{cases} \tag{3.17}$$

Let n be the index of the neutral point on the alternating side. We have:

$$\begin{cases} V_{ao} = V_{an} + V_{no} \\ V_{bo} = V_{bn} + V_{no} \\ V_{co} = V_{cn} + V_{no} \end{cases} \tag{3.18}$$

Given that the neutral is isolated and the load is balanced, then:

$$V_{an} + V_{bn} + V_{cn} = 0 \tag{3.19}$$

By using the Equation (3.19) and the Equations (3.18), we get:

$$V_{no} = \frac{1}{3}(V_{ao} + V_{bo} + V_{co}) \tag{3.20}$$

By substituting the Equation (3.20) in the Equations (3.18), we get the simple voltages:

$$\begin{cases} V_{an} = \frac{1}{3}(2V_{ao} - V_{bo} - V_{co}) \\ V_{bn} = \frac{1}{3}(-V_{ao} + 2V_{bo} - V_{co}) \\ V_{cn} = \frac{1}{3}(-V_{ao} - V_{bo} + 2V_{co}) \end{cases} \tag{3.21}$$

As functions of the switches S_1, S_2, and S_3, these voltages can be expressed as follows:

$$\begin{cases} V_{an} = \frac{1}{3}V_{DC}(2S_1 - S_2 - S_3) \\ V_{bn} = \frac{1}{3}V_{DC}(-S_1 + 2S_2 - S_3) \\ V_{cn} = \frac{1}{3}V_{DC}(-S_1 - S_2 + 2S_3) \end{cases} \tag{3.22}$$

Depending on the states of the switches S_1, S_2, and S_3, there is eight possible vectors that can be obtained as illustrated in Figure 3.8 [132]:

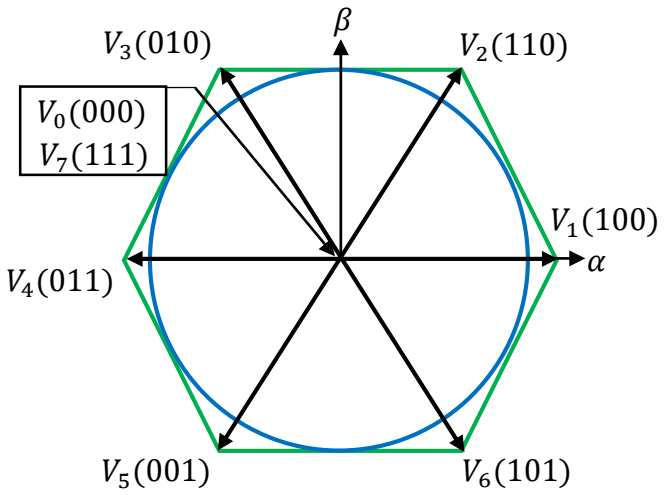

Figure 3.8. Vectors generated by two level voltage inverter in $\alpha - \beta$ frame.

The corresponding voltages of each of the eight states are summarized in Table 3.1[133]:

Table 3.1. Voltages generated by two level voltage inverter.

Vrs	Switches			Phase voltages			Phase to phase voltages		
$n°$	S_1	S_2	S_3	V_{an}	V_{bn}	V_{cn}	V_{ab}	V_{bc}	V_{ca}
0	0	0	0	0	0	0	0	0	0
1	0	0	1	$-\frac{1}{3}V_{DC}$	$-\frac{1}{3}V_{DC}$	$\frac{2}{3}V_{DC}$	0	$-V_{DC}$	V_{DC}
2	0	1	0	$-\frac{1}{3}V_{DC}$	$\frac{2}{3}V_{DC}$	$-\frac{1}{3}V_{DC}$	$-V_{DC}$	V_{DC}	0
3	0	1	1	$-\frac{2}{3}V_{DC}$	$\frac{1}{3}V_{DC}$	$\frac{1}{3}V_{DC}$	$-V_{DC}$	0	V_{DC}
4	1	0	0	$\frac{2}{3}V_{DC}$	$-\frac{1}{3}V_{DC}$	$-\frac{1}{3}V_{DC}$	V_{DC}	0	$-V_{DC}$
5	1	0	1	$\frac{1}{3}V_{DC}$	$-\frac{2}{3}V_{DC}$	$\frac{1}{3}V_{DC}$	V_{DC}	$-V_{DC}$	0
6	1	1	0	$\frac{1}{3}V_{DC}$	$\frac{1}{3}V_{DC}$	$-\frac{2}{3}V_{DC}$	0	V_{DC}	$-V_{DC}$
7	1	1	1	0	0	0	0	0	0

3.5.2. Induction motor model

Three-phase induction machines have been considered one of the most widely used electrical machines in industrial applications due to their inexpensive, simple, and robust construction. Its use in high-performance variable-speed drive systems requires the imposition of specific and complex control structures based on the mathematical model of the machine [134]. Several hypotheses are typically used in the modeling of the IM. We assume that if the winding is supplied with sinusoidal currents, they will be dispersed to produce a magnetomotive sinusoidal force. Additionally, we presumptively operate in an unsaturated regime. A uniform thickness is also expected for the motor air gap. Eddy currents and the hysteresis phenomenon are neglected [135].

The IM shown in Figure 3.9 is composed of a stationary stator circuit with three identical phases offset by 120 degrees and a mobile rotor circuit with three identical phases in staggered short circuits separated by 120 degrees. The angle θ marks the position of the rotor phase in relation to that of the stator phase and ω is the electrical speed of the induction motor [136].

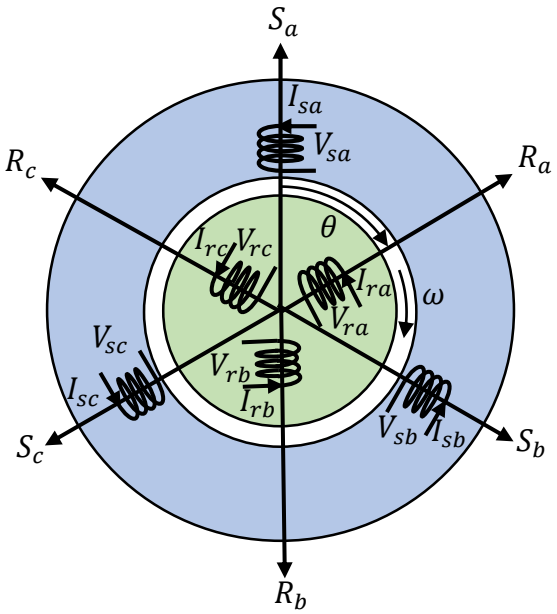

Figure 3.9. Representation of a three-phase induction motor.

According to Faraday law, we can write:

$$V = R \cdot I + \frac{d\phi}{dt} \tag{3.23}$$

By applying this law on each motor winding, we get the electrical equations of the IM:

$$\begin{cases} [V_s] = [R_{ss}][I_s] + \frac{d}{dt}[\phi_s] \\ [V_r] = 0 = [R_{rr}][I_r] + \frac{d}{dt}[\phi_r] \end{cases} \tag{3.24}$$

where:

- $[V_s] = [V_{sa} \quad V_{sb} \quad V_{sc}]^T$: Instantaneous voltages a, b, and c of the stator phases.
- $[I_s] = [I_{sa} \quad I_{sb} \quad I_{sc}]^T$: Instantaneous currents a, b, and c of the stator phases.
- $[\phi_s] = [\phi_{sa} \quad \phi_{sb} \quad \phi_{sc}]^T$: Instantaneous flux a, b, and c of the stator phases.
- $[V_r] = [V_{ra} \quad V_{rb} \quad V_{rc}]^T$: Instantaneous voltages a, b, and c of the rotor phases.
- $[I_r] = [I_{ra} \quad I_{rb} \quad I_{rc}]^T$: Instantaneous currents a, b, and c of the rotor phases.
- $[\phi_r] = [\phi_{ra} \quad \phi_{rb} \quad \phi_{rc}]^T$: Instantaneous flux a, b, and c of the rotor phases.

- $[R_{ss}] = \begin{bmatrix} R_s & 0 & 0 \\ 0 & R_s & 0 \\ 0 & 0 & R_s \end{bmatrix}$: Resistances a, b, and c of the stator phases.
- $[R_{rr}] = \begin{bmatrix} R_r & 0 & 0 \\ 0 & R_r & 0 \\ 0 & 0 & R_r \end{bmatrix}$: Resistances a, b, and c of the rotor phases.

Under the hypothesis of operation without magnetic saturation, the IM magnetic equations could be written as follows:

$$\begin{cases} [\phi_s] = [L_{ss}][I_s] + [M_{sr}][I_r] \\ [\phi_r] = [M_{rs}][I_s] + [L_{rr}][I_r] \end{cases} \tag{3.25}$$

with:

$$[L_{ss}] = \begin{bmatrix} l_s & m_s & m_s \\ m_s & l_s & m_s \\ m_s & m_s & l_s \end{bmatrix}; \qquad [L_{rr}] = \begin{bmatrix} l_r & m_r & m_r \\ m_r & l_r & m_r \\ m_r & m_r & l_r \end{bmatrix};$$

$$[M_{sr}] = [M_{rs}]^T = m_{sr} \begin{bmatrix} \cos\theta & \cos(\theta + \frac{2\pi}{3}) & \cos(\theta - \frac{2\pi}{3}) \\ \cos(\theta - \frac{2\pi}{3}) & \cos\theta & \cos(\theta + \frac{2\pi}{3}) \\ \cos(\theta + \frac{2\pi}{3}) & \cos(\theta - \frac{2\pi}{3}) & \cos\theta \end{bmatrix}$$

where:

- l_s and l_r: Inductances of a stator phase and a rotor phase, respectively.
- m_s and m_r: Mutual inductances between two stator phases and between two rotor phases, respectively.
- m_{sr}: Maximum value of mutual inductance between stator phase and rotor phase.

The two-phase model of the IM is carried out by a transformation of the three-phase reference $(a - b - c)$ into a two-phase reference, which leads to the reduction order of the machine equations. The most common transformation into a two-phase model is known as the Park transformation, where the new reference $(d - q)$ could be positioned either in the stator, the rotor, or in a rotating field. The principle of these transformations is illustrated in Figure 3.10 [96].

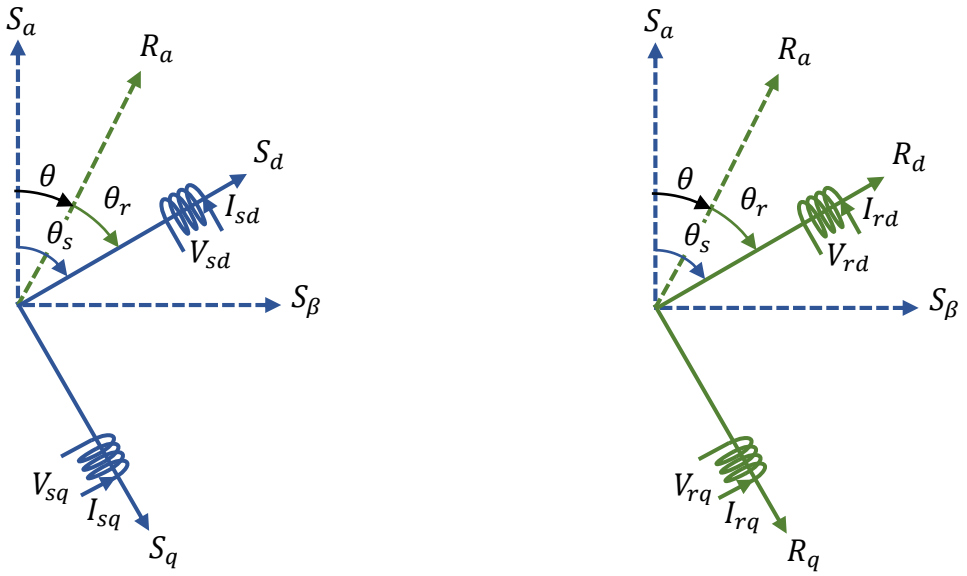

Figure 3.10. Representation of a two-phase induction motor.

Based on Figure 3.10 The transformation matrix from $(a-b-c)$ reference to $(d-q)$ reference is defined as:

$$T = k\begin{bmatrix} \cos\theta_s & \cos\left(\theta_s - \frac{2\pi}{3}\right) & \cos\left(\theta_s - \frac{4\pi}{3}\right) \\ -\sin\theta_s & -\sin\left(\theta_s - \frac{2\pi}{3}\right) & -\sin\left(\theta_s - \frac{4\pi}{3}\right) \end{bmatrix} \tag{3.26}$$

where k is a constant that which plays a crucial role in characterizing the transformation. When power conservation is not a concern, k can be assigned a value of $\frac{2}{3}$. On the other hand, in scenarios where power conservation is paramount, k assumes the value of $\sqrt{\frac{2}{3}}$, facilitating a transformation that upholds power conservation principles.

Then, the inverse of the transformation matrix is:

$$T^{-1} = k\begin{bmatrix} \cos\theta_s & -\sin\theta_s \\ \cos\left(\theta_s - \frac{2\pi}{3}\right) & -\sin\left(\theta_s - \frac{2\pi}{3}\right) \\ \cos\left(\theta_s - \frac{4\pi}{3}\right) & -\sin\left(\theta_s - \frac{4\pi}{3}\right) \end{bmatrix} \tag{3.27}$$

Based on the transformation matrix T, the electrical equations of the IM in $(d-q)$ frame are deduced as follows:

$$\begin{cases} V_{sd} = R_s \cdot I_{sd} + \frac{d\phi_{sd}}{dt} - \frac{d\theta_s}{dt}\phi_{sq} \\ V_{sq} = R_s \cdot I_{sq} + \frac{d\phi_{sq}}{dt} + \frac{d\theta_s}{dt}\phi_{sd} \\ V_{rd} = 0 = R_r \cdot I_{rd} + \frac{d\phi_{rd}}{dt} - \frac{d\theta_r}{dt}\phi_{rq} \\ V_{rq} = 0 = R_r \cdot I_{rq} + \frac{d\phi_{rq}}{dt} + \frac{d\theta_r}{dt}\phi_{rd} \end{cases} \quad (3.28)$$

with:

$$\theta = \theta_s - \theta_r \quad (3.29)$$

where:

- V_{sd} and V_{sq}: Instantaneous voltages d and q of the stator phases in $(d-q)$frame.
- V_{rd} and V_{rq}: Instantaneous voltages d and q of the rotor phases in $(d-q)$frame.
- I_{sd} and I_{sq}: Instantaneous currents d and q of the stator phases in $(d-q)$frame.
- I_{rd} and I_{rq}: Instantaneous currents d and q of the rotor phases in $(d-q)$frame.
- ϕ_{sd} and ϕ_{sq}: Instantaneous flux d and q of the stator phases in $(d-q)$frame.
- ϕ_{rd} and ϕ_{rq}: Instantaneous flux d and q of the rotor phases in $(d-q)$frame.
- θ_s and θ_r: The angles between the stator phase a and the direct axis d and between the rotor phase a and the direct axis d, respectively.

In a reference frame linked to the rotating field, where $\frac{d\theta_r}{dt}=\omega_{sl}$ is the sliding pulse and $\frac{d\theta_s}{dt}=\omega_s$, the electrical equations become:

$$\begin{cases} V_{sd} = R_s \cdot I_{sd} + \frac{d\phi_{sd}}{dt} - \omega_s \cdot \phi_{sq} \\ V_{sq} = R_s \cdot I_{sq} + \frac{d\phi_{sq}}{dt} + \omega_s \cdot \phi_{sd} \\ V_{rd} = 0 = R_r \cdot I_{rd} + \frac{d\phi_{rd}}{dt} - \omega_{sl} \cdot \phi_{rq} \\ V_{rq} = 0 = R_r \cdot I_{rq} + \frac{d\phi_{rq}}{dt} + \omega_{sl} \cdot \phi_{rd} \end{cases} \quad (3.30)$$

In a reference frame linked to the rotor, θ_r=0, then $\theta_s = \theta$, and $\frac{d\theta_s}{dt} = \frac{d\theta}{dt} = \omega$, the electrical equations become:

$$\begin{cases} V_{sd} = R_s \cdot I_{sd} + \frac{d\phi_{sd}}{dt} - \omega \cdot \phi_{sq} \\ V_{sq} = R_s \cdot I_{sq} + \frac{d\phi_{sq}}{dt} + \omega \cdot \phi_{sd} \\ V_{rd} = 0 = R_r \cdot I_{rd} + \frac{d\phi_{rd}}{dt} \\ V_{rq} = 0 = R_r \cdot I_{rq} + \frac{d\phi_{rq}}{dt} \end{cases} \quad (3.31)$$

In a reference frame linked to the stator, θ_s=0, then $\theta_r = -\theta$, and $\frac{d\theta_r}{dt} = -\frac{d\theta}{dt} = -\omega$, the electrical equations are deduced in $(\alpha - \beta)$ frame as follows:

$$\begin{cases} V_{s\alpha} = R_s \cdot I_{s\alpha} + \frac{d\phi_{s\alpha}}{dt} \\ V_{s\beta} = R_s \cdot I_{s\beta} + \frac{d\phi_{s\beta}}{dt} \\ V_{r\alpha} = 0 = R_r \cdot I_{r\alpha} + \frac{d\phi_{r\alpha}}{dt} - \omega \cdot \phi_{r\beta} \\ V_{r\beta} = 0 = R_r \cdot I_{r\beta} + \frac{d\phi_{r\beta}}{dt} + \omega \cdot \phi_{r\alpha} \end{cases} \quad (3.32)$$

By applying the transformation to $(d - q)$ frame, the magnetic equations become:

$$\begin{cases} \phi_{sd} = L_s \cdot I_{sd} + L_m \cdot I_{rd} \\ \phi_{sq} = L_s \cdot I_{sq} + L_m \cdot I_{rq} \\ \phi_{rd} = L_r \cdot I_{rd} + L_m \cdot I_{sd} \\ \phi_{rq} = L_r \cdot I_{rq} + L_m \cdot I_{sq} \end{cases} \quad (3.33)$$

with:

$$\begin{cases} L_s = l_s - m_s \\ L_r = l_r - m_r \\ L_m = \frac{3}{2} m_{sr} \end{cases} \quad (3.34)$$

The fundamental relation of the dynamics makes it possible to write the mechanical equation of the IM as follows:

$$J.\frac{d\Omega}{dt} = T_e - T_L - f \cdot \Omega \quad (3.35)$$

where:

- T_e: Electromagnetic torque.
- T_L: Load torque.
- Ω: Motor mechanical speed.
- J: Motor inertia.
- f: Viscous damping coefficient.

3.6. Conclusion

In conclusion, autonomous vehicle modeling is a crucial aspect of the development of self-driving cars. It involves creating mathematical models that simulate the behavior of autonomous vehicles and their interactions with the environment. These models help engineers and researchers to test and validate the safety and efficiency of autonomous driving systems before they are deployed on public roads.

In this chapter, we first have introduced the main representations of an autonomous vehicle. From these representations, it appears that the bicycle representation seems to achieve a good compromise in terms of representativeness and simplicity for the description of the lateral and longitudinal evolution of the vehicle in normal driving situations. Then a wide description on the forces created at the level of tire-ground contact as well as the moments created at this level have been presented. These efforts present the only interface between vehicle and ground that causes the movement of the vehicle. After that, a detailed presentation on the existing vehicle modeling tools was presented. Some modeling techniques are based only on the position, velocity, and acceleration of the vehicle, while some other modeling techniques make use of the applied forces to describe the dynamics of the vehicle. Finally, we have been given a detailed mathematical description of the voltage inverter and the induction motor that represent a part of the traction system of the autonomous vehicle in order to use them later to control vehicle speed.

Despite its challenges, autonomous vehicle modeling will continue to play a vital role in the advancement of autonomous driving technology and the eventual realization of safe and efficient self-driving cars.

CHAPTER 4

VEHICLE LATERAL CONTROL

Contents **Page**

4.1. Introduction

In the field of autonomous vehicle, lateral control is a crucial component of ensuring precise and accurate movement along a predetermined path. At its core, lateral control involves the control of the lateral deviation of a vehicle from a reference trajectory, with the goal of minimizing this deviation and ensuring that the vehicle follows the desired path. This is accomplished through the use of advanced control algorithms that are capable of adjusting the value of the front steering angle to achieve the desired deviation. By effectively controlling the lateral deviation of the vehicle, we can ensure that it moves along the intended trajectory with high precision and accuracy.

The development and refinement of lateral control algorithms for autonomous vehicles are at the forefront of research and technological advancements, driven by the relentless pursuit of enhanced safety, comfort, and efficiency on the roads. Accurate and robust lateral control plays a pivotal role in maintaining lane discipline, mitigating the risk of collisions, and facilitating seamless cooperation among vehicles in complex traffic scenarios. Through the utilization of advanced control techniques and the fusion of data from diverse sensors, autonomous vehicles are now able to achieve unprecedented levels of precision and reliability in their lateral control capabilities. This remarkable progress brings us closer to a future where self-driving cars seamlessly coexist with conventional vehicles, revolutionizing transportation as we know it and shaping a new era of intelligent mobility.

In this chapter, a lateral control law based on super-twisting algorithm is designed to control the lateral motion of autonomous vehicle through predefined trajectories. We will begin by outlining the fundamental principles of SMC. This will involve discussing the sliding surface choice and the design of the control law used in SMC. Following the introduction of the general principles of SMC, we will then present the super-twisting algorithm, a well-established algorithm that has been widely adopted in the field of control engineering. This algorithm provides a highly efficient approach to deal with the challenges associated with nonlinear systems and uncertainties. Finally, we will apply the super-twisting algorithm to lateral control, a critical aspect of autonomous vehicle navigation. We will discuss how the algorithm can be effectively used to guide the vehicle towards a desired trajectory, while taking into account various environmental factors such as road curvature and vehicle velocity.

4.2. Preliminaries on sliding mode control

SMC is a powerful control technique that has gained significant attention in through the years due to its ability to handle nonlinear, uncertain and time-varying systems with high accuracy and robustness. In order to avoid any confusion, we will first establish some basic definitions and concepts related to SMC.

- **Switching surface:** is a specific hypersurface in the state space of the system. It is designed to guide the system's state trajectories to a desired equilibrium point or trajectory, despite disturbances and uncertainties in the system. The switching surface is characterized by the property that the system dynamics change when the state trajectory crosses the surface. Specifically, when the state of the system lies on the switching surface, the control input is switched to a different value, causing the system to "slide" along the surface towards the desired equilibrium point or trajectory.
- **Sliding mode:** involves defining a switching surface S that includes the origin $x = 0$ and ensuring that the system trajectory $x(t)$ lies on or "slides" along this surface. More precisely, for any initial state x_0 on S, the system is designed to evolve such that $x(t)$ remains on S for all $t > t_0$. This behavior is guaranteed by ensuring that the tangent or velocity vectors of the state trajectory always point towards the switching surface in the vicinity of S.
- **Sliding surface:** it is a specific type of switching surface, denoted by $S = \{x | s(x) = 0\}$, that exhibits sliding mode behavior. This behavior occurs when trajectories in the system reach the surface from both sides, and then remain on the surface indefinitely. In other words, once the system enters the sliding mode, it "slides" along the surface without leaving it. This sliding behavior is characterized by high-frequency switching between different modes of motion, which enables the system to achieve fast and accurate tracking of desired trajectories.
- **Reaching condition:** is a sufficient condition that must be met for the existence of a sliding mode. It states that the system's state trajectory must be stable towards the sliding surface, which is defined as the set of points where the function $s(x) = 0$. This stability must be

ensured in a region around the sliding surface. The reaching condition is critical for achieving robust and accurate control with sliding mode, and failure to meet this condition may result in suboptimal performance.

- **Region of attraction:** refers to the biggest area surrounding the sliding surface S where the reaching condition is met. This area is considered to be the domain within which the system's state trajectory is guaranteed to converge towards the sliding surface and eventually slide along it towards the desired equilibrium point or trajectory.

The use of First Order Sliding Control (FOSC) for lateral control in various studies has shown promising results. In [137-139], the application of SMC has enabled the achievement of constant and minimal lateral errors, even at higher speeds. Moreover, the experimental results obtained with this control technique have been comparable to, and in some cases, superior to those obtained with self-adjusting gain linear controllers, as reported in [138]. SMC is also highly effective in compensating for model parametric uncertainties and rejecting disturbances that are commonly encountered in automotive applications. Another advantage of this methodology is that it produces control laws that are of low complexity, compared to other robust control approaches, as highlighted by Ferrara and Vecchio [140]. Overall, the application of SMC has shown great potential in lateral control, providing a robust and efficient control strategy with relatively low complexity.

One of the primary challenges associated with sliding mode control is the issue of "chattering", which can negatively impact the system's performance. However, this issue can be mitigated by utilizing Higher Order Sliding Control techniques (HOSC). In recognition of this, Imine and Madani [141] employed the super-twisting control to provide active steering assistance for heavy vehicles at low speeds. This approach offers an effective solution to the chattering problem, enabling the system to maintain a high degree of stability and accuracy in its steering control. The super-twisting algorithm is particularly well-suited to heavy vehicles, where precise and responsive steering is crucial for safety and maneuverability. By utilizing this advanced control technique, Imine and Madani were able to achieve exceptional results in their research, demonstrating the efficacy of higher-order sliding mode control for challenging automotive applications.

4.3. First order sliding mode control

The development of a robust control law involves a three-stage process that begins with the identification of a sliding surface aligned with the desired control objectives. Then, a sliding mode reaching law must be identified. Next, a discontinuous control law is derived, which effectively constrains the state trajectories of the system to converge onto and remain within this surface, even in the face of various uncertainties, parametric variations, and external disturbances (Figure 4.1). This approach enables the control system to achieve stability and enhanced performance by effectively regulating the system's behavior through precise and efficient manipulation of control inputs. By combining these three stages, the control law synthesis achieves a high degree of precision and reliability, making it an indispensable tool for controlling complex systems.

Consider a general system:

$$\dot{x} = A(x) + B(x) \cdot u \tag{4.1}$$

with a sliding surface:

$$S = \{x | s(x) = 0\} \tag{4.2}$$

where $A(x)$, $B(x)$ are general nonlinear functions of x, and $x \in R^n$, $u \in R^m$.

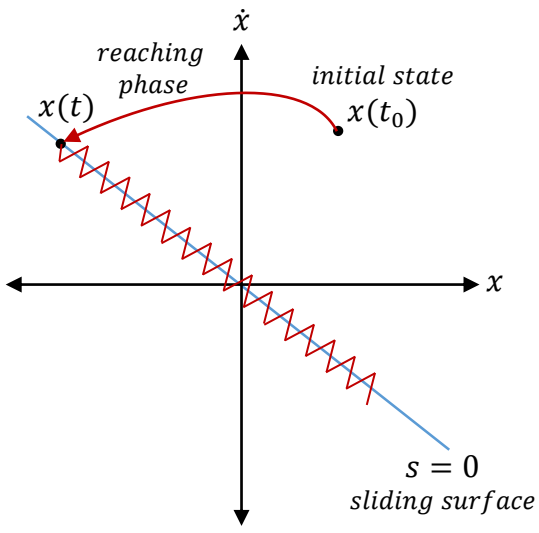

Figure 4.1. Sliding system convergence.

4.3.1. Sliding surface design

This passage discusses sliding surfaces, which can be categorized as either linear or nonlinear. While the design theory for linear switching surfaces in linear dynamics systems has been extensively explored and comprehensively understood, developing sliding surfaces for more complex nonlinear systems still poses a major challenge. One approach to defining the sliding surface of a single input system is by considering the desired control bandwidth [142,143], which can be achieved as follows:

$$s(x) = \left(\frac{\partial}{\partial t} + \lambda_s\right)^{n-1} e(x) \tag{4.3}$$

where x represents the variable that is used for control, e is the difference between the desired and actual values, λ_s is a constant that is always greater than zero, and it is used to determine the range of the closed-loop system, and n is the relative degree of the system.

It is apparent that s is solely reliant on the tracking error e, as demonstrated by the following illustration when n is equal to 2:

$$s = \dot{e} + \lambda_s \cdot e \tag{4.4}$$

which represents a calculation involving a weighted sum of the position and velocity errors. On the other hand, when n is set to 3, the sliding surface will be different:

$$s = \ddot{e} + 2 \cdot \lambda_s \cdot \dot{e} + {\lambda_s}^2 \cdot e \tag{4.5}$$

In general, the sliding surface is chosen as a hypersurface passing through the origin of the state space, and is in most cases linear with respect to the state variables. A necessary condition for the establishment of a sliding regime is that the sliding variable has a relative degree equal to 1 with respect to the control input.

4.3.2. Reaching law:

The conditions of existence and convergence of the control law are the criteria that ensure that the system trajectories converge to the sliding surface and remain there for all time, regardless of the magnitude of the external disturbances or uncertainties, also called conditions of attractiveness.

There are two types of conditions for accessing the sliding surface and ensuring the mode of convergence.

4.3.2.1. The direct switching function approach

This approach of convergence is the oldest. It is a question of giving the surface convergent dynamics towards zero. It is given by:

$$s \cdot \dot{s} < 0 \tag{4.6}$$

and a similar condition was also proposed in [144] as:

$$\lim_{s \to 0^+} \dot{s} < 0 \; and \; \lim_{s \to 0^-} \dot{s} > 0 \tag{4.7}$$

The variable structure control is produced by these laws, which generate sliding surfaces at both the individual switching level and their intersection. Although the reaching achieved is global, it does not ensure that reaching time will be finite.

4.3.2.2. The Lyapunov function approach

This approach involves choosing a candidate Lyapunov function (positive definite $V > 0$) for the state variables of the system and choosing a control law that will make this function decrease ($\dot{V} < 0$). It is used to guarantee the stability of nonlinear systems. By defining Lyapunov's candidate function for the system as follows:

$$V(x) = \frac{1}{2} s^T \cdot s \tag{4.8}$$

For the Lyapunov function to decrease, it suffices to ensure that its derivative is negative. This is checked if:

$$\dot{V}(x) = \dot{s} \cdot s < 0 \tag{4.9}$$

The variable structure control produced by this reaching law ensures sliding mode only at the point where all switching surfaces intersect, which is called the eventual sliding mode. However, it is uncertain whether points on each individual switching surface will belong to the sliding surface or not.

4.3.3. Control law design:

Once the sliding surface is chosen, as well as the convergence criterion, the next step consists in choosing a command stabilizing in zero the sliding variable in a finite time. The objective of the control law is to constrain the trajectories of the state of the system to reach and then to remain on the sliding surface despite the presence of uncertainties on the system. In other words, the control law must make the sliding surface locally attractive. Thus, the control law must be calculated by verifying a convergence condition of $s(x)$ towards zero.

The behavior of the looped system can be described by two phases:

- **The convergence phase:** This phase corresponds to the time interval of $[0, t]$ during which the state trajectories of the system are not on the sliding surface s . During this phase, the system remains sensitive to parameter variations. However, to avoid a major influence of these variations, one solution consists in shortening the duration of this phase.
- **The sliding phase:** This phase corresponds to the time interval of $[t, \infty[$ during which the state trajectories are confined in the sliding surface s. The sliding regime enjoys the property of insensitivity to disturbances occurring in the same direction as the control input. In fact, the system is insensitive to such disturbances only in the sliding regime, but it remains sensitive during the transient regime. This is the reason why the behavior of the perturbed system is not identical to the same unperturbed system during the transient state.

The control law u is comprised of two components, namely the equivalent component (u_{eq}) and a discontinuous component (u_{dis}). The former is utilized to attain the sliding regime and stabilize the system on the sliding surface, while the latter guarantees that the system is insensitive to parameter variations. By combining these two components, the control law u can be tailored to achieve optimal control performance and robustness against uncertainties [145].

4.3.3.1. Equivalent control

To discover the comparable control, it is important to acknowledge that for the state trajectory to remain on the sliding surface $s(x) = 0, \dot{s}(x) = 0$ must be a mandatory requirement:

$$\dot{s} = \frac{\partial s}{\partial x}\dot{x} = \frac{\partial s}{\partial x}A(x) + \frac{\partial s}{\partial x}B(x) \cdot u_{eq} = 0 \tag{4.10}$$

By solving Equation (4.10) the equivalent control law is deduced as:

$$u_{eq} = -\frac{\partial s}{\partial x} A(x) \cdot \left(\frac{\partial s}{\partial x} B(x)\right)^{-1} \tag{4.11}$$

so that the equivalent command can take a finite value it is necessary that $\frac{\partial s}{\partial x} \cdot B(x) \neq 0$.

4.3.3.2. Discontinuous control

The discontinuous control represents the mode of convergence, the simplest function that can be used to accomplish the function of that command is defined by:

$$s(x) \cdot \dot{s}(x) < 0 \tag{4.12}$$

It is generally of the form:

$$u_{dis} = -k_s \cdot sign\big(s(x)\big) \tag{4.13}$$

with:

$$sign\big(s(x)\big) = \begin{cases} 1 & if \;\; s(x) > 0 \\ 0 & if \;\; s(x) = 0 \\ -1 & if \;\; s(x) < 0 \end{cases} \tag{4.14}$$

Figure 4.2 summarizes the steps for deriving the sliding mode control law:

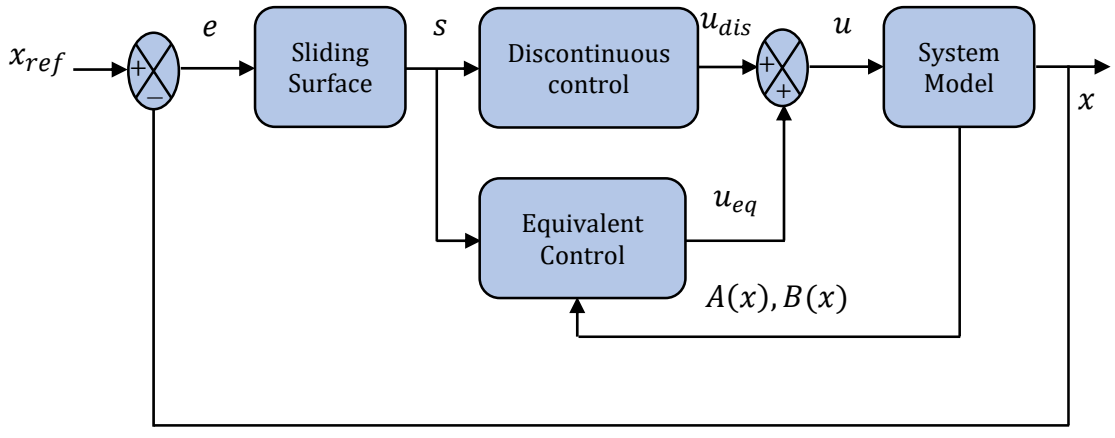

Figure 4.2. Sliding mode control law.

4.3.4. Chattering problem and its reduction

As previously stated, sliding mode controllers require a rapid switching mechanism to ensure the desired behavior of the closed-loop system. However, in actual physical systems, using the control algorithms developed above directly will inevitably result in oscillations near the switching surface, commonly referred to as the chattering phenomenon, due to the limitations of the real world. According to [146], there are two potential causes of chattering. The first is switching non-idealities, such as time delays or time constants, which exist in all implementations of switching devices. The second cause of chattering is the presence of parasitic dynamics, which refers to unmodelled dynamics that appear in the vicinity of the sliding surface. These parasitic dynamics include the fast dynamics of actuators, sensors, and other high-frequency modes of the controlled process. Reducing the chattering effect has long been a primary goal of SMC research. The following is a summary of the existing methods for reducing chattering in SMC design.

4.3.4.1. Continuous functions sliding mode control

To address the issue known as the "chattering phenomenon," which involves the discontinuous "sign" term in sliding mode control, researchers have proposed using approximate smoothed implementations of the technique. This involves replacing the discontinuous term with a continuous smooth approximation. Two instances of this approach are provided as examples:

$$u_{dis} = -k_s \cdot sat(s(x), \varepsilon) \equiv -k_s \frac{s}{|s|+\varepsilon} \tag{4.15}$$

$$u_{dis} = -k_s \cdot tanh\left(\frac{s}{\varepsilon}\right) \tag{4.16}$$

with $\varepsilon > 0$ and $\varepsilon \approx 0$.

While approximating the discontinuous "sign" function with a continuous function in the vicinity of the sliding surface can help mitigate the issue of chattering, it comes at a cost to precision, control robustness, and convergence time. Striking a balance between minimizing chattering and maintaining robustness is crucial. This requires carefully considering the trade-offs between different design objectives and identifying an optimal compromise that yields satisfactory performance. Ultimately, the effectiveness of any approach to mitigating chattering will depend on the specific system requirements and constraints, as well as the experience of the designer.

4.3.4.2. Observer-based sliding mode control

The phenomenon of chattering can be effectively eliminated in a closed-loop system by incorporating an asymptotically stable observer, despite the presence of control discontinuity. Instead of generating a sliding regime in the system itself, the observer is designed to generate the regime, resulting in an ideal sliding mode in the closed-loop of the observer. As the observer is independent of any unmodelled dynamics, the system output follows the observer output smoothly and without any chattering. However, it is important to note that synthesizing an asymptotically stable observer is not a straightforward task, especially for nonlinear and uncertain systems. Despite this limitation, the use of an asymptotical stable observer in closed-loop systems has proven to be a highly effective technique for eliminating chatter and improving system performance [146,147]. This approach is depicted in Figure 4.3.

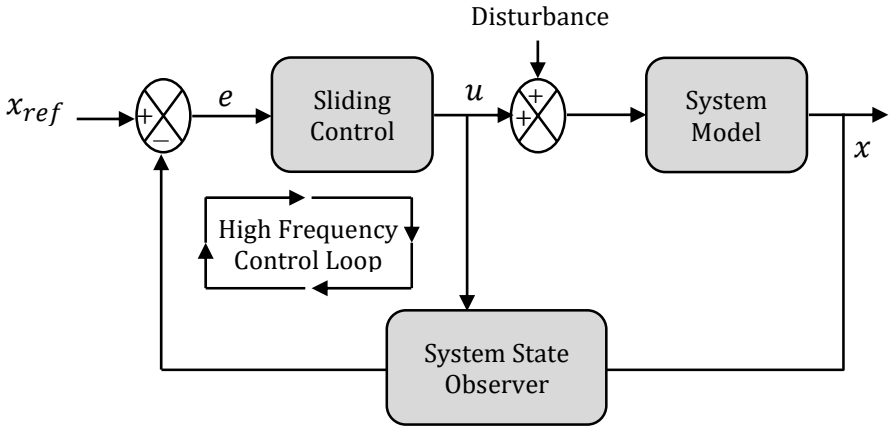

Figure 4.3. Block diagram of observer based sliding mode control.

4.3.4.3. Higher order sliding mode control

In situations where the control action relies on the higher-order time derivatives of the sliding variable, the HOSC technique can be employed. By defining a discontinuous control signal, $\dot{u}$, both the sliding variable, s, and its time derivative, $\dot{s}$, can be steered towards zero. This approach results in the plant input, u, becoming a continuous control signal, which helps to prevent chattering. Despite this method's efficacy, there is a challenge involved in the fact that there is no universal method for adjusting the parameters that differentiate the various algorithms. Therefore, determining the appropriate parameters remains a significant challenge for researchers [148,149].

4.4. Second order sliding mode control

Super-twisting control is a nonlinear control technique that has gained popularity in recent years due to its ability to provide robust control of uncertain dynamic systems. The main advantage of super-twisting controller is its ability to handle systems with uncertainties in their parameters, external disturbances, and nonlinearities. This is achieved by designing a sliding surface, which is a hyperplane in the state space that separates the system trajectory into two regions: one where the system dynamics follow a specific reference model, and the other where the system dynamics are forced to converge to the sliding surface in a finite time. This sliding mode ensures that the system trajectory is insensitive to external disturbances and model uncertainties. Super-twisting also includes a control law that generates a control signal that drives the system to the sliding surface and maintains it there. This control law is based on the concept of super-twisting algorithm, which uses a high-order sliding mode to achieve finite-time convergence to the sliding surface. The super-twisting algorithm is robust to uncertainties and disturbances, and it can handle both continuous and discrete-time systems.

The super-twisting algorithm is a higher-order sliding mode control technique that has been specifically designed to deal with the challenges posed by controlling systems with a relative degree equal to 1. The relative degree of a system refers to the order of its highest time derivative that appears in the system's equations of motion. When the relative degree is 1, the system is said to have a single integrator in its dynamics, and this can make it difficult to achieve precise tracking performance. The super-twisting algorithm addresses this challenge by introducing a second-order sliding mode. This allows the controller to generate a control signal that converges to the sliding surface faster than a first-order sliding mode, leading to improved tracking performance.

By considering the system in Equation (4.1), we define a sliding variable of relative degree equal to 1, whose second derivative can be expressed as follows:

$$\ddot{s}(t,s) = \Phi(t,s) + \Gamma(t,s) \cdot \dot{u}(t) \tag{4.17}$$

where $\Phi(t,s)$ and $\Gamma(t,s)$ are unknown but bounded signals. The assumption that these are unknown but bounded is critical for the effectiveness of the super-twisting control algorithm in handling uncertainties in practical control systems.

The purpose of the controller is to ensure convergence towards the sliding surface defined by $s = 0$. Only the measurement of s in real time is necessary.

Suppose the positive constants S_M, Γ_M, Γ_m, Φ_M, U_M such that $\forall x \in R^n$ and $|s(t,x)| < S_M$, the system fulfills the following conditions:

$$\begin{cases} |u(t)| < U_M \\ \Gamma_m < \Gamma(t,s) < \Gamma_M \\ |\Phi(t,s)| < \Phi_M \end{cases} \tag{4.18}$$

The uncertain function Γ has both upper and lower bounds, represented by Γ_M and Γ_m respectively. Likewise, the uncertain function Φ has an upper bound, represented by Φ_M. Also, the control law is upper bounded by U_M.

The second order sliding mode control based on the super-twisting-algorithm is given by the following expression [150]:

$$u = u_1 + u_2 \tag{4.19}$$

The initial component u_1 allows to get soft response by ensuing $\dot{s} = 0$ and it is given as:

$$u_1 = -\alpha_s \cdot |s|^{\rho} \cdot sign(s) \tag{4.20}$$

while the second part u_2 guarantees that the sliding surface approaches zero, and its expression is as follows:

$$\dot{u}_2 = -\beta_s \cdot sign(s) \tag{4.21}$$

In this context, ρ is a constructive factor employed to regulate the level of nonlinearity and its range is between 0 and 0.5. Typically, this factor is set at 0.5 to attain the highest level of second-order sliding mode control. α_s and β_s are affirmative amplifications utilized in the super-twisting controller, and in order to fulfill the requirements for the system's convergence, these gains should be selected as indicated in [151]:

$$\beta_s > \frac{\Phi_M}{\Gamma_M} \tag{4.22}$$

$$\alpha_s \geq \frac{4 \cdot \Phi_M \cdot \Gamma_M (\beta_s + \Phi_M)}{{\Gamma_m}^3 (\beta_s - \Phi_M)} \tag{4.23}$$

The design of super-twisting control has several advantages over first order sliding control:

- Chattering reduction: STC has a smoother control action, which reduces chattering compared to FOSC, making it more suitable for systems with complex mechanical components.
- Faster convergence: STC has a faster convergence rate, which means that it can reach the desired control output more quickly and with greater precision.
- Robustness: STC is more robust to uncertainties and disturbances, which means that it can still maintain control performance even in the presence of external disturbances.
- Better tracking performance: STC has better tracking performance compared to FOSC, which is important in systems where the control output needs to track a reference signal with high precision.

4.5. Autonomous vehicle lateral control by a super-twisting algorithm

In order to develop an effective control law, the dynamic bicycle model was employed as a foundational framework. By incorporating a linear model of pneumatic forces, a more refined and accurate Linear Variant Parameter (LVP) model was derived. This model specifically focuses on lateral displacement and yaw, two critical aspects of the system's behavior [137, 152]:

$$\begin{cases} \ddot{y} = -\frac{\mu(C_f + C_r)}{m \cdot v_x}\dot{y} - \left(\frac{\mu(L_f \cdot C_f - L_r \cdot C_r)}{m \cdot v_x} + v_x\right)\dot{\psi} + \frac{\mu \cdot C_f}{m}\delta \\ \ddot{\psi} = -\frac{\mu(L_f \cdot C_f - L_r \cdot C_r)}{I_z \cdot v_x}\dot{y} - \frac{\mu({L_f}^2 \cdot C_f + {L_r}^2 \cdot C_r)}{I_z \cdot v_x}\dot{\psi} + \frac{\mu \cdot L_f \cdot C_f}{I_z}\delta \end{cases} \tag{4.24}$$

where y and ψ represent respectively the lateral position and the yaw angle of the vehicle; δ, the steering angle at the tire, v_x, the longitudinal speed; m, the mass of the vehicle; I_z, the moment of inertia; L_f, the front axle-center of gravity distance; L_r, the rear axle distance - center of gravity distance; C_f, the drift stiffness of the front tire; C_r, the drift stiffness of the rear tire; and μ, the coefficient of adhesion. The values of these parameters could be found in Appendix A.1.

For a coefficient of adhesion $\mu = 1$ and $\dot{y} = v_x \cdot \beta$, the LVP model becomes:

$$\begin{cases} \dot{\beta} = -\frac{C_f + C_r}{m \cdot v_x}\beta - \left(\frac{L_f \cdot C_f - L_r \cdot C_r}{m \cdot {v_x}^2} + 1\right)\dot{\psi} + \frac{C_f}{m \cdot v_x}\delta \\ \ddot{\psi} = -\frac{L_f \cdot C_f - L_r \cdot C_r}{I_z}\beta - \frac{{L_f}^2 \cdot C_f + {L_r}^2 \cdot C_r}{I_z \cdot v_x}\dot{\psi} + \frac{L_f \cdot C_f}{I_z}\delta \end{cases} \quad (4.25)$$

where β is the sliding angle at the center of gravity.

The dynamic equation of the lateral error at the center of gravity of the vehicle, with respect to a reference trajectory, is given by:

$$\ddot{e}_{ST} = a_y - a_{y_{ref}} \quad (4.26)$$

where a_y and $a_{y_{ref}}$ are respectively the lateral acceleration of the vehicle and the desired lateral acceleration.

The lateral acceleration could be expressed according to [152] as:

$$a_y = v_x\left(\dot{\beta} + \dot{\psi}\right) \quad (4.27)$$

Assuming that the desired lateral acceleration can be written as:

$$a_{y_{ref}} = {v_x}^2 \cdot \kappa \quad (4.28)$$

where κ is the curvature of the road.

By substituting Equations (4.27) and (4.28) in Equation (4.26), we get:

$$\ddot{e}_{ST} = v_x\left(\dot{\beta} + \dot{\psi}\right) - {v_x}^2 \cdot \kappa \quad (4.29)$$

By substituting $\dot{\beta}$ by its expression in Equation (4.25), we get:

$$\ddot{e}_{ST} = -\frac{C_f + C_r}{m}\beta - \frac{L_f \cdot C_f - L_r \cdot C_r}{m \cdot v_x}\dot{\psi} - {v_x}^2 \cdot \kappa + \frac{C_f}{m}\delta \quad (4.30)$$

The control input is the steering angle δ and the output is the lateral error e_{ST}. The purpose of the command is to cancel the lateral error. Let us choose the sliding variable s as follows:

$$s = \dot{e}_{ST} + \lambda_s \cdot e_{ST} \tag{4.31}$$

The time derivative of the sliding surface:

$$\dot{s} = \ddot{e}_{ST} + \lambda_s \cdot \dot{e}_{ST} \tag{4.32}$$

By replacing $\ddot{e}_{ST}$ by its expression in (4.30), we have:

$$\dot{s} = -\frac{C_f + C_r}{m}\beta - \frac{L_f \cdot C_f - L_r \cdot C_r}{m \cdot v_x}\dot{\psi} - {v_x}^2 \cdot \kappa + \frac{C_f}{m}\delta + \lambda_s \cdot \dot{e}_{ST} \tag{4.33}$$

The variable s has a relative degree $r = 1$. The control input δ appears in the first derivative of s. By applying the super-twisting algorithm, the control input can be defined by the following equation:

$$\delta_{ST} = \delta_1 + \delta_2 \tag{4.34}$$

where:

$$\delta_1 = -\alpha_s \cdot |s|^{0.5} \cdot sign(s) \tag{4.35}$$

and:

$$\dot{\delta}_2 = -\beta_s \cdot sign(s) \tag{4.36}$$

To avoid large peaks during the transient phases, we add an equivalent command δ_{eq}. This term plays the role of an anticipation which makes it possible to approach the system at the sliding surface, and it is obtained by solving the equation $\dot{s} = 0$:

$$\dot{s} = -\frac{C_f + C_r}{m}\beta - \frac{L_f \cdot C_f - L_r \cdot C_r}{m \cdot v_x}\dot{\psi} - {v_x}^2 \cdot \kappa + \frac{C_f}{m}\delta + \lambda_s \cdot \dot{e}_s = 0 \tag{4.37}$$

By solving the Equation (4.37), we get:

$$\delta_{eq} = \frac{C_f + C_r}{C_f}\beta + \frac{L_f \cdot C_f - L_r \cdot C_r}{C_f \cdot v_x}\dot{\psi} + \frac{m \cdot {v_x}^2}{C_f}\kappa - \frac{m \cdot \lambda_s}{C_f}\dot{e}_s \tag{4.38}$$

Therefore, the steering angle, representing the system control input, is defined by the following equation:

$$\delta_{SM} = \delta_{ST} + \delta_{eq} \tag{4.39}$$

In order to ensure stability of the control law, the super-twisting control needs to meet the Lyapunov stability condition. This involves defining a positive definite Lyapunov candidate as follows:

$$V_{SM} = \frac{1}{2}s^2 \tag{4.40}$$

Its time derivative must be negative definite:

$$\dot{V}_{SM} = s \cdot \dot{s} < 0 \tag{4.41}$$

By substituting Equation (4.39) in Equation (4.33) we obtain:

$$\dot{s} = \frac{C_f}{m}\delta_{ST} = -\frac{C_f}{m}(\alpha_s \cdot |s|^{0.5} \cdot sign(s) + \int \beta_s \cdot sign(s) \cdot dt) \tag{4.42}$$

Then, the time derivative of Lyapunov candidate is:

$$\dot{V}_{SM} = -s\frac{C_f}{m}(\alpha_s \cdot |s|^{0.5} \cdot sign(s) + \int \beta_s \cdot sign(s) \cdot dt) \tag{4.43}$$

and it becomes:

$$\dot{V}_{SM} = -\frac{C_f}{m}\left(\alpha_s \cdot |s|^{\frac{3}{2}} \cdot sign(s) + s \cdot \beta_s \int sign(s) \cdot dt\right) \tag{4.44}$$

By observing the expression for the time derivative of the Lyapunov candidate, it becomes apparent that its negativity is contingent on the positivity of α_s and β_s. This observation, in turn, leads to the conclusion that the system under consideration satisfies the stability condition. This finding is of great significance as it guarantees the stability of the system, which is an essential requirement in the analysis and design of control systems. Therefore, we can confidently assert that the system will remain in a stable state as long as the values of α_s and β_s remain positive.

4.6. Simulation results

This section presents an in-depth analysis of the performance of the proposed super-twisting control technique through simulations. To ensure the robustness and versatility of our method, we conducted simulations on two distinct trajectories, each with its own unique set of features and profiles. The first trajectory has the shape of an eight with a total distance of 2.66 km, while the second trajectory has a total distance of 3.35 km, as illustrated in Figure 4.4. The vehicle's initial position is set to $(0, 0)$, and it proceeds in an anticlockwise direction until reaching the endpoint at the same coordinates as the starting point. By analyzing the simulation results of both trajectories, we aim to demonstrate the performance enhancement of the proposed super-twisting control technique in terms of tracking accuracy, even in challenging and varying circumstances.

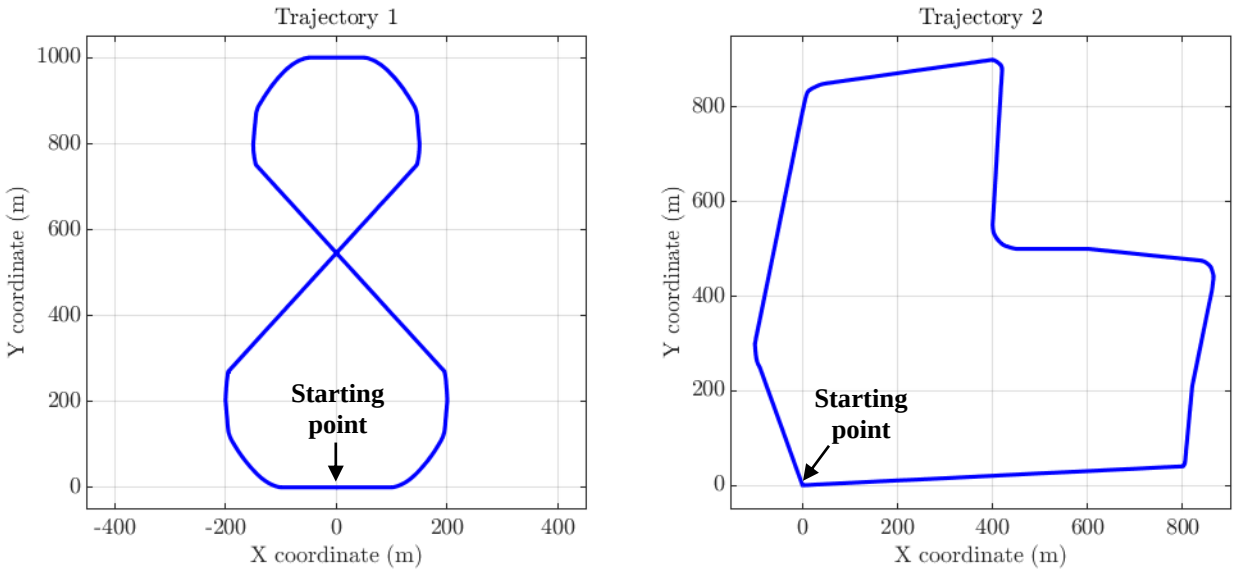

Figure 4.4. Vehicle predefined trajectories.

In this chapter, we explore the vehicle's navigation performance through desired trajectories using a constant velocity profile. The study begins with the vehicle at a standstill, starting with an initial velocity of 0 m/s. To ensure passenger comfort and safety, the vehicle gradually accelerates at a carefully calculated rate 2 m/s^2. The acceleration is precisely controlled to ensure a smooth motion while maintaining the desired velocity profile. Throughout the study, the vehicle velocity

increases gradually, reaching a maximum speed of 70 km/h (19.44 m/s), which is demonstrated in detail in Figure 4.5. By meticulously monitoring the vehicle's velocity profile and controlling the acceleration, we ensure that the vehicle's performance is safe, efficient, and comfortable for all passengers.

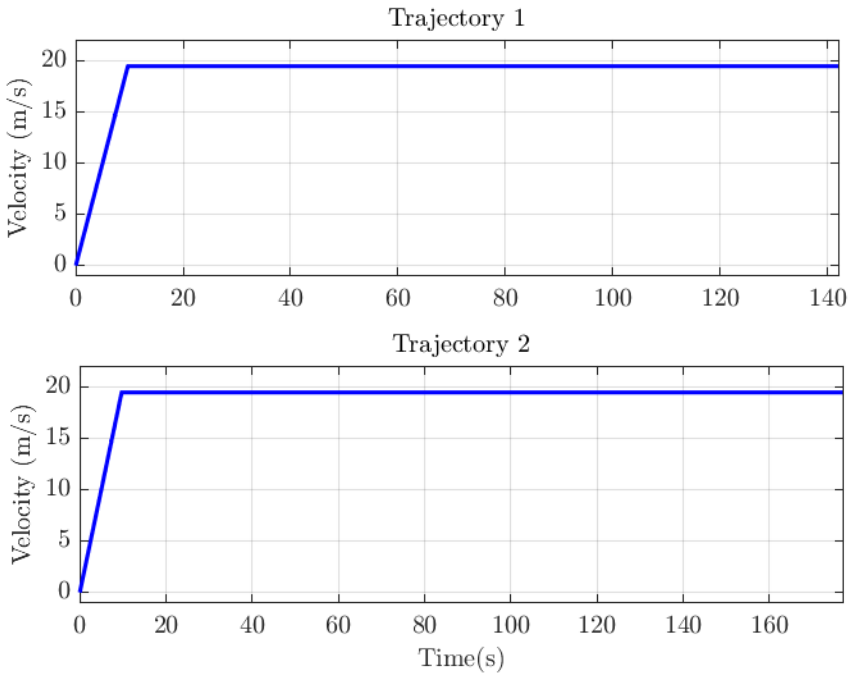

Figure 4.5. Speed profiles for trajectories 1&2 using constant speed.

Figure 4.6 presents a detailed representation of the curvatures associated with each trajectory. The curvature values for the first trajectory range from $-0.022\,m^{-1}$ to $0.021\,m^{-1}$, while the second trajectory's curvature values range from $-0.021\,m^{-1}$ and $0.051\,m^{-1}$. These values provide valuable insight into the extent of deviation from a straight-line path, with the second trajectory exhibiting a higher degree of curvature than the first. The analysis of curvatures presented in Figure 4.6 serves as a powerful tool for understanding the dynamics of the trajectories, which in turn can aid in the development of improved trajectory planning algorithms. By carefully analyzing the curvature values associated with each trajectory, we gain a better understanding of the complexity of each trajectory. This insight is crucial for designing optimal navigation plans that can navigate through complex trajectories with good precision and high efficiency.

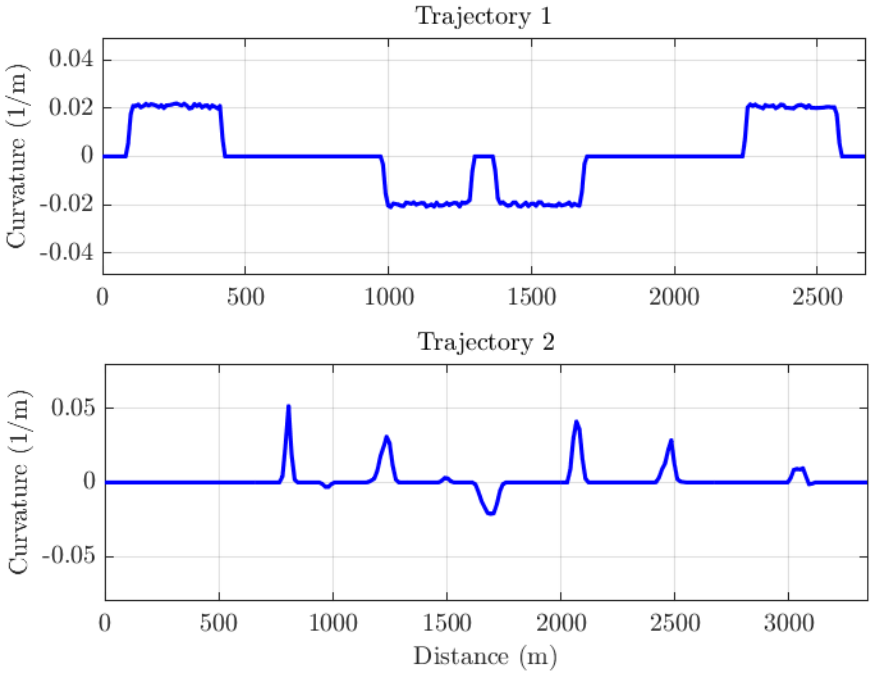

Figure 4.6. Curvatures for trajectories 1&2.

The vehicle tracking results, showcased in Figure 4.7, reveal the impressive performance of the super-twisting controller. The blue line denotes the reference trajectory, while the red line signifies the real trajectory of the vehicle. The graph unmistakably exhibits that the vehicle position

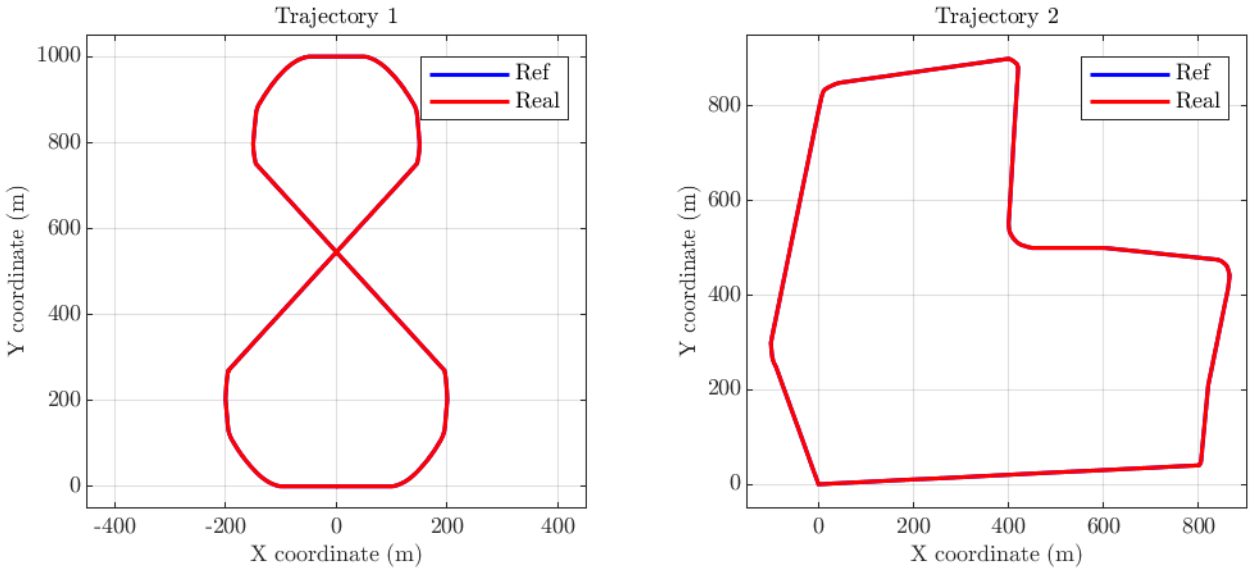

Figure 4.7. Vehicle tracking trajectories using constant speed.

closely tracking the reference trajectory, providing concrete evidence of the effectiveness of the super-twisting controller. Moreover, the reference and actual trajectories are practically indistinguishable, which emphasizes the exceptional precision and accuracy of the controller.

Figures 4.8 and 4.9 offer a detailed visualization of the lateral and orientation errors obtained from the rigorous experimentation process. The distance error, which measures the instantaneous distance between the reference and the vehicle's actual position, and the orientation error, indicating the deviation between the desired vehicle heading direction and the actual heading direction, were the chosen metrics to assess the performance of the controller. The outcomes demonstrated that the implemented super-twisting controller was exceptionally effective in tracking the reference trajectory, with only minimal distance and orientation errors observed consistently. Notably, the occasional irregular peaks noticed in some parts of the figures were due to sudden turns that the vehicle had to execute to handle the trajectories curvatures and remain within the designated safety boundaries, as highlighted in Figure 4.6. Overall, the obtained results provide strong confirmation of the exceptional efficacy demonstrated by the designed super-twisting controller in effectively preserving both the precise position and desired orientation of the vehicle along its designated trajectories.

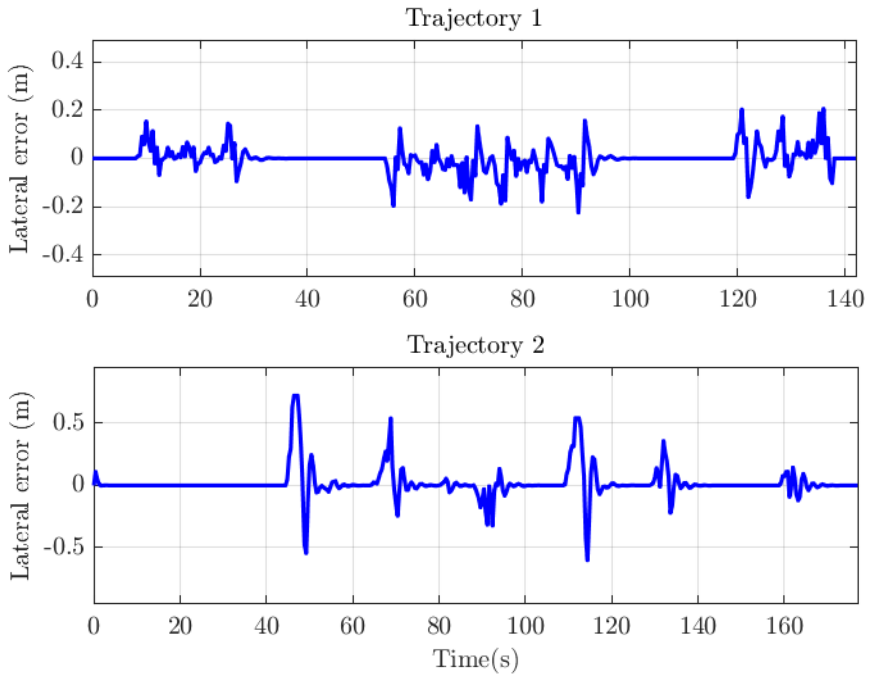

Figure 4.8. Lateral error for trajectories 1&2 using constant speed.

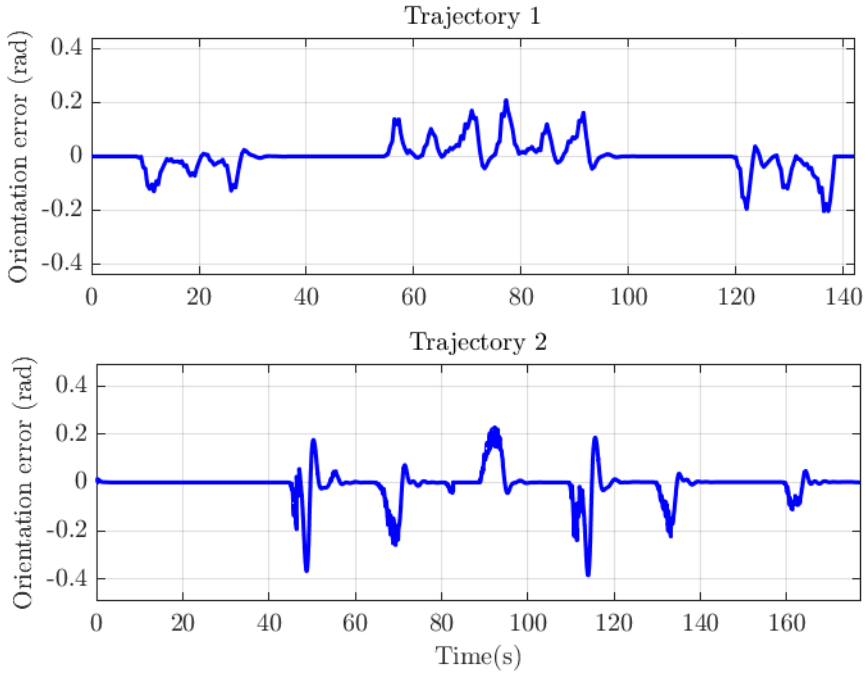

Figure 4.9. Orientation error for trajectories 1&2 using constant speed.

Figures 4.10 and 4.11 provide a comprehensive and insightful representation of the steering angle command and yaw rate achieved during the trajectory-tracking task. These figures play a vital role in evaluating the vehicle's performance and assessing the effectiveness of the implemented controller throughout the task. They vividly demonstrate the controller's remarkable ability to maintain the vehicle's trajectory, highlighting its competence and reliability. The vehicle autonomously maneuvered around the designated testing area for multiple rounds, showcasing the exceptional performance of the implemented controller throughout the entire simulation process. Notably, the super-twisting controller stands out for its ability to achieve an impressively smooth steering angle curve, effectively minimizing any shuddering effects. This aspect is crucial in ensuring the stability of the vehicle during navigation, as even the slightest deviation from the intended path could have disastrous consequences. The consistent and precise steering angle command produced by the controller is of paramount importance in ensuring the seamless and accurate motion of the vehicle as it traces the intended path. The achieved stability and accuracy emphasize the controller's effectiveness in enabling a smooth and steady navigation experience. In real-world scenarios, where safety and efficiency are of utmost importance, such performance becomes even more critical.

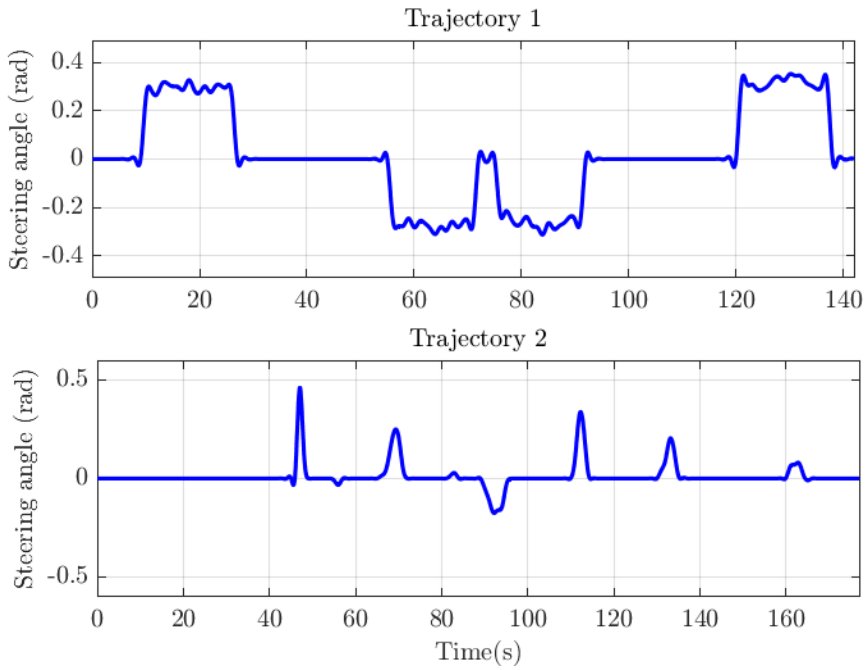

Figure 4.10. Steering angle for trajectories 1&2 using constant speed.

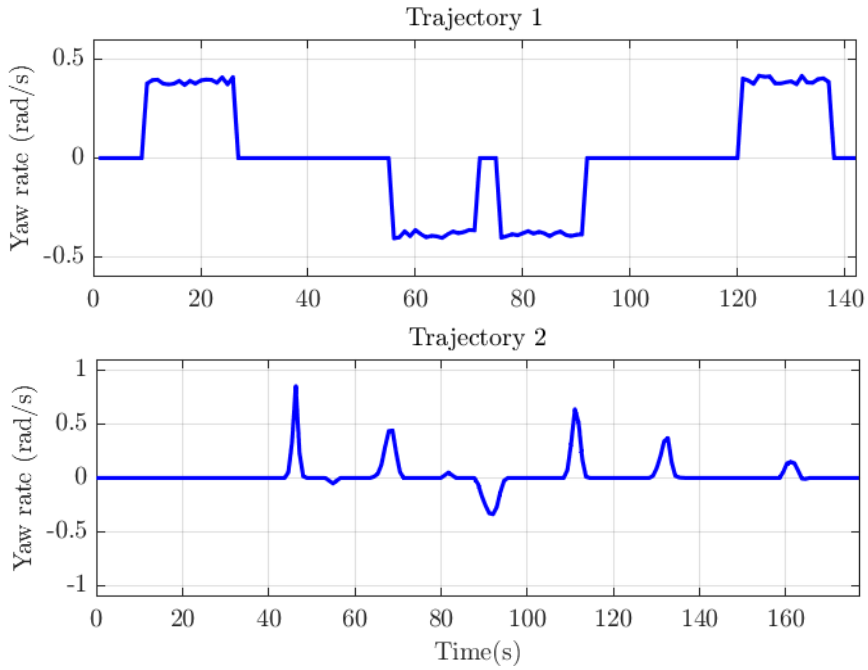

Figure 4.11. Yaw rate for trajectories 1&2 using constant speed.

Table 4.1 and Table 4.2 provide a comprehensive summary of the lateral and orientation errors observed during trajectory tracking in sharp curves, when using constant velocity. The Root Mean

Square (RMS) errors for trajectory 1 are $0.054\,m$ and $0.059\,rad$, while for trajectory 2, they are $0.209\,m$ and $0.086\,rad$. Notably, the maximum errors recorded for all the sharp curves are $0.224\,m$ and $0.720\,m$ for lateral error, and $0.209\,rad$ and $0.385\,rad$ for orientation error, for trajectories 1 and 2, respectively. These results are indicative of the exceptional transient response and robustness exhibited by the designed super-twisting controller. Additionally, the average errors of trajectory 1 are found to be lower than those of trajectory 2. This is largely due to the presence of sharper curves in the latter trajectory. It is worth noting that despite the presence of such challenging conditions, the designed super-twisting controller is able to deliver satisfactory performance through the whole trajectory.

Table 4.1. Lateral and orientation errors for trajectory 1 using constant speed.

Curve	1	2	3	4	Average
MAX lateral error (m)	0.153	0.200	0.224	0.205	0.195
RMS lateral error (m)	0.041	0.051	0.060	0.063	0.054
MAX orientation error (rad)	0.129	0.170	0.209	0.203	0.178
RMS orientation error (rad)	0.043	0.057	0.066	0.069	0.059

Table 4.2. Lateral and orientation errors for trajectory 2 using constant speed.

Curve	1	2	3	4	5	6	Average
MAX lateral error (m)	0.720	0.538	0.322	0.600	0.356	0.143	0.447
RMS lateral error (m)	0.354	0.353	0.101	0.265	0.115	0.065	0.209
MAX orientation error (rad)	0.367	0.258	0.227	0.385	0.223	0.112	0.262
RMS orientation error (rad)	0.112	0.093	0.094	0.102	0.064	0.052	0.086

4.7. Conclusion

In this chapter, we have outlined a comprehensive control design for lateral vehicle navigation along a pre-defined trajectory at a constant velocity. The main focus of this chapter is to identify the key research areas in this field. In terms of lateral control, we believe that the dynamic bicycle model is the most suitable for our high-speed automatic driving application. This model is known for its nonlinear and time-varying behavior, which accurately represents the complex dynamics of a vehicle in motion.

For the control law, we have designed a highly effective lateral control strategy for autonomous vehicles that is based on a second-order sliding mode control approach. This approach leverages the super-twisting algorithm, which enables robust and accurate tracking of the reference trajectory while minimizing unwanted chatter. This algorithm is a powerful tool for controlling dynamic systems, particularly in high-speed and complex environments.

The obtained results using Matlab/Simulink software on two distinct trajectories, each with its own unique set of features and profiles, have showed that our autonomous vehicle is able to maintain precise control over its lateral movements, and navigate through challenging road conditions with ease. This designed control law represents a significant advancement in the field of autonomous driving, and has the potential to revolutionize the way we think about vehicle control and navigation.

CHAPTER 5

VEHICLE VELOCITY PLANNING

Contents **Page**

5.1. Introduction

Speed planning in autonomous vehicles refers to the process of determining the appropriate speed for the vehicle to travel. It is a crucial aspect of autonomous driving that affects the safety, efficiency, and comfort of the vehicle. With the increasing demand for autonomous vehicles, speed planning has become a key area of research and development in the field of autonomous driving.

Autonomous vehicle longitudinal control refers to the control of the vehicle's speed and acceleration. Longitudinal control involves adjusting the vehicle's speed to match the flow of traffic, maintain a safe following distance, and comply with speed limits. Broadly speaking, autonomous vehicle longitudinal control works together with the speed planning process to achieve the goal of safe and efficient autonomous driving. The speed planning process determines the target speed for the vehicle, and the longitudinal control system ensures that the vehicle maintains this speed by controlling its acceleration and deceleration. The vehicle's longitudinal control system is constantly monitoring road conditions and adjusting the vehicle's speed and acceleration as needed to maintain the target speed determined by the speed planning system.

Autonomous vehicle speed planning may depend on several factors, including:

- Path geometry: The path conditions, such as curves and inclines, can affect the vehicle's speed and acceleration.
- Speed limits: Autonomous vehicles must abide by speed limits to ensure the safety of passengers and other road users.
- Obstacles: The presence of obstacles, such as other vehicles, pedestrians, or roadwork, can impact the vehicle's speed planning.
- Regulations and laws: Autonomous vehicles must comply with traffic regulations and laws, such as right-of-way rules.

In this study, we will focus on path geometry and speed limits to design a speed planning algorithm that generates a suitable speed profile for vehicle navigation through a predetermined trajectory. The speed algorithm works on adapting the vehicle speed with trajectory curvatures such that the highly curved sections of the trajectory lead to low speeds and vice versa, to tune an ideal performance and ensure the stability and safety of the autonomous vehicle system. First, we

will start by identifying the main curves included in the predefined trajectory. Then, the curves main characteristics will be identified. After that, the velocity of each sharp curve will be calculated. Finally, we will design an algorithm to produce a speed profile for vehicle navigation through the whole trajectory.

5.2. Curve identification

Identification of curves included in a predefined trajectory refers to the process of determining the type and properties of curves within a known path followed by an object over time. This may involve fitting various mathematical functions to different segments of the trajectory data in order to identify specific curves such as parabolic or sinusoidal patterns. The goal of this process is to provide a detailed understanding of the object's motion, including the types and properties of curves present in the trajectory, in order to make predictions or analyze the data further.

5.2.1. Curve types

The trajectory can be represented by a set of coordinates that describe the position of the object at various points in time. A curve in a trajectory can be seen as a smooth and continuous function that refers to the degree to which a path deviates from a straight line. The curve can be used to describe the amount of bend or turning in the trajectory, and it is characterized by its starting point, which is called the Point of Curvature (PC) and its ending point, which is called the point of Tangency (PT).

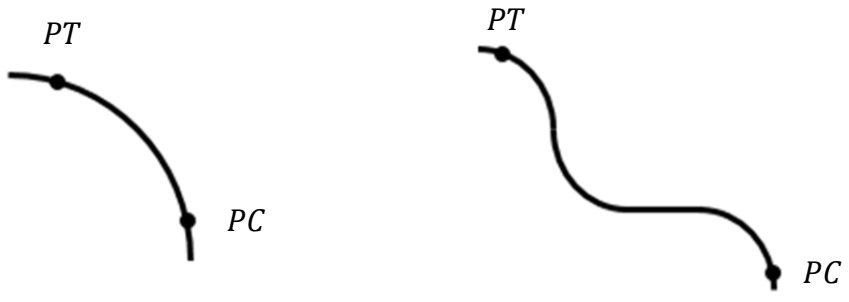

Figure 5.1. Curve types.

Generally, curves can be classified into two fundamental types: simple curves and compound curves. Both types are commonly used in the design of highways, railways, and other transportation systems to provide smooth and safe travel for vehicles and passengers. The change in curvature makes the trajectory more complex, but can also make it more flexible and capable of accommodating changes in direction. A simple curve in a trajectory refers to a curve with constant curvature and is mathematically represented as a segment of a circle, as shown in Figure 5.1 (a). A compound curve, on the other hand, is composed of multiple consecutive short curves, as illustrated in Figure 5.1 (b).

The main difference between a simple curve and a compound curve in a trajectory is the amount and change of curvature. A simple curve has a constant radius of curvature, meaning that it has the same degree of curvature along its entire length. This type of curve is often used in the design of highways, railways, and other transportation systems to provide a smooth and gradual change in direction. From the other side, a compound curve is made up of two or more simple curves with different radii of curvature. This results in a change in the degree of curvature along the length of the curve. Compound curves are used in situations where a more complex trajectory is required, such as navigating around obstacles or accommodating changes in direction.

An important parameter in defining the compound curve is the distance that separates two consecutive simple curves. According to The American Association of State Highway and Transportation Officials (AASHTO), a tangent that separates two consecutive horizontal curves should be at least $183\ m$ in length [153]. Therefore, in the case illustrated in Figure 5.2 (a), the

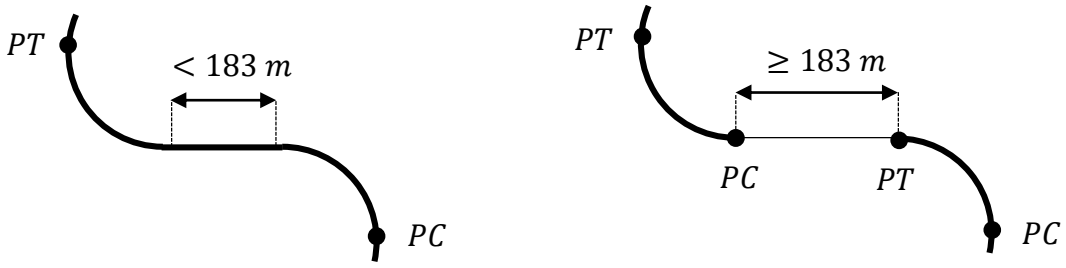

a b

Figure 5.2. Curve classification.

tow simple curves and the line between them form together a compound curve because the length of the inner line is less than $183\ m$. However, the case illustrated in Figure 5.2 (b) presents two separate simple curves because the line that separates them is longer than $183\ m$.

5.2.2. Curve detection

The ability to accurately detect the curves present in a predetermined trajectory is a vital aspect in the optimization of speed planning procedures. As such, it is necessary to develop and implement a robust and efficient algorithm for curve detection that can accurately detect and classify these curves in a reliable manner. For the algorithm to automatically detect curvatures in a predetermined trajectory, it could use the following steps:

- Preprocessing: Clean and smooth the data points in the trajectory to reduce noise and improve accuracy.
- Curve segmentation: Divide the trajectory into segments based on the regions of significant curvature.
- Segments inclination: Evaluate the degree of inclination of each two consecutive segments in the curve.
- Thresholding: Set a threshold on the value of the inclination to identify regions with significant curvature.
- Curve classification: Evaluate the degree of inclination of each curve segment to classify them into different categories based on the threshold value.
- Postprocessing: Verify the accuracy of the curve fits and make adjustments as needed to improve the final result.

The trajectory is created by connecting a series of discrete data points, with each line segment formed between two consecutive points. These line segments, when combined, form the overall trajectory, which represents the path of a moving object over time. The bearing angle α is a key measurement that represents the inclination between two consecutive line segments in the curve, as illustrated in Figure 5.3. This calculation plays a crucial role in the curve detection algorithm, as it provides important information about the direction of the curve at each point. By accurately determining the bearing angle, the algorithm can understand the shape and behavior of the curve.

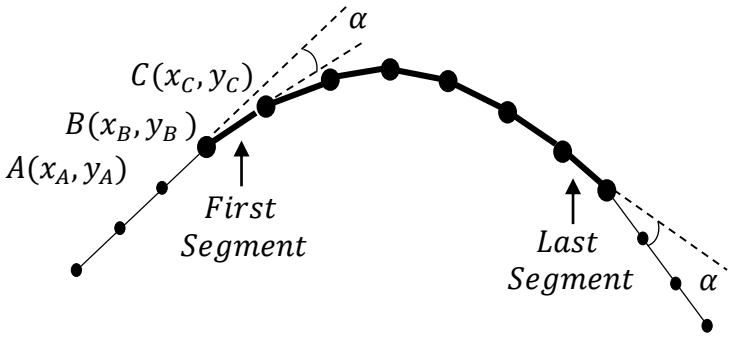

Figure 5.3. Bearing angle.

The bearing angle α between the segments AB and BC in Figure 5.3 can be calculated utilizing the geographic coordinates of points A, B, and C through the following equations [154]:

$$\cos\left(\frac{\alpha\cdot\pi}{180}\right) = \frac{\overrightarrow{AB}.\overrightarrow{BC}}{|\overrightarrow{AB}|\cdot|\overrightarrow{BC}|} = \frac{(x_B-x_A)(x_C-x_B)+(y_B-y_A)(y_C-y_B)}{\sqrt{(x_B-x_A)^2+(y_B-y_A)^2}\cdot\sqrt{(x_C-x_B)^2+(y_C-y_B)^2}} \tag{5.1}$$

$$\alpha = \cos^{-1}\left(\frac{(x_B-x_A)(x_C-x_B)+(y_B-y_A)(y_C-y_B)}{\sqrt{(x_B-x_A)^2+(y_B-y_A)^2}\cdot\sqrt{(x_C-x_B)^2+(y_C-y_B)^2}}\right)\frac{180}{\pi} \tag{5.2}$$

where (x_A, y_A), (x_B, y_B), and (x_C, y_C) are the coordinates of the points A, B, and C, respectively.

The success of the curve identification algorithm lies in the precise determination of the threshold value for the bearing angle. This value holds significant influence in ensuring the accuracy of the curves extracted by the algorithm. Careful consideration is therefore imperative in the selection of the threshold value for the bearing angle. This value holds immense importance in identifying the precise starting and ending points of genuine curves, making it a critical component in the curve identification process. When the calculated bearing angle between the current segment and the next segment exceeds the threshold, it indicates the start or continuation of a real curve. On the other hand, if the calculated bearing angle between the current segment and the previous segment is less than or equal to the threshold, it suggests the absence of a real curve or the end of a previously detected curve [155]. In this research, a bearing angle threshold of 5° was utilized. After detecting the real curves, each one is defined by its curvature point, and its tangency point.

A comprehensive description of the curve identification algorithm is presented in flowchart in Figure 5.4, allowing for a clear understanding and easy interpretation of the method.

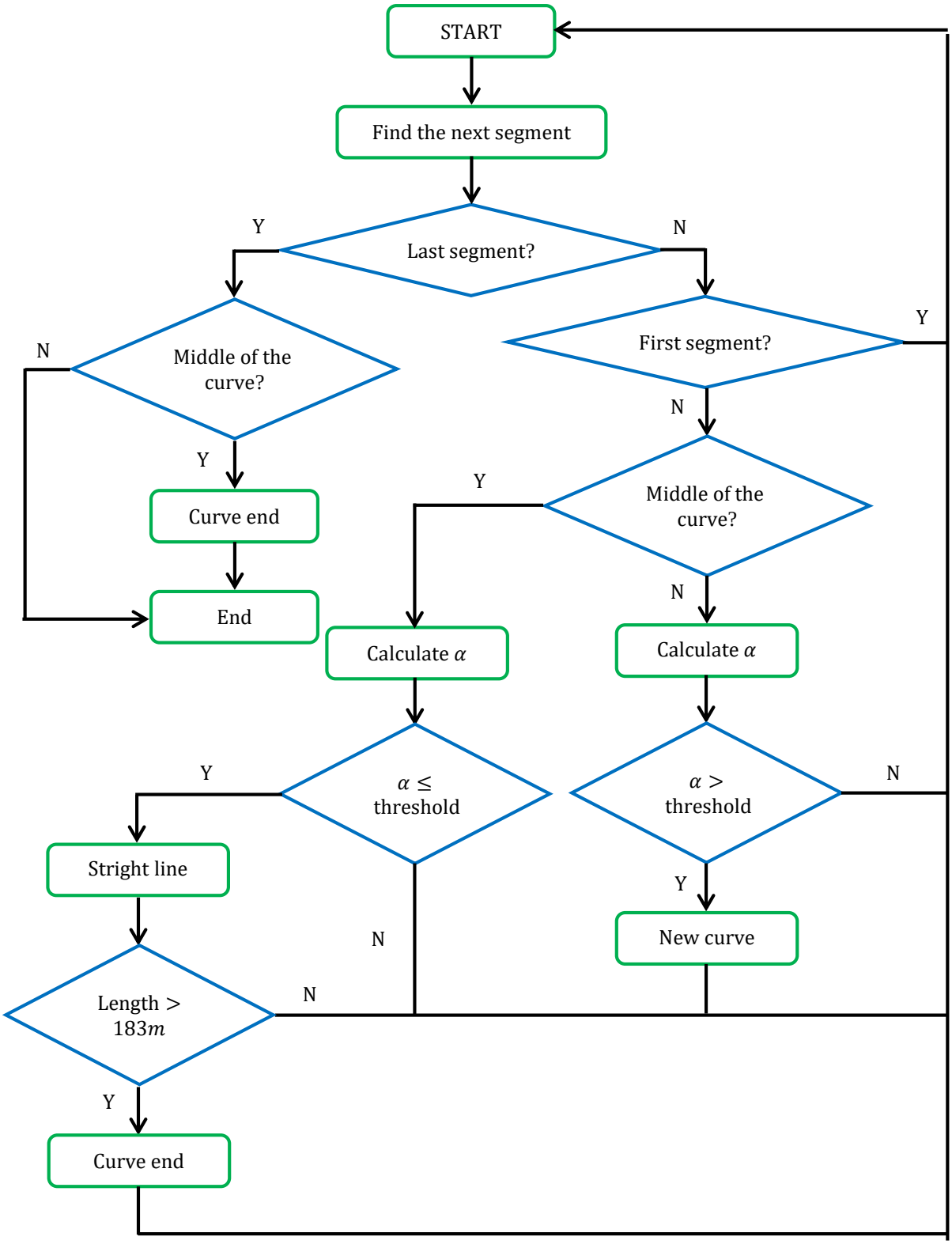

Figure 5.4. Curve identification algorithm.

5.3. Curve characteristics

After the curve identification algorithm has been utilized to extract the actual curves from the predefined trajectory and to define them through their curvature points and tangency points, the next step is to extract the main characteristics of each curve. This information is crucial in understanding the behavior and behavior patterns of the curve, and it allows for the formulation of a suitable approach in dealing with it. These characteristics can be studied mathematically through the use of functions, derivatives, and integrals. By fully comprehending the main characteristics of each curve, a more informed and effective approach can be taken in dealing with it, leading to improved performance and safety. The main components of a curve are represented in Figure 5.5 and include [156]:

- Intersection Point (IP): The intersection point is a significant junction at which the two tangents, representing the direction of curvature in opposite directions, intersect and come together to form a common point.
- Intersection angle (ι): The intersecting angle is a significant measure of deviation at the point of intersection.
- Curve Radius (R_c): The radius of a curve is a crucial component of geometric study and is defined as a straight line that originates from the center of the curve and extends to its circumference.
- Curve Length (L_c): The length of a curve is a fundamental aspect of its geometry, representing the total distance covered when traversing the curve from its curvature point to its tangency point.
- Curve Length Chord (C_c): A chord in geometry is defined as a straight line connecting two points on a curve. A long chord of a curve is a chord that starts from the point of curvature and extends to the point of tangency.
- Curve Center (O_c): The center of a curve refers to a central point or average position of the points on the curve.
- Central angle (ϑ): The central angle is the angle formed by two radii drawn from the center of the circle (O_c) to the point of curvature and the point of tangency.

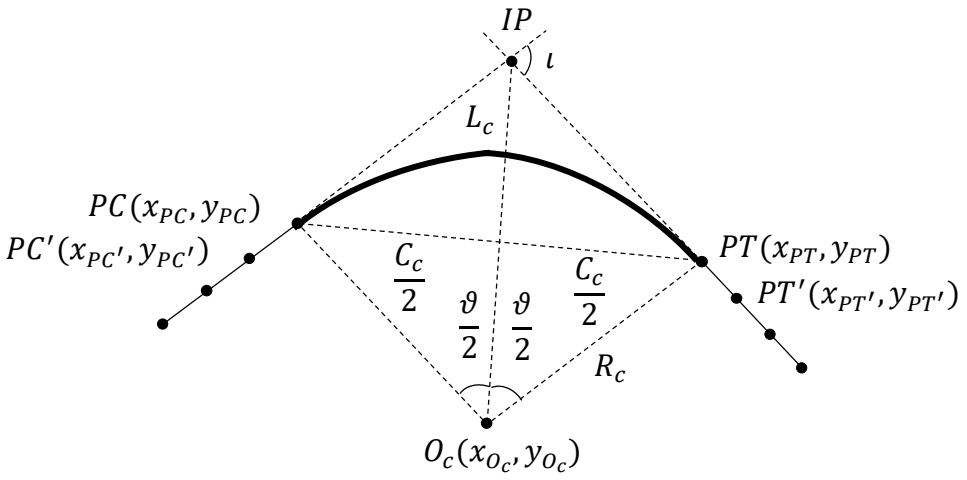

Figure 5.5. Curve parameters.

The parameters that define the curve shown in Figure 5.5 are crucial for a complete understanding of its characteristics and behavior. These parameters are obtained by applying a set of mathematical equations, which serve as a structured and systematic method for determining the key features of the curve. The equations used in this process are detailed below [157]. The precise calculation of these parameters is crucial, as it forms the foundation of the analysis and provides valuable insight into the nature of the curve.

$$a_{(O_c-PC)} = \frac{(x_{PC'}-x_{PC})}{(y_{PC}-y_{PC'})} \tag{5.3}$$

$$b_{(O_c-PC)} = (y_{PC} - x_{PC})\frac{(x_{PC'}-x_{PC})}{(y_{PC}-y_{PC'})} \tag{5.4}$$

$$a_{(O_c-PT)} = \frac{(x_{PT'}-x_{PT})}{(y_{PT}-y_{PT'})} \tag{5.5}$$

$$b_{(O_c-PT)} = (y_{PT} - x_{PT})\frac{(x_{PT'}-x_{PT})}{(y_{PT}-y_{PT'})} \tag{5.6}$$

$$x_{O_c} = \frac{b_{(O_c-PT)}-b_{(O_c-PC)}}{a_{(O_c-PC)}-a_{(O_c-PT)}} \tag{5.7}$$

$$y_{O_c} = a_{(O_c-PC)} \frac{b_{(O_c-PT)} - b_{(O_c-PC)}}{a_{(O_c-PC)} - a_{(O_c-PT)}} + b_{(O_c-PC)} \tag{5.8}$$

$$R_c = \sqrt{\left(x_{PC} - x_{O_c}\right)^2 + \left(y_{PC} - y_{O_c}\right)^2} \tag{5.9}$$

$$C_c = \sqrt{(x_{PT} - x_{PC})^2 + (y_{PT} - y_{PC})^2} \tag{5.10}$$

$$\vartheta = 2 \cdot \sin^{-1}\left(\frac{C_c}{2R_c}\right) \cdot \frac{180}{\pi} \tag{5.11}$$

$$L_c = \frac{\vartheta.\pi}{180} R_c \tag{5.12}$$

The slopes of lines $O_c - PC$ and $O_c - PT$ are represented by $a_{(O_c-PC)}$ and $a_{(O_c-PT)}$ respectively, while their intercepts are denoted by $b_{(O_c-PC)}$ and $b_{(O_c-PT)}$. The coordinates of the center point of the curve are represented by x_{O_c} and y_{O_c}.

The extracted curves present in a particular trajectory can display a wide range of shapes and curvatures, making it challenging to compare and analyze them effectively. To address this, various parameters have been devised to quantify the severity of a curve, with the central angle being one of the most commonly utilized metrics. When the central angle of a curve is large, it indicates that the curve is sharp, with a tight radius and steep incline. In contrast, a low central angle indicates that the curve is less sharp, has a larger radius, and a gentler incline. As a result, the central angle can provide valuable insight into the comparison of the sharpness of curves within a particular trajectory.

In the context of identifying hazardous curves, only those curves that are considered sharp are of interest. To determine what constitutes a sharp curve, a set of criteria have been established based on the AASHTO's guidelines. According to "A Policy on Geometric Design of Highways and Streets" [153], a sharp curve is classified as such if its central angle falls within a specific range, specifically between 30° and 180°. This range of central angles is considered to pose a greater risk to drivers and therefore are considered dangerous curves that require special attention and measures to mitigate their potential dangers. In this study, the emphasis is placed solely on sharp curves for adjusting vehicle speed during trajectory tracking

5.4. Curve speed calculation

Curve speed calculation is crucial in autonomous vehicle driving because it directly affects the safety and performance of the vehicle. By accurately calculating the appropriate speed for navigating a curve, an autonomous vehicle can ensure that it stays on the road and avoids potential accidents. If the vehicle takes a curve at a speed that is too high, it can lose traction and spin out of control, potentially colliding with other vehicles or objects. On the other hand, if the vehicle takes the curve at a speed that is too slow, it can impede traffic flow and cause delays. Therefore, accurate curve speed calculation is critical for ensuring the safe and efficient operation of autonomous vehicles. This involves taking into account various factors such as the curvature of the road and the forces applied on the vehicle to determine the ideal speed for navigating the curve.

Figure 5.6 showcases the comprehensive forces that were meticulously considered in our vehicle model. The centrifugal force, slope force, and rolling resistance force were all precisely incorporated into the model, as they play a significant role in determining the vehicle's trajectory and overall behavior. However, in the interest of precision and accuracy, the aerodynamic force was excluded from our model. While the aerodynamic force is undoubtedly a relevant factor in vehicle dynamics, its contribution to the overall behavior of the vehicle is typically relatively minor when compared to other forces that have been taken into account. Moreover, for the specific purpose of our study, the effects of aerodynamic forces are negligible, allowing us to focus on other forces that have a more significant impact on the vehicle's performance.

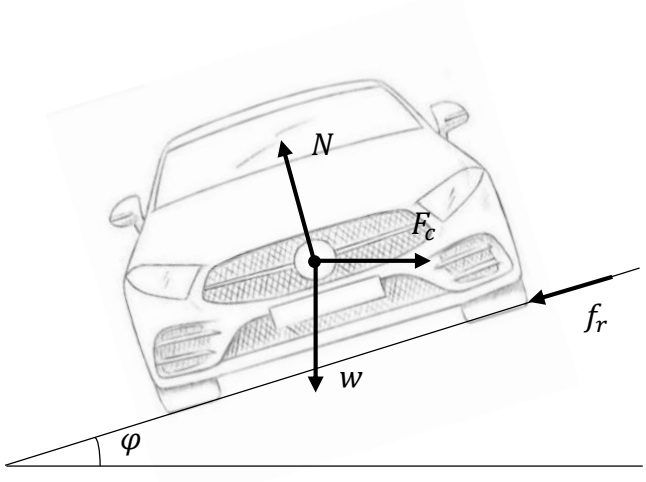

Figure 5.6. Forces applied in the vehicle.

Estimating the speed of a curve is a crucial aspect of safe driving and relies on the interplay between two opposing forces: centripetal and centrifugal. The centripetal force, arising from the friction between the tires and the road surface, is responsible for keeping the vehicle on track along the curve. Conversely, the centrifugal force is an outward force that seeks to push the vehicle away from the curve. Therefore, to mitigate the effects of the centrifugal force, road designers incorporate a banked angle φ into curves, which tilts the roadway and provides an incline that counters the centrifugal force, thereby enhancing vehicle stability and safety.

The expression for the centrifugal force exerted on the vehicle can be conveyed as follows:

$$F_c = m\frac{v^2}{R_c} \tag{5.13}$$

The centrifugal force can be expressed as the resultant of the normal force N and the friction force f_r in the horizontal direction:

$$F_c = N \cdot \sin\varphi + f_r \cdot \cos\varphi \tag{5.14}$$

When considering the vertical direction, the weight force w can be represented as the sum of the normal force N and the friction force f_r acting in the opposite direction:

$$w = N \cdot \cos\varphi - f_r \cdot \sin\varphi \tag{5.15}$$

Newton's second law states that the force acting on an object is proportional to its mass and acceleration. Therefore, the weight force can be mathematically expressed as the product of an object's mass and the acceleration due to gravity g:

$$w = m \cdot g \tag{5.16}$$

The expression for the friction force applied on a vehicle wheel can be given by the product of the coefficient of friction, μ, between the tire and the road surface and the normal force, N, acting on the wheel. The friction force is essential for ensuring the vehicle's ability to accelerate, decelerate, and turn safely and efficiently. Mathematically, this can be represented as:

$$f_r = N \cdot \mu \tag{5.17}$$

By substituting the Equations (5.16) and (5.17) in the Equation (5.15), the expression of the normal force could be derived as:

$$N = \frac{m \cdot g}{\cos\varphi - \mu \cdot \sin\varphi} \tag{5.18}$$

By substituting the Equations (5.17) and (5.18) in the Equation (5.14), the expression of the centrifugal force could be derived as:

$$F_c = \frac{\tan\varphi + \mu}{1 - \mu \cdot \tan\varphi} m \cdot g \tag{5.19}$$

When we set Equations (5.13) and (5.19) to be equal to each other, we obtain:

$$\frac{\tan\varphi + \mu}{1 - \mu \cdot \tan\varphi} g = \frac{v^2}{R_c} \tag{5.20}$$

By defining the super-elevation $\xi = \tan\varphi$ and the curvature $\kappa = \frac{1}{R_c}$, the optimal speed of a curve can be expressed as follows:

$$v_c = \sqrt{\frac{(\xi + \mu)g}{(1 - \mu \cdot \xi)\kappa}} \tag{5.21}$$

Super-elevation is an essential factor in designing curves to ensure vehicle safety by resisting the effects of centripetal force. The American Association of State Highway and Transportation Officials recommends a super-elevation rate between 4% to 12% to prevent the vehicle from sliding or tipping over when navigating a curve [153]. However, the friction coefficient is another critical aspect to consider, as it depends on various factors such as the vehicle velocity, tire quality, and road surface type. The friction coefficient value typically ranges between 0.1 to 0.16, and exceeding this limit can compromise vehicle safety, especially in wet or slippery conditions [15]. Therefore, it is crucial to design the super-elevation and friction coefficient values according to the specific road geometry and environmental factors, including weather and traffic conditions, to ensure safe and efficient travel around the curve. Road designers and engineers must carefully consider these parameters to determine the optimal super-elevation and friction coefficient values, highlighting the importance of road design in ensuring passenger safety.

5.5. Speed profile generation

Navigating an unfamiliar road with sharp curves can pose a significant risk to drivers if they fail to adjust their speed accordingly. In such situations, the driver must possess the skill and ability to simultaneously maneuver the steering wheel and reduce speed to navigate through the curve safely without leaving their lane. However, with the advent of autonomous driving systems, the same principles of safe navigation must be applied. Autonomous driving systems must be programmed to adapt the vehicle speed with the path curvature and speed limits. Such programming would require an understanding of the physics of driving as this helps to maintain the autonomous vehicle stability, prevents the vehicle from veering off course, and ensures the safety of passengers and other road users.

Speed profile planning is a critical aspect of trajectory planning that involves determining the optimal speed for navigating through sharp curves v_c and adhering to vehicle speed limits. By extracting the ideal speed for each segment of the trajectory, a speed profile is created that guides the autonomous vehicle along the designated path. However, the challenge of maintaining a comfortable ride for passengers during variable velocity navigation requires controlling the speed variation within acceleration limits. To achieve smooth motion and human comfort, a crucial factor in speed profile planning is determining the appropriate distance required for the vehicle to reach the desired speed within defined acceleration boundaries. This distance is influenced by the current speed v_a, desired speed v_d, and acceleration value a, and can be calculated using the following equation [158]:

$$d = \frac{{v_d}^2 - {v_a}^2}{2 \cdot a} \tag{5.21}$$

Once the real curves in the predetermined trajectory have been defined, the optimal speed for each curve has been calculated, and the required distance necessary to achieve the desired speed while maintaining passenger comfort has been determined, the speed profile can be generated and applied to the vehicle throughout the entire trajectory. The algorithm for generating the speed profile is illustrated in Figure 5.7. By following the generated speed profile, the autonomous vehicle can navigate the trajectory with precision, avoiding any potential hazards and ensuring a comfortable ride for all passengers.

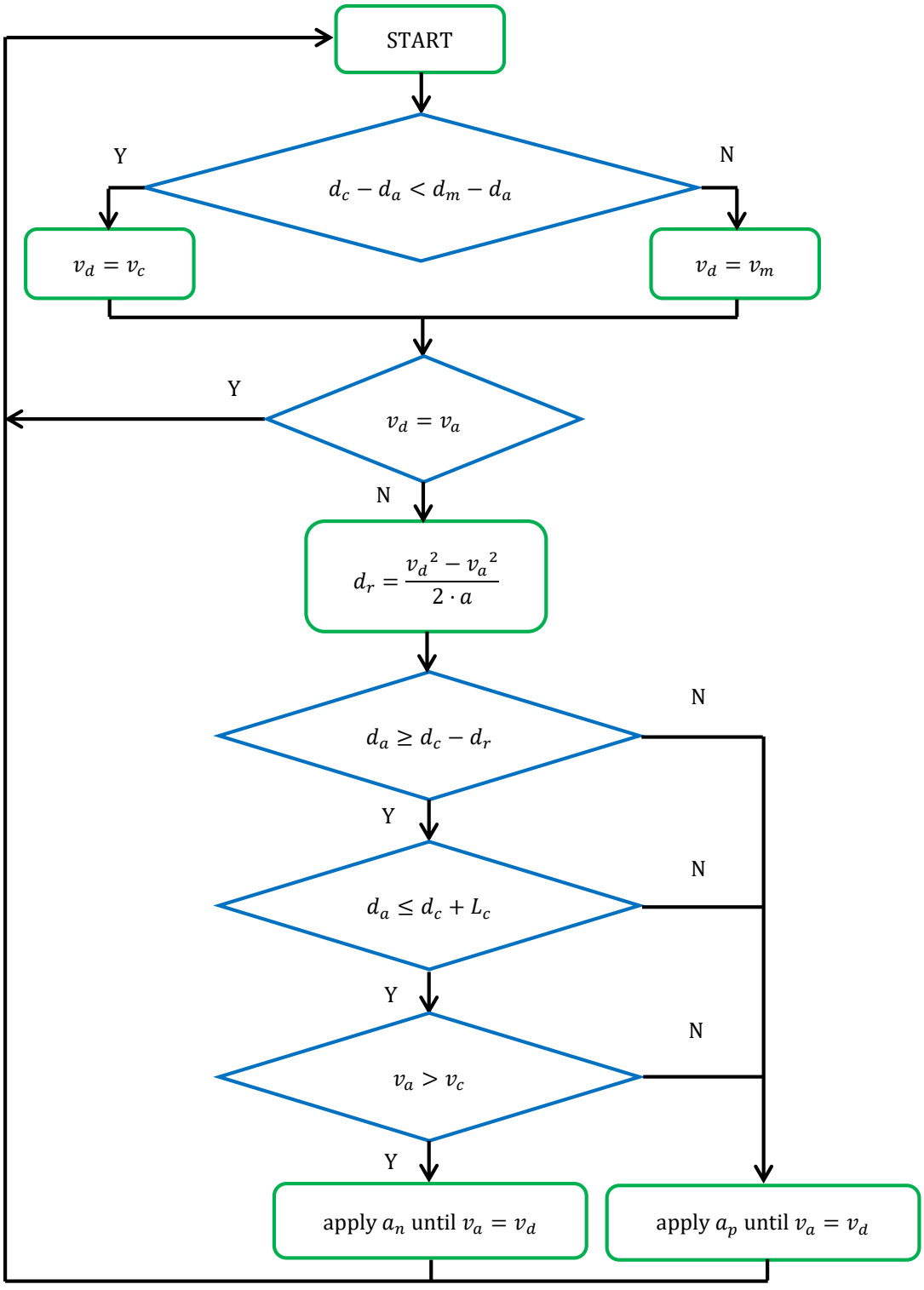

Figure 5.7. Speed planning algorithm.

Based on the information presented in Figure 5.7, the implementation of the speed planning algorithm can be achieved through the execution of a series of well-defined steps:

- At the onset of the motion, the vehicle begins from a stationary position with an initial velocity v_i, and the maximum permissible speed is capped at v_m.
- The algorithm for determining the desired speed of a vehicle takes into account various factors, including the actual traveled distance d_a, the upcoming curve distance d_c, and the distance to maximum speed d_m. Based on these inputs, the algorithm intelligently selects the appropriate speed for the vehicle to achieve. If the difference between the curve distance and the actual traveled distance is smaller than the difference between the distance to maximum speed and the actual traveled distance, the algorithm selects the next curve speed as the desired speed. In this way, the vehicle can safely navigate the curve without risking any accidents or losing control. However, if the difference between the distance to the maximum speed limit and the actual traveled distance is greater than the difference between the curve distance and the actual traveled distance, the algorithm selects the maximum speed limit as the desired speed. This allows the vehicle to make up for lost time and cover more ground quickly while staying within safe limits.
- Once the actual speed and the desired speed have been established, Equation (5.21) is used to calculate the required distance d_r that is necessary to achieve the desired speed. This calculation takes into account any discrepancies between the actual speed and the desired speed. By using this equation, the system can determine the distance needed to reach the desired speed, allowing for more precise control of the vehicle's acceleration.
- The vehicle applies a deceleration a_n to reach the desired speed, but only if one of these conditions are met. Firstly, the actual distance travelled must exceed the difference between the curve distance and the required distance to reach the curve. Secondly, the actual distance travelled must be less than the sum of the curve distance and the curve length L_c. Lastly, the vehicle's actual speed must be greater than the speed required for the upcoming curve. In the event that all of these conditions are not met, an acceleration a_p is applied instead to achieve the desired speed. By adhering to these parameters, the vehicle can maintain safe and efficient speed while navigating curves.

5.6. Simulation results

In this section, we showcase the exceptional vehicle navigation performance achieved through the utilization of our speed planning algorithm with super-twisting control on the two predefined trajectories discussed in Chapter 4. Our method stands out in its ability to guarantee robustness and versatility, a fact that we demonstrate through extensive simulations. By presenting the outcomes of our simulations, we aim to provide valuable insights into the potential of our algorithm to revolutionize vehicle navigation in real-world scenarios.

Figure 5.8 illustrates the complete workflow for vehicle trajectory-tracking, which employs the technique of speed planning with super-twisting control. The trajectory coordinates are analyzed to extract crucial information about sharp curves in the path, which is then utilized to compute the optimal velocity for each curve. Then a speed profile algorithm is used to enable the vehicle to travel along the path at a variable velocity, with smooth and precise navigation. The generated speed profile is integrated into the lateral control law formula, which calculates the required steering angle, ensuring that the vehicle maintains its trajectory without any sudden or jerky changes in direction.

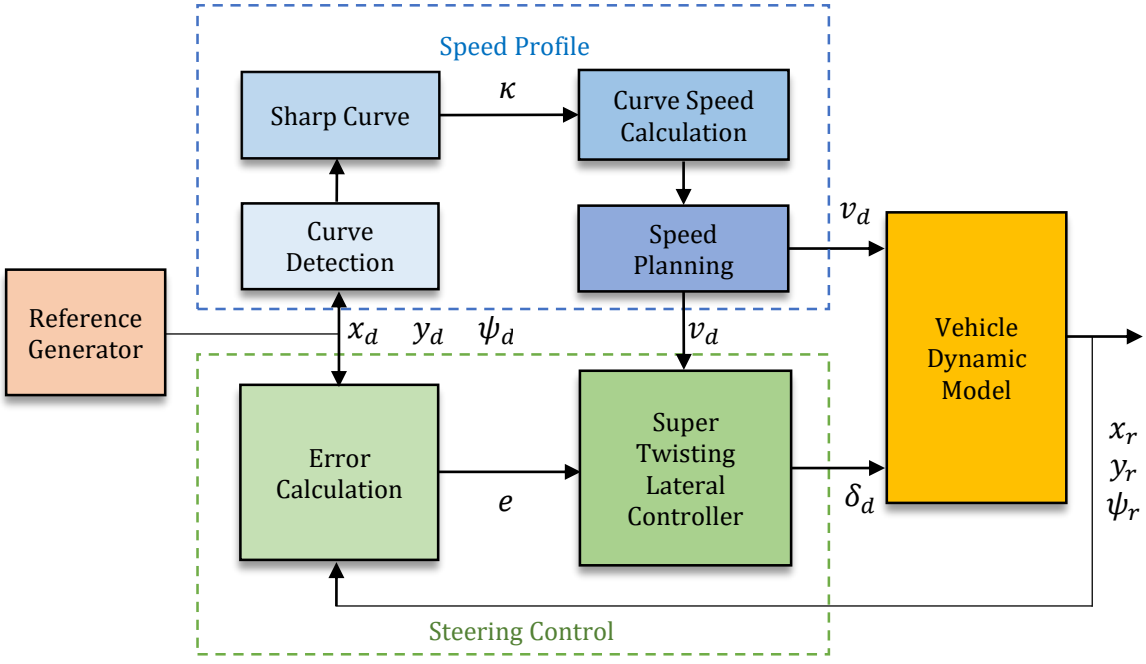

Figure 5.8. Trajectory tracking structure using speed profile generation.

In Figure 5.9, we present the sharp curves that were identified in each trajectory using the curve identification algorithm according to "A Policy on Geometric Design of Highways and Streets" criteria. The visual representation of these curves allows for a more comprehensive understanding of the trajectories and their complexity. The first trajectory is found to contain four sharp curves, whereas the second trajectory contains six sharp curves, as depicted in the figure. The use of the curve identification algorithm provides an efficient and effective way to analyze trajectories, enabling us to design speed planning algorithms that can handle the challenges posed by sharp curves. This information is crucial for the development of advanced navigation systems that can accurately and reliably guide vehicles through complex terrains.

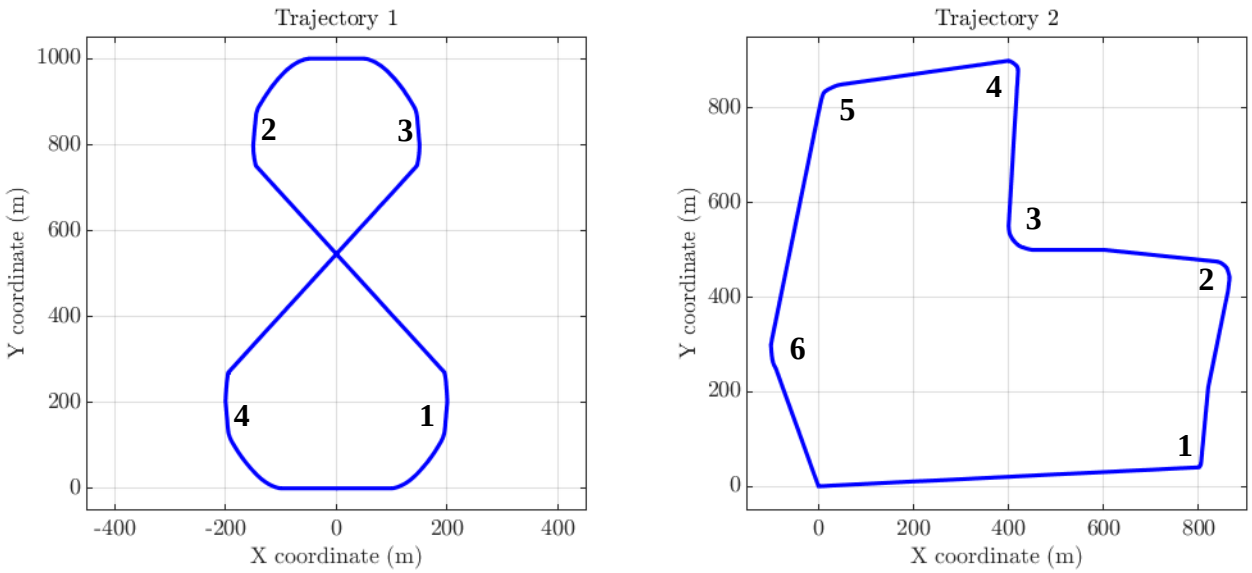

Figure 5.9. Trajectories sharp curves.

In Figure 5.10, the speed profile generated for vehicle tracking is presented. The sophisticated speed planning algorithm takes into consideration the trajectory curvatures to produce an appropriate speed profile for the vehicle to travel at, ensuring not only smooth tracking but also high precision. By dynamically adjusting the vehicle's speed, the algorithm enables it to precisely follow the intended trajectory, while taking into account various factors. This precision in tracking can improve the safety of the vehicle, reduce energy consumption, and enhance the overall driving experience.

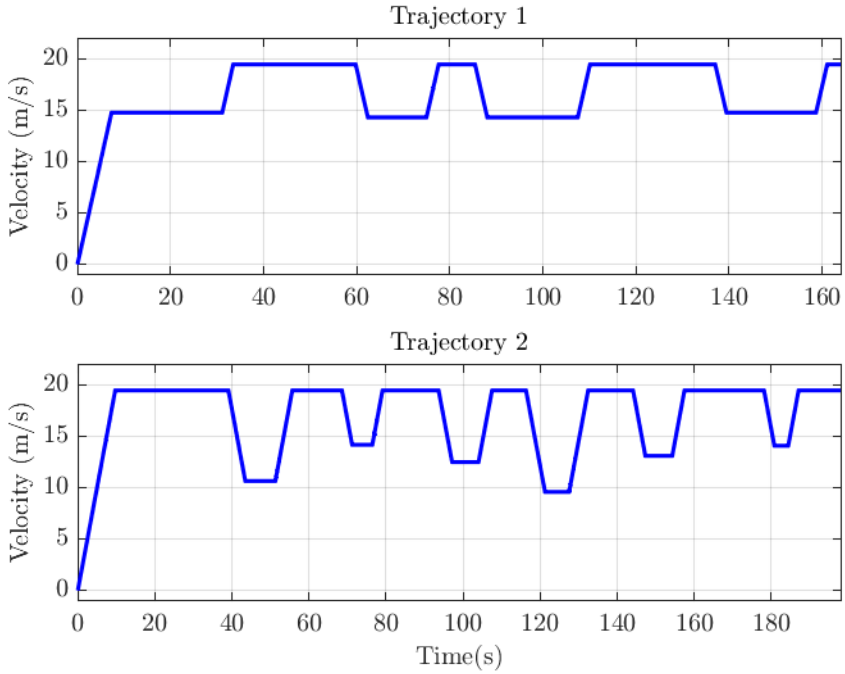

Figure 5.10. Speed profiles for trajectories 1&2 using speed planning.

Figure 5.11 displays the outcomes of tracking the vehicle, indicating the impressive performance of the speed planning algorithm combined with the super-twisting controller. The blue line in the figure represents the reference trajectory, while the red line shows the real trajectory of the vehicle.

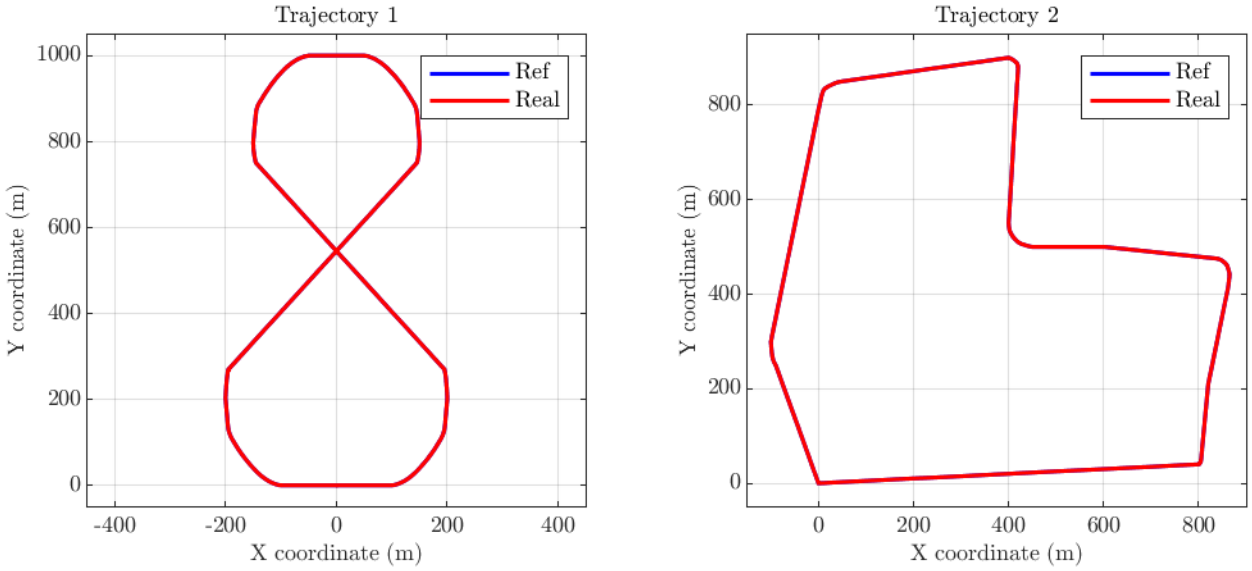

Figure 5.11. Vehicle tracking trajectories using speed planning.

The graph clearly shows that the vehicle closely follows the reference trajectory, providing solid evidence of the efficiency of the speed planning algorithm when used with the super-twisting controller. Additionally, the reference and actual trajectories are even more similar than when using the super-twisting algorithm with constant velocity, highlighting the outstanding precision and accuracy of this method.

Figures 5.12 and 5.13 illustrate the outcomes of the lateral and orientation error measurements of the entire path, respectively. These figures reveal a noteworthy finding that the lateral and orientation errors obtained from the integration of the speed planning algorithm are significantly lower than those obtained from using the constant velocity approach in Chapter 4. This indicates that the algorithm plays a crucial role in reducing the errors by optimizing the vehicle velocity during sharp curves. By doing so, it allows the vehicle to more accurately track the real trajectory, resulting in a more precise and accurate path. This noteworthy finding showcases the exceptional effectiveness of the designed algorithm in enhancing the overall path planning process, positioning it as a valuable asset in numerous autonomous vehicle systems and opening up potential applications across a broad spectrum.

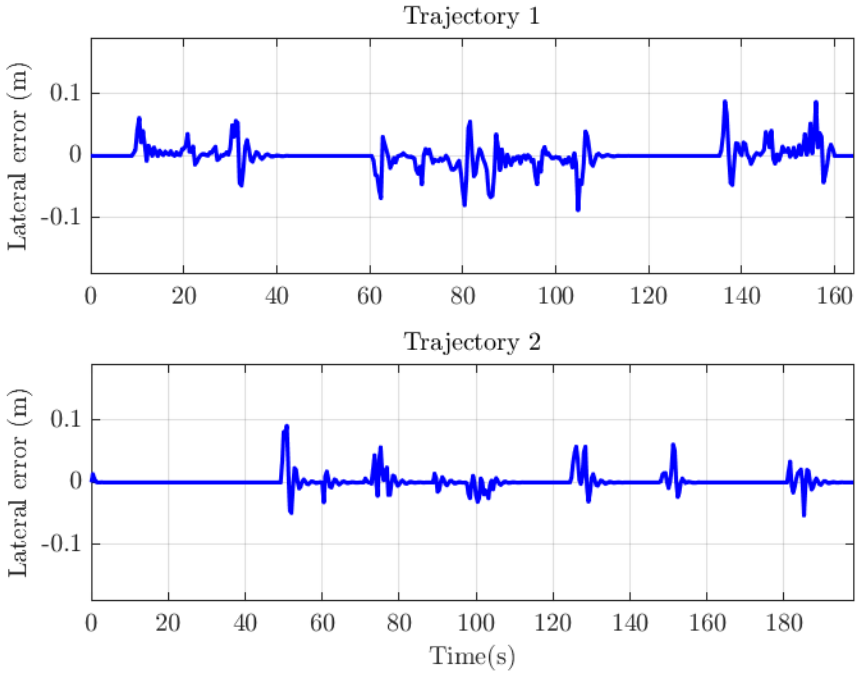

Figure 5.12. Lateral error for trajectories 1&2 using speed planning.

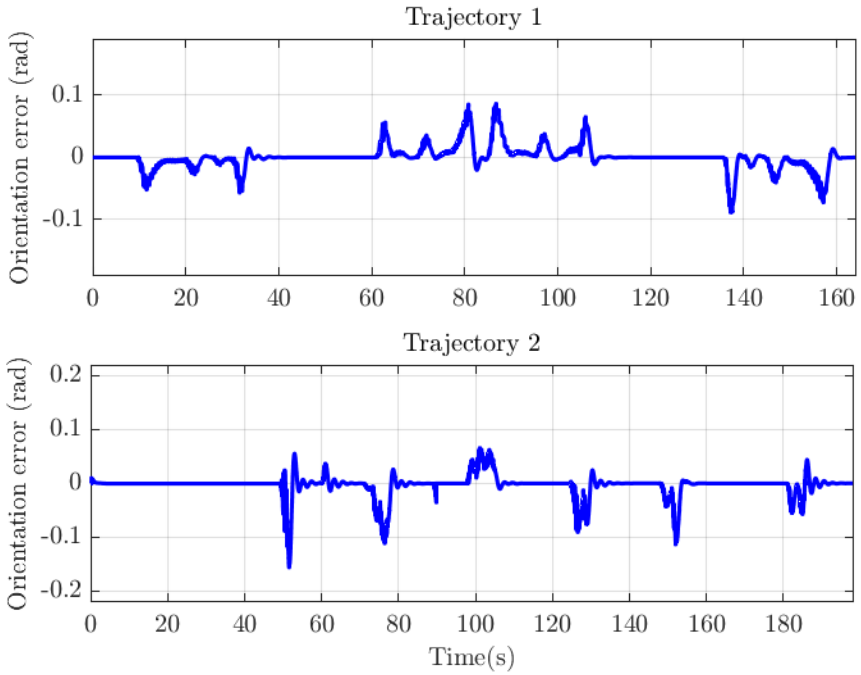

Figure 5.13. Orientation error for trajectories 1&2 using speed planning.

Figures 5.14 and 5.15 provide a visualization of the front steering angle and vehicle yaw rate as the vehicle navigates through the desired trajectories. The speed planning algorithm plays a critical role in the generation of an ideal speed profile, which is then utilized in the lateral control block to provide a steering angle set point that is applied to the vehicle's steering wheel. This approach is highly effective, as it provides a smooth tracking performance, resulting in better control and stability during navigation. By incorporating the generated speed profile in the steering angle calculation procedure, the generated angle is more appropriate, which significantly enhances the vehicle's overall maneuverability and performance. Furthermore, the steering angle response is more precise and stable, leading to more accurate tracking of the desired trajectory and comfortable travel for the passengers. The combination of the trajectory curvatures and the obtained speed profile from the speed planning algorithm into the lateral control block offers a robust solution for trajectory tracking tasks in autonomous vehicle fields, enabling them to navigate complex environments with greater accuracy and efficiency. This approach has the potential to revolutionize the field of autonomous vehicle technology, paving the way for safer and more reliable transportation systems.

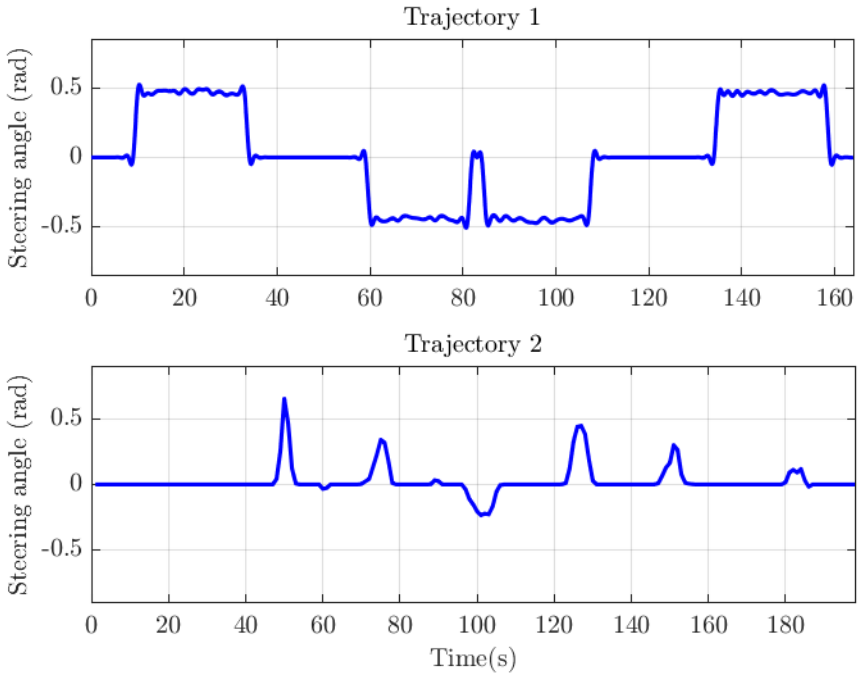

Figure 5.14. Steering angle for trajectories 1&2 using speed planning.

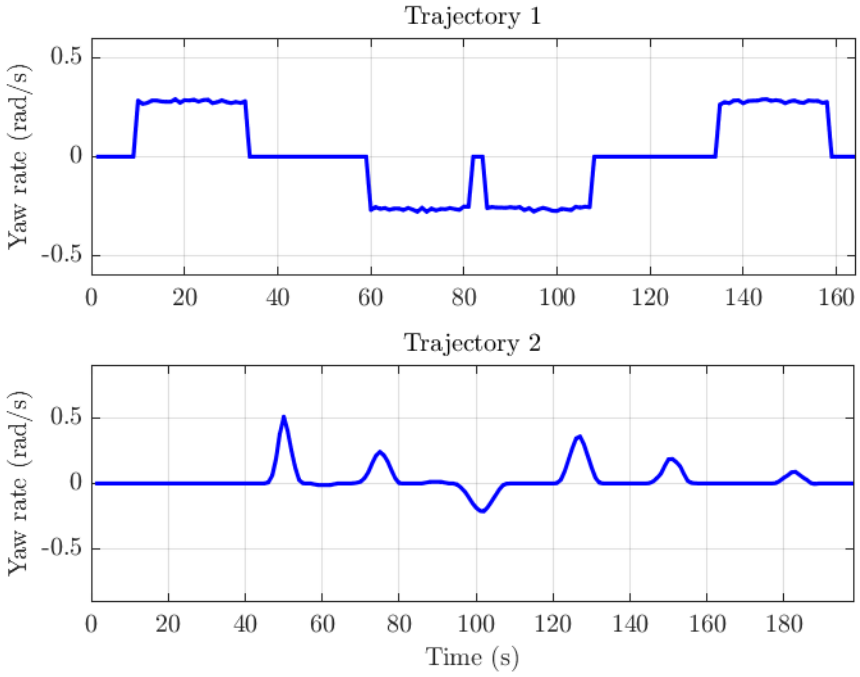

Figure 5.15. Yaw rate for trajectories 1&2 using speed planning.

Table 5.1 and Table 5.2 provide a comprehensive summary of the lateral and orientation error results obtained from trajectory tracking using the speed planning algorithm. The values of the RMS

errors obtained from trajectory 1 and trajectory 2 are $0.016\,m$ and $0.020\,m$, and $0.015\,rad$ and $0.027\,rad$, respectively. These results indicate that the speed planning algorithm significantly reduces the errors in trajectory tracking during sharp curves. Moreover, the maximum error values obtained from all the sharp curves are $0.088\,m$ and $0.091\,m$ for lateral error, and $0.088\,rad$ and $0.035\,rad$ for orientation error, respectively, for both trajectories 1 and 2. These findings highlight the robustness of the speed planning algorithm in decreasing the errors in the trajectory tracking, leading to more accurate and reliable navigation of the path. Broadly speaking, the use of this algorithm offers a promising solution to enhance the trajectory tracking performance of autonomous vehicles driving.

Table 5.1. Lateral and orientation errors for trajectory 1 using speed planning.

Curve	1	2	3	4	Average
MAX lateral error (m)	0.060	0.080	0.087	0.088	0.079
RMS lateral error (m)	0.013	0.017	0.016	0.018	0.016
MAX orientation error (rad)	0.056	0.085	0.086	0.088	0.079
RMS orientation error (rad)	0.011	0.016	0.016	0.018	0.015

Table 5.2. Lateral and orientation errors for trajectory 2 using speed planning.

Curve	1	2	3	4	5	6	Average
MAX lateral error (m)	0.091	0.056	0.031	0.057	0.063	0.051	0.058
RMS lateral error (m)	0.038	0.020	0.010	0.023	0.018	0.013	0.020
MAX orientation error (rad)	0.156	0.111	0.066	0.090	0.113	0.057	0.099
RMS orientation error (rad)	0.035	0.031	0.025	0.026	0.027	0.020	0.027

The results of the comparison between the vehicle navigation errors with and without using the speed planning algorithm are presented in Figures 5.16 and 5.17. These figures show a significant improvement in the performance of the algorithm, as demonstrated by the reduction in the lateral RMS error by 70.37% and 45.45% for trajectory 1 and 2, respectively. Moreover, the orientation RMS error was also significantly reduced by 90.43% and 68.60% for the same trajectories, indicating the effectiveness of the speed-planning algorithm with super-twisting controller in providing high-precision trajectory-tracking with minimal error. These remarkable results demonstrate the superiority of this combined designed techniques over other existing algorithms. The success of this algorithm in reducing the navigation errors can be attributed to its ability to generate optimal speed based on real-time information about the vehicle's motion, while also taking into account the constraints of the vehicle and the environment.

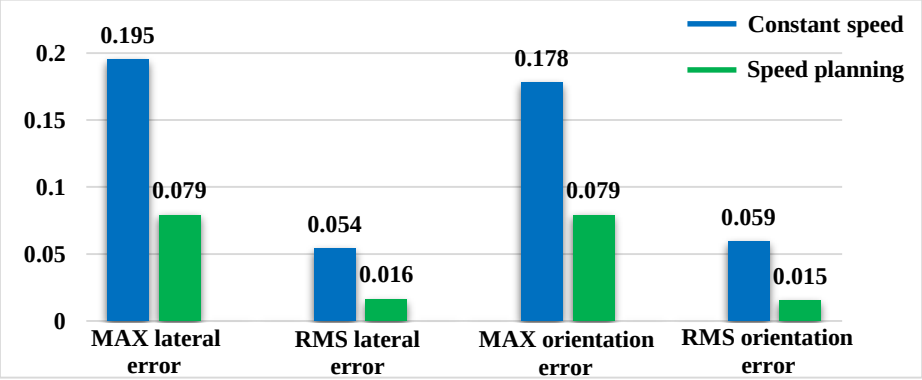

Figure 5.16. Average errors for trajectory 1.

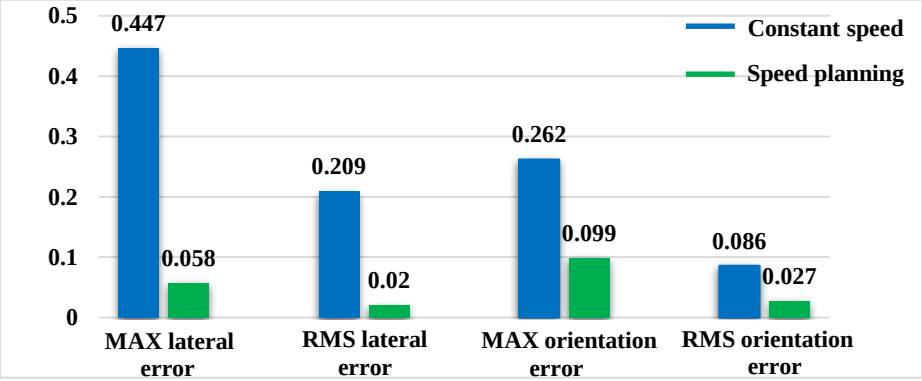

Figure 5.17. Average errors for trajectory 2.

5.7. Conclusion

In this chapter, we have developed a speed planning algorithm that is capable of creating an appropriate speed profile for navigating a predetermined trajectory with a vehicle. The first step of the algorithm was to detect and recognize the primary curves that are present within the pre-established trajectory. Once the primary curves had been identified, their fundamental properties were extracted. Next, the algorithm calculated the velocity required for each sharp curve. Finally, a method for generating a speed profile that would allow for successful navigation of the entire trajectory with a vehicle was proposed.

The primary benefit of the speed planning algorithm we have developed lies in its ability to adapt to different scenarios, as it can be integrated into the vehicle's lateral control system. This integration allows the vehicle to maintain appropriate speeds while navigating through straight and curved sections of a route. Additionally, the algorithm is capable of identifying sharp curves ahead of time and gradually reducing the vehicle's speed by applying a comfortable deceleration value. This ensures that the vehicle reaches an optimal speed in preparation for traversing the curve safely and comfortably.

The obtained results using Matlab/Simulink software showed impressive improvement in autonomous vehicle performance. The tracking results using our approach showed significant reduction of lateral errors. This improvement may potentially prevent accidents and reduce severe injuries in real driving scenarios, which is exactly the aim of any autonomous vehicle.

CHAPTER 6

VEHICLE VELOCITY CONTROL

Contents **Page**

6.1. Introduction

In the preceding chapter, we introduced a cutting-edge speed planning algorithm meticulously crafted to optimize the velocity of autonomous vehicles as they traverse predetermined trajectories. The fundamental concept underpinning this algorithm is to leverage the key attributes of trajectory curvature, enabling the generation of an ideal speed profile. By leveraging this approach, our algorithm ensures that the vehicle attains an elevated speed level in advance, thus facilitating a safe and comfortable maneuvering of curves.

To accurately emulate the behavior of an autonomous electric vehicle, we employ the derived speed profiles from the meticulously designed speed planning algorithm to govern the drive speed of the vehicle, rather than directly manipulating its overall velocity. Deliberately chosen for this research, the induction motor serves as the prime traction element of the autonomous electric vehicle. This deliberate selection stems from the motor's remarkable ability to effectively reach the desired reference speed, all while adhering to strict current limits to ensure operational safety. Moreover, the induction motor demonstrates exceptional energy efficiency, optimizing the vehicle's overall energy consumption [75-79]. By leveraging the unique characteristics of the induction motor, we establish a robust and efficient framework for achieving precise speed control in our autonomous electric vehicle system.

To regulate the speed of the induction motor, a multitude of control techniques have been devised. In this study, however, we introduce a back-stepping SVM approach meticulously crafted to ensure unparalleled performance and robustness of the induction motor. By attaining precise control over the induction motor, our approach enables the autonomous vehicle to effortlessly navigate through predefined trajectories, guaranteeing a safe and comfortable traversal of curves and other demanding road conditions. This advanced control technique serves as a key enabler for enhancing the overall capabilities and efficiency of autonomous electric vehicles.

To assess the effectiveness of the back-stepping SVM technique, comprehensive evaluations were conducted using both numerical simulations and experimental implementation. MATLAB/Simulink was utilized for conducting simulations, providing a reliable platform for analyzing and optimizing the control algorithm. Additionally, real-time experiments were carried out with the dSpace 1104 board to validate the theoretical findings and ensure practical feasibility.

6.2. Back-stepping approach

Back-stepping control is a nonlinear control technique that aims to control complex systems with uncertain dynamics. It provides a systematic approach to design control laws for achieving stability and tracking performance in nonlinear systems. This control theory has gained significant attention in recent years due to its effectiveness in dealing with complex and uncertain systems. In this section, we will explore the principles and key concepts of back-stepping control theory and its applications in various fields [159].

6.2.1. Principles of back-stepping control:

The main principles of the back-stepping approach are based on the following steps [160]:

- **Lyapunov Stability Analysis:** At the core of back-stepping control lies the utilization of Lyapunov stability analysis. This analysis involves the selection of a Lyapunov function that can prove the stability of the system. In the case of back-stepping control, a series of Lyapunov functions are designed to stabilize the system incrementally. This stepwise approach ensures that the system achieves stability in a systematic manner.
- **Recursive Design:** Back-stepping control follows a recursive design procedure. To tackle the control problem effectively, it is broken down into a sequence of subsystems. Each subsystem is responsible for stabilizing a specific dynamics aspect of the overall system. By designing control laws for each subsystem, the stability and tracking performance of the entire system can be achieved through a cascaded structure.
- **Virtual Control:** An integral concept employed in back-stepping control is virtual control. This involves introducing a desired control input to guide the system towards a desired trajectory or behavior. The virtual control input is determined based on the system's error, which represents the deviation from the desired behavior, and the desired system behavior itself. By manipulating the virtual control input, the system can be steered towards the desired state while maintaining stability.

By incorporating these steps, back-stepping control provides a systematic framework for designing control laws that achieve stability and performance objectives in a recursive manner.

6.2.2. Recursive control design

The concept of Recursive control design involves stabilizing a larger system by initially stabilizing a smaller subsystem and then gradually extending the controlled stability outward. This approach is based on the assumption that a lower-order subsystem, represented by the Equation (6.1) has already been stabilized at the origin using a control $u\,(x)$ such that $u\,(0) = 0$. The stabilization of this subsystem cannot be achieved directly through conventional methods. Additionally, it is assumed that a Lyapunov function V is known for the stabilized subsystem [161].

$$\dot{x} = A(x) + B(x) \cdot u \tag{6.1}$$

To extend the controlled stability to the larger system, a control $u_1(x, z_1)$ is designed for the system in Equation (6.2) in such a way that z_1 follows the desired control $u\,(x)$.

$$\dot{z}_1 = A_1(x, z_1) + B_1(x, z_1) \cdot u_1 \tag{6.2}$$

The design of this control is based on an augmented Lyapunov function candidate:

$$V_1(x, z_1) = V(x) + \frac{1}{2}(z_1 - u)^2 \tag{6.3}$$

where the control u_1 can be chosen to ensure that $\dot{V}_1$ is bounded away from zero.

Similarly, a control $u_2(x, z_1, z_2)$ is designed for the system in Equation (6.4) so that z_2 follows the desired control $u_1(x, z_1)$.

$$\dot{z}_2 = A_2(x, z_1, z_2) + B_2(x, z_1, z_2) \cdot u_2 \tag{6.4}$$

The design of this control is based on an augmented Lyapunov function candidate:

$$V_2(x, z_1, z_2) = V_1(x, z_1) + \frac{1}{2}(z_2 - u_1)^2 \tag{6.5}$$

where the selection of control u_1 ensures that $\dot{V}_2$ remains at a significant distance from zero.

This process continues recursively until the actual control u is determined. At each step, the fictitious controls are used to stabilize the corresponding fictitious states to the desired control of the previous step. Finally, the fictitious control u stabilizes the state x to the origin.

6.3. Electric vehicle speed control using back-stepping approach

6.3.1. Induction motor presentation

To regulate the speed of an induction motor, one can derive dynamic equations from the induction motor model presented in Chapter 3 by taking into account the stator current and rotor flux as state variables in the stationary reference $(\alpha - \beta)$ frame:

$$\frac{di_{s\alpha}}{dt} = -\frac{\gamma}{\sigma \cdot L_s} \cdot i_{s\alpha} + \frac{T_{mr}}{\sigma \cdot L_s \cdot T_r} \phi_{r\alpha} + \frac{T_{mr} \cdot \omega}{\sigma \cdot L_s} \phi_{r\beta} + \frac{1}{\sigma \cdot L_s} V_{s\alpha} \tag{6.6}$$

$$\frac{di_{s\beta}}{dt} = -\frac{\gamma}{\sigma \cdot L_s} \cdot i_{s\beta} + \frac{T_{mr}}{\sigma \cdot L_s \cdot T_r} \phi_{r\beta} - \frac{T_{mr} \cdot \omega}{\sigma \cdot L_s} \phi_{r\alpha} + \frac{1}{\sigma \cdot L_s} V_{s\beta} \tag{6.7}$$

$$\frac{d\phi_{r\alpha}}{dt} = \frac{L_m}{T_r} i_{s\alpha} - \frac{1}{T_r} \phi_{r\alpha} - \omega \cdot \phi_{r\beta} \tag{6.8}$$

$$\frac{d\phi_{r\beta}}{dt} = \frac{L_m}{T_r} i_{s\beta} - \frac{1}{T_r} \phi_{r\beta} - \omega \cdot \phi_{r\alpha} \tag{6.9}$$

$$J.\frac{d\Omega}{dt} = T_e - T_L - f \cdot \Omega \tag{6.10}$$

The electromagnetic torque equation is the result of multiplying the rotor flux and stator currents through a cross product. It describes the magnetic field's influence on the produced torque:

$$T_e = \eta(\phi_{r\alpha} \cdot i_{s\beta} - \phi_{r\beta} \cdot i_{s\alpha}) \tag{6.11}$$

The magnitude of the rotor flux, ϕ_r, is determined by:

$$\phi_r = \sqrt{{\phi_{r\alpha}}^2 + {\phi_{r\beta}}^2} \tag{6.12}$$

where: $\sigma = 1 - \frac{{L_m}^2}{L_s \cdot L_r}$; $\gamma = R_s + \frac{L_s(1-\sigma)}{T_r}$; $T_{mr} = \frac{L_m}{L_r}$; $T_r = \frac{L_r}{R_r}$; $\eta = p\frac{L_m}{L_r}$.

Additionally, $V_{s\alpha\_\beta}$, $i_{s\alpha\_\beta}$, $\phi_{r\alpha\_\beta}$, R_s, R_r, L_s, L_r, L_m, ω, Ω, J, f, p, and T_L are stator $\alpha - \beta$ frame voltage, stator $\alpha - \beta$ frame current, stator $\alpha - \beta$ frame flux, stator resistance, rotor resistance, stator inductance, rotor inductance, mutual inductance, electrical speed, mechanical speed, motor inertia, viscous damping coefficient, number of pair poles, and load torque.

6.3.2. Back-stepping SVM control design

This section describes a stationary reference $(\alpha - \beta)$ frame back-stepping control technique that is used to regulate the speed of an AEV induction motor. The designed controller comprises four control loops - two outer loops and two inner loops - each with its own control law. The outer loops are responsible for regulating the speed and rotor flux, respectively. The outputs of these two loops, which involve the subtraction of cross multiplication and the summation of direct multiplication of the global stator currents and rotor flux, serve as set-points for the two inner loops. By selecting an appropriate Lyapunov function, the control law of the overall system can be ensured. These findings are a significant contribution to the field of electrical engineering, as they demonstrate a practical approach to optimizing the performance of induction motors in AEVs, with potential applications in a variety of industries.

6.3.2.1. Outer loops control

The control of the speed and rotor flux is included in the outer loops, and as such, the tracking errors for these loops are defined as follows:

$$e_1 = \Omega_{ref} - \Omega \tag{6.13}$$

$$e_2 = \phi_{r_{ref}}^2 - {\phi_r}^2 \tag{6.14}$$

Consequently, the dynamic errors' gradients are as follows:

$$\frac{de_1}{dt} = \frac{d\Omega_{ref}}{dt} - \frac{d\Omega}{dt} \tag{6.15}$$

$$\frac{de_2}{dt} = \frac{d\phi_{r_{ref}}^2}{dt} - \frac{d{\phi_r}^2}{dt} \tag{6.16}$$

Utilizing the magnetic, mechanical, and electromagnetic torque equations, Equations (6.15) and (6.16) can be transformed into:

$$\frac{de_1}{dt} = \frac{d\Omega_{ref}}{dt} - \frac{1}{J}[\eta(\phi_{r\alpha} \cdot i_{s\beta} - \phi_{r\beta} \cdot i_{s\alpha}) - T_L - f \cdot \Omega] \tag{6.17}$$

$$\frac{de_2}{dt} = \frac{d\phi_{r_{ref}}^2}{dt} - \frac{2 \cdot L_m}{T_r}\left(\phi_{r\alpha} \cdot i_{s\alpha} + \phi_{r\beta} \cdot i_{s\beta}\right) + \frac{2}{T_r}{\phi_r}^2 \tag{6.18}$$

To guarantee the stability of the outer loops regulating speed and rotor flux, a Lyapunov candidate V_{B1} is defined as a first positive definite function:

$$V_{B1} = \frac{1}{2}e_1^2 + \frac{1}{2}e_2^2 \tag{6.19}$$

The derivative of Equation (6.19) with respect to time is:

$$\frac{dV_{B1}}{dt} = e_1\frac{de_1}{dt} + e_2\frac{de_2}{dt} \tag{6.20}$$

Substituting Equations (6.17) and (6.18) into Equation (6.20) results in the following:

$$\frac{dV_{B1}}{dt} = e_1\left(\frac{d\Omega_{ref}}{dt} - \frac{1}{J}\left[\eta\left(\phi_{r\alpha}\cdot i_{s\beta} - \phi_{r\beta}\cdot i_{s\alpha}\right) - T_L - f\cdot\Omega\right] + k_1\cdot e_1\right) - k_1\cdot e_1^2 +$$
$$e_2\left(\frac{d\phi_{rref}^2}{dt} - \frac{2.L_m}{T_r}\left(\phi_{r\alpha}\cdot i_{s\alpha} + \phi_{r\beta}\cdot i_{s\beta}\right) + \frac{2}{T_r}{\phi_r}^2 + k_2\cdot e_2\right) - k_2\cdot e_2^2 \tag{6.21}$$

where the constants k_1 and k_2 are closed loop constants with positive values, ensuring the convergence of the errors in speed and rotor flux to zero.

To guarantee the asymptotic stability of the outer loops, the derivative of a positive definite Lyapunov function must be semi-negative definite:

$$\frac{dV_{B1}}{dt} = -k_1\cdot e_1^2 - k_2\cdot e_2^2 < 0 \tag{6.22}$$

Equating Equations (6.21) and (6.22) leads to the deduction of the outer loops' outcome as follows:

$$C_{1_{ref}} = \frac{J}{\eta}\left(\frac{d\Omega_{ref}}{dt} + \frac{T_L}{J} + \frac{f}{J}\Omega + k_1\cdot e_1\right) \tag{6.23}$$

$$C_{2_{ref}} = \frac{T_r}{2\cdot L_m}\left(\frac{d\phi_{rref}^2}{dt} + \frac{2}{T_r}{\phi_r}^2 + k_2\cdot e_2\right) \tag{6.24}$$

6.3.2.2. Inner loops control

The inner loops calculate the control laws $V_{s\alpha}$ and $V_{s\beta}$ using the outcome of the outer loops as a reference. The tracking errors are defined as follows:

$$e_3 = C_{1_{ref}} - C_1 \tag{6.25}$$

$$e_4 = C_{2_{ref}} - C_2 \tag{6.26}$$

Therefore, the gradients of these dynamic errors are:

$$\frac{de_3}{dt} = \frac{dC_{1_{ref}}}{dt} - \frac{dC_1}{dt} \tag{6.27}$$

$$\frac{de_4}{dt} = \frac{dC_{1_{ref}}}{dt} - \frac{dC_2}{dt} \tag{6.28}$$

Utilizing the outcome of the outer loops for speed and rotor flux, as well as the electrical and magnetic equations, the gradients of the errors for the inner loops are as follows:

$$\frac{de_3}{dt} = \frac{f-k_1 \cdot J}{\eta \cdot J}(\eta \cdot C_1 - f \cdot \omega - T_L) + \left(\frac{1}{T_r} + \frac{\gamma}{\sigma \cdot L_s}\right) C_1 + \omega \cdot C_2 + \frac{T_{mr}}{\sigma \cdot L_s}\omega \cdot \phi_r^2 + \frac{\phi_{r\beta}}{\sigma \cdot L_s} V_{s\alpha} - \frac{\phi_{r\alpha}}{\sigma \cdot L_s} V_{s\beta} \tag{6.29}$$

$$\frac{de_4}{dt} = \frac{2-k_2 \cdot T_r}{L_m}\left(\frac{L_m}{T_r} C_2 - \frac{1}{T_r}\phi_r^2\right) + \left(\frac{1}{T_r} + \frac{\gamma}{\sigma \cdot L_s}\right) C_2 - \omega \cdot C_1 - \frac{T_{mr}}{T_r \cdot \sigma \cdot L_s} \cdot \phi_r^2 - \frac{L_m}{T_r}\left(i_{s\alpha}^2 + i_{s\beta}^2\right) - \frac{\phi_{r\alpha}}{\sigma \cdot L_s} V_{s\alpha} - \frac{\phi_{r\beta}}{\sigma \cdot L_s} V_{s\beta} \tag{6.30}$$

To ensure the stability of the inner loops, a second positive definite Lyapunov candidate V_{B2} is defined as follows:

$$V_{B2} = \frac{1}{2} e_3^2 + \frac{1}{2} e_4^2 \tag{6.31}$$

Its derivative is calculated in the following manner:

$$\frac{dV_{B2}}{dt} = e_3 \frac{de_3}{dt} + e_4 \frac{de_4}{dt} \tag{6.32}$$

Using Equations (6.29) and (6.30), Equation (6.32) can be expressed as follows:

$$\frac{dV_{B2}}{dt} = e_3\left(\frac{f-k_1 \cdot J}{\eta \cdot J}(\eta \cdot C_1 - f \cdot \omega - T_L) + \left(\frac{1}{T_r} + \frac{\gamma}{\sigma \cdot L_s}\right) C_1 + \omega \cdot C_2 + \frac{T_{mr}}{\sigma \cdot L_s}\omega \cdot \phi_r^2 + \frac{\phi_{r\beta}}{\sigma \cdot L_s} V_{s\alpha} - \frac{\phi_{r\alpha}}{\sigma \cdot L_s} V_{s\beta} + k_3 \cdot e_3\right) + e_4\left(\frac{2-k_2 \cdot T_r}{L_m}\left(\frac{L_m}{T_r} C_2 - \frac{1}{T_r}\phi_r^2\right) + \left(\frac{1}{T_r} + \frac{\gamma}{\sigma \cdot L_s}\right) C_2 - \omega \cdot C_1 - \frac{T_{mr}}{T_r \cdot \sigma \cdot L_s}\phi_r^2 - \frac{L_m}{T_r}\left(i_{s\alpha}^2 + i_{s\beta}^2\right) - \frac{\phi_{r\alpha}}{\sigma . L_s} V_{s\alpha} - \frac{\phi_{r\beta}}{\sigma . L_s} V_{s\beta} + k_4 \cdot e_4\right) - k_3 \cdot e_3^2 - k_4 \cdot e_4^2 \tag{6.33}$$

where the constants k_3 and k_4 are positive and utilized to manage the rate of convergence of the inner loops.

In order to ensure the overall stability of the system, both the inner loops and the entire system must have asymptotic stability. This is achieved by making sure that the derivative of the second candidate Lyapunov function is semi negative definite:

$$\frac{dV_{B2}}{dt} = -k_3 \cdot e_3^2 - k_4 \cdot e_4^2 < 0 \tag{6.34}$$

The control law is obtained as follows to meet Equation (6.34):

$$V_{s\alpha} = \frac{\sigma \cdot L_s}{\phi_r^2}\left[\phi_{r\alpha}\left(\frac{2-k_2 \cdot T_r}{L_m}\left(\frac{L_m}{T_r}C_2 - \frac{1}{T_r}\phi_r^2\right) + \left(\frac{1}{T_r} + \frac{\gamma}{\sigma \cdot L_s}\right)C_2 - \omega \cdot C_1 - \frac{T_{mr}}{T_r \cdot \sigma \cdot L_s} \cdot \phi_r^2 - \frac{L_m}{T_r}\left(i_{s\alpha}^2 + i_{s\beta}^2\right) + k_4 \cdot e_4\right) - \phi_{r\beta}\left(\frac{f - k_1 \cdot J}{\eta \cdot J}(\eta \cdot C_1 - f \cdot \omega - T_L) + \left(\frac{1}{T_r} + \frac{\gamma}{\sigma \cdot L_s}\right)C_1 + \omega \cdot C_2 + \frac{T_{mr}}{\sigma \cdot L_s}\omega \cdot \phi_r^2 + k_3 \cdot e_3\right)\right. \tag{6.35}$$

$$V_{s\beta} = \frac{\sigma \cdot L_s}{\phi_r^2}\left[\phi_{r\beta}\left(\frac{2-k_2 \cdot T_r}{L_m}\left(\frac{L_m}{T_r} \cdot C_2 - \frac{1}{T_r} \cdot \phi_r^2\right) + \left(\frac{1}{T_r} + \frac{\gamma}{\sigma \cdot L_s}\right)C_2 - \omega \cdot C_1 - \frac{T_{mr}}{T_r \cdot \sigma \cdot L_s}\phi_r^2 - \frac{L_m}{T_r}\left(i_{s\alpha}^2 + i_{s\beta}^2\right) + k_4 \cdot e_4\right) + \phi_{r\alpha}\left(\frac{f - k_1 \cdot J}{\eta \cdot J}(\eta \cdot C_1 - f \cdot \omega - T_L) + \left(\frac{1}{T_r} + \frac{\gamma}{\sigma \cdot L_s}\right)C_1 + \omega \cdot C_2 + \frac{T_{mr}}{\sigma \cdot L_s}\omega \cdot \phi_r^2 + k_3 \cdot e_3\right)\right] \tag{6.36}$$

6.3.3. Load torque estimation

In the previous control loop design, the load torque was considered an unknown variable. However, using a torque sensor to measure it directly can be expensive. To address this, a back-stepping observer is proposed in this section. This observer is used to estimate the applied load torque and reduce uncertainty in the system. The applied load torque can be expressed based on the mechanical equation of the induction motor as follows:

$$T_L = T_e - f \cdot \Omega - J\frac{d\Omega}{dt} \tag{6.37}$$

The difference between the estimated load torque and the actual load torque is expressed as:

$$e_5 = T_L - \widehat{T_L} \tag{6.38}$$

The rate of change of the estimation error is obtained as:

$$\frac{de_5}{dt} = \frac{dT_L}{dt} - \frac{d\widehat{T_L}}{dt} \tag{6.39}$$

If it is assumed that the load torque remains constant except at certain moments, Equation (6.39) can be simplified to:

$$\frac{de_5}{dt} = -\frac{d\widehat{T_L}}{dt} \tag{6.40}$$

To ensure stability in the estimated load torque error, a positive definite Lyapunov function V_{B3} is introduced as follows:

$$V_{B3} = \frac{1}{2}{e_5}^2 \tag{6.41}$$

We can represent the time derivative of Equation (6.41) as follows:

$$\frac{dV_{B3}}{dt} = e_5\left(\frac{de_5}{dt} + k_5 \cdot e_5\right) - k_5 \cdot {e_5}^2 \tag{6.42}$$

where k_5 is a positive constant.

To ensure that the system is asymptotically stable, the derivative of the Lyapunov function must be negative semi-definite.

$$\frac{dV_{B3}}{dt} = -k_5 \cdot {e_5}^2 < 0 \tag{6.43}$$

Thus, the formula for the estimated load torque can be derived as:

$$\widehat{T_L} = T_e - f \cdot \Omega - J\frac{d\Omega}{dt} - \frac{1}{k_5} \cdot \frac{d\widehat{T_L}}{dt} \tag{6.44}$$

6.3.4. SVM strategy control

Space vector modulation has proven to be an effective technique for switching power inverters in Alternative Current (AC) drives. Its aim is to minimize current harmonic distortion by selecting appropriate switching vectors. This technique has demonstrated its capability to reduce torque and flux ripple phenomena, thereby enhancing the efficiency of the control loop. SVM is widely used in modern AC drives, and it has become a very important tool in industrial automation and control

applications. Its effectiveness in improving drive performance makes it a preferred choice for engineers and researchers in the field.

SVM is a distinct modulation technique compared to the conventional Pulse Width Modulation (PWM) method, as it utilizes the space vector representation of the inverter output instead of individual modulators for each phase. The reference voltages are generated by space voltage vector, which are components of voltage vectors in the complex plane [162]. The basic idea behind SVM is to predict the inverter voltage vector by projecting the reference vector V_{s_ref} onto the adjacent vectors corresponding to two non-zero switching states [163]. The switching vectors diagram for a two-level inverter takes the form of a hexagon, which is divided into six sectors with an expansion of 60° for each sector as depicted in Figure 6.1.

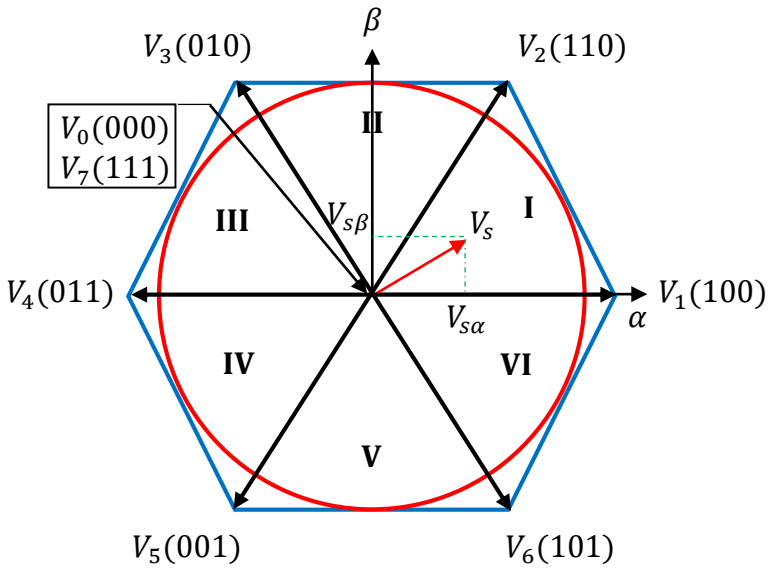

Figure 6.1. Diagram of voltage space vector.

The time required for each vector to be applied can be determined through vector calculations, while the remaining time interval will be allocated to applying the zero vector. If the reference voltage falls under sector 1 (as shown in Figure 6.2), it can be produced by utilizing the vectors V_1, V_2, and V_0 (which represents zero vector**)** [164]:

$$V_{s\_ref} = \frac{V_1 \cdot T_1 + V_2 \cdot T_2 + V_0 \cdot T_0}{T_z} \tag{6.45}$$

where:

$$T_z = T_1 + T_2 + T_0 \tag{6.46}$$

T_1, T_2, and T_0 are the corresponding application times of the voltage vectors V_1, V_2, and V_0, respectively, where T_z is the sampling time.

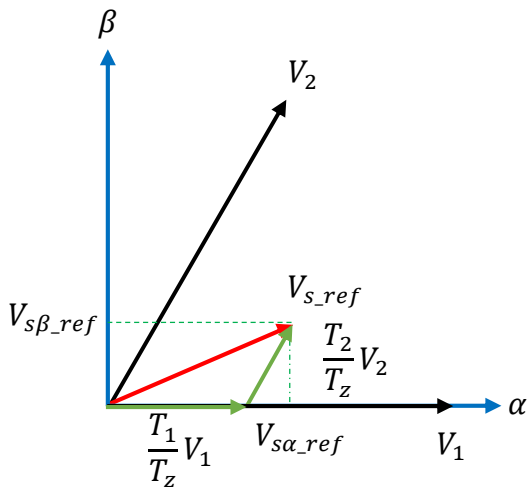

Figure 6.2. Reference vector formed by combining neighboring vectors in sector 1.

To find the durations T_1 and T_2 that correspond to voltage vectors, straightforward projections are used:

$$T_1 = \frac{T_z}{2V_{dc}}(\sqrt{6} \cdot V_{s\beta_{ref}} - \sqrt{2} \cdot V_{s\alpha\_ref}) \tag{6.47}$$

$$T_2 = \sqrt{2} \cdot \frac{T_z}{V_{dc}} \cdot V_{s\alpha\_ref} \tag{6.48}$$

Here, V_{DC} is the DC bus voltage.

The computation of switching times, also known as duty cycles, is represented by the following equation [96]:

$$T_a = \frac{T_z - T_1 - T_2}{2} \tag{6.49}$$

$$T_b = T_a + T_1 \tag{6.50}$$

$$T_c = T_b + T_2 \tag{6.51}$$

Table 6.1 gives a summary of the output, which includes switching times for every sector:

Table 6.1. Switching times for each sector.

Sector	1	2	3	4	5	6
S_1	T_b	T_a	T_a	T_c	T_b	T_c
S_2	T_a	T_c	T_b	T_b	T_c	T_a
S_3	T_c	T_b	T_c	T_a	T_a	T_b

Figure 6.3 illustrates the structure of the global back-stepping control method incorporating SVM strategy and load torque estimation.

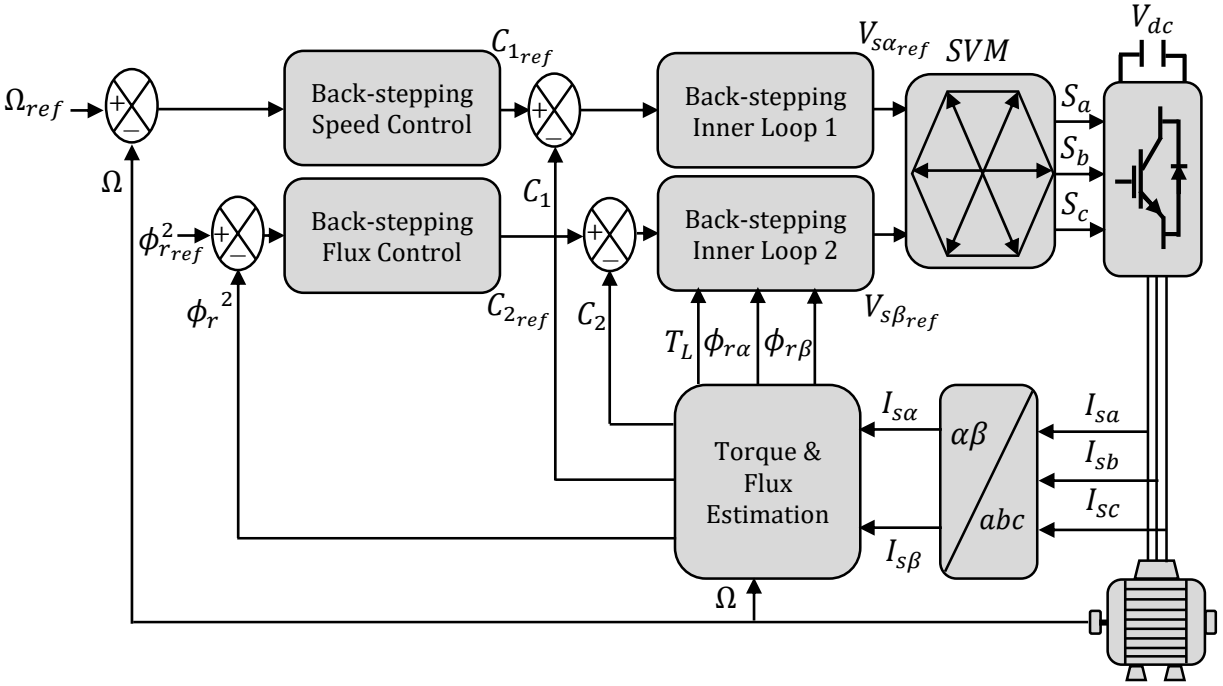

Figure 6.3. Control scheme of IM back-stepping.

6.4. Back-stepping SVM and classical DTC comparative Analysis

This section demonstrates the results obtained from applying the back-stepping control algorithm to a 3 kW squirrel-cage induction motor with three phases. The motor's characteristics can be found in the Appendix A.2, and the simulation was carried out using Matlab/Simulink software. To showcase the effectiveness of the back-stepping control technique, a comparative analysis was performed against the classical DTC method under various operating conditions. The initial startup and steady-state performance of the controlled motor with load introduction are presented first. Subsequently, the reversal of rotation direction and low-speed operation are shown. The figures for the classical DTC method are displayed in the left of the pages, while those for the back-stepping SVM technique are shown in the right of the pages.

6.4.1. Starting up and steady state with load application

In this portion, we discuss the initial and stable phases of the induction motor using a speed step reference of 1000 rpm. Subsequently, at $t = 0.5\ s$, a load of 10 $N.m$ is applied. Figures 6.4 to 6.9 illustrate the rotor speed, electromagnetic torque, stator phase current, flux components, flux magnitude, and flux angle, respectively.

Figure 6.4 presents a comparison of the speed response. It is evident that both techniques achieve satisfactory tracking of the rotor speed reference without overshooting. However, the back-stepping SVM technique surpasses classical DTC by exhibiting a faster response in the transient phase and effectively compensating for speed errors caused by the applied load torque. Moving on to Figure 6.5, it displays the response of the electromagnetic torque. The results indicate that both techniques exhibit fast dynamics and good response. However, classical DTC shows high torque ripples, while back-stepping demonstrates a lower level of ripple. Next, Figure 6.6 illustrates the stator phase current. The current waveform displays a good sinusoidal shape. Upon closer inspection, it can be observed that the SVM back-stepping technique produces a smoother current waveform and reduces harmonics due to the optimal selection of the voltage reference. Finally, Figures 6.7 to 6.9 depict the flux components, magnitude, and angle. Both techniques yield favorable waveforms for the flux components and fast tracking responses for the flux magnitude. However, the back-stepping SVM technique demonstrates lower flux ripples.

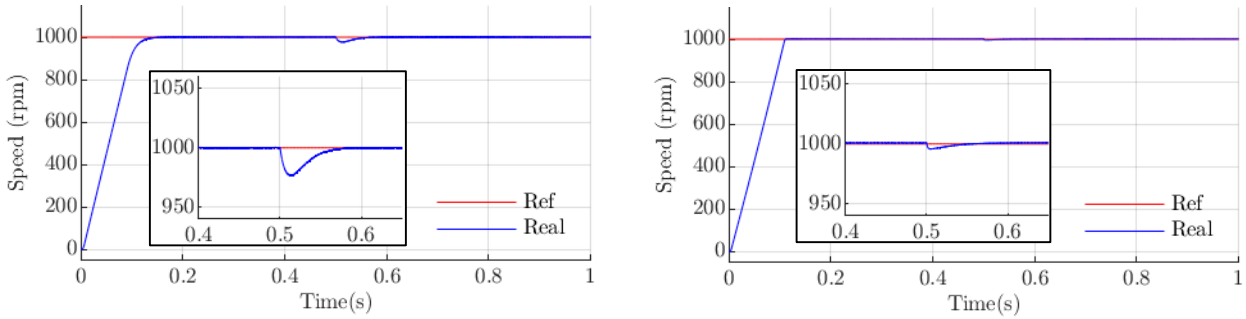

Figure 6 4. Rotor speed response at starting up and steady states with load application.

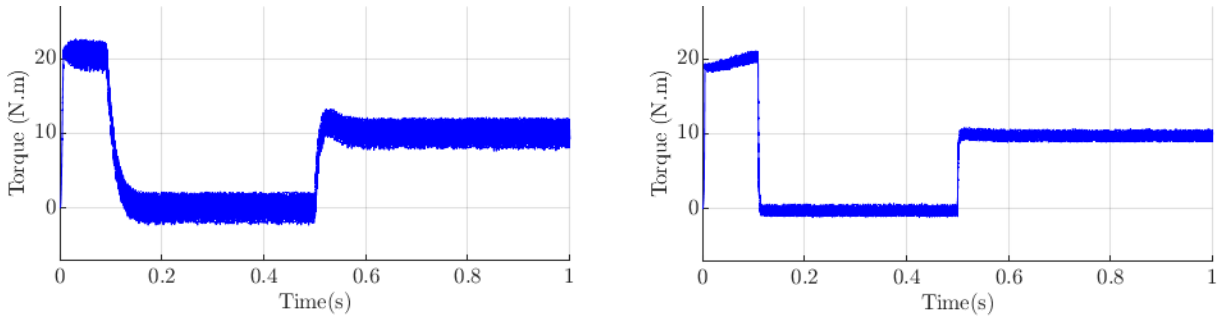

Figure 6.5. Electromagnetic torque at starting up and steady states with load application.

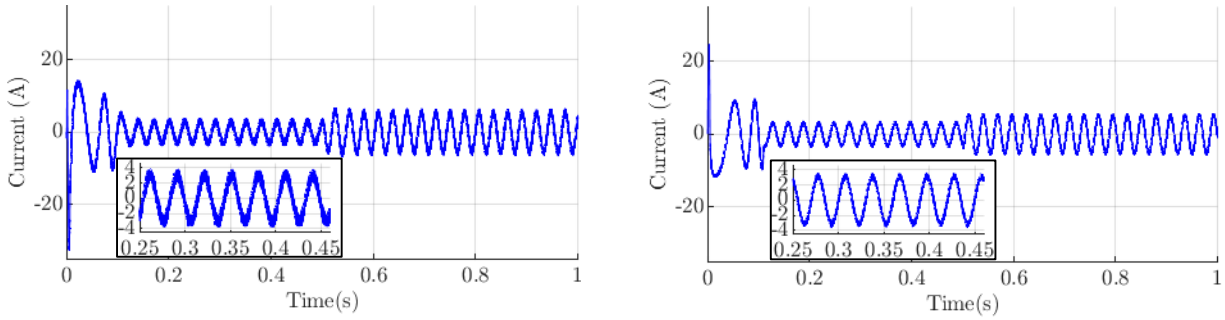

Figure 6.6. Stator current at starting up and steady states with load application.

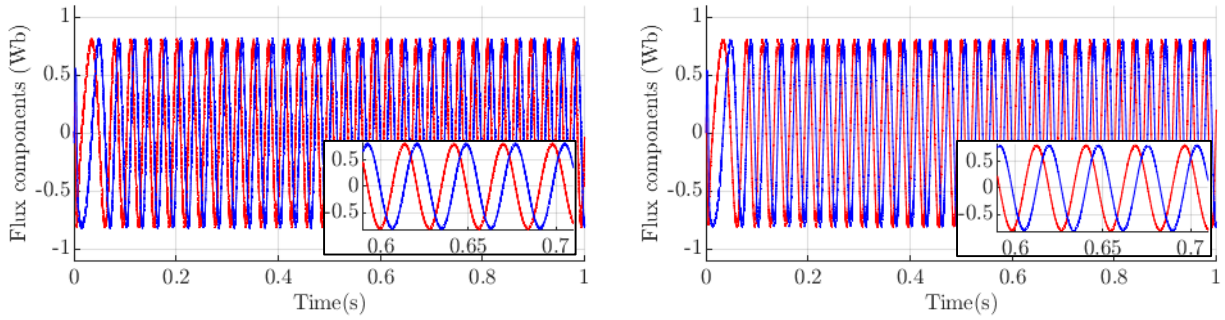

Figure 6.7. Flux components at starting up and steady states with load application.

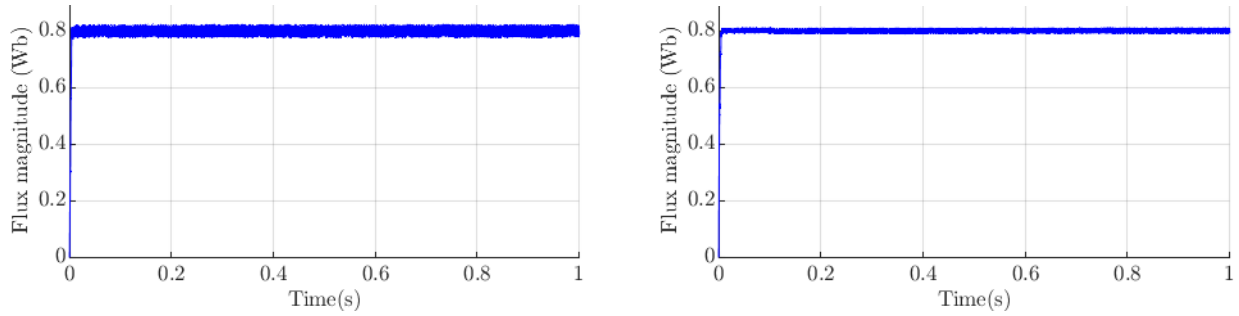

Figure 6.8. Flux magnitude at starting up and steady states with load application.

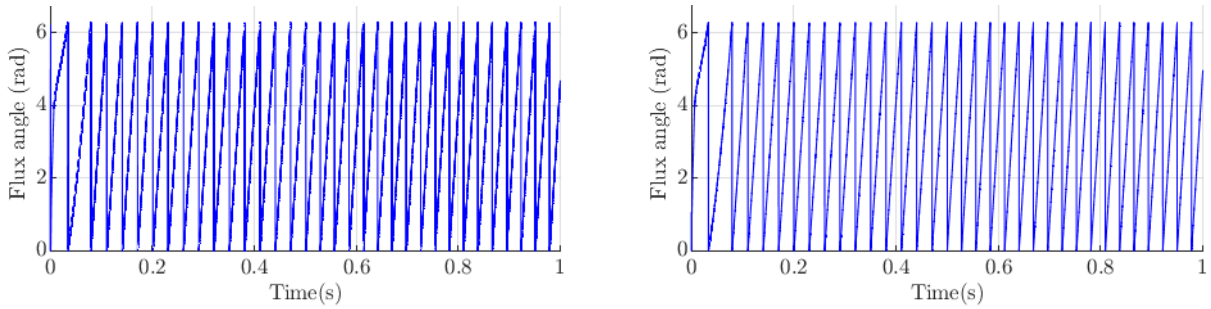

Figure 6.9. Flux angle at starting up and steady states with load application.

6.4.2. Speed reversing with load application

In this section, we examine the reversal of rotation direction in the induction motor, specifically from speeds of $1000\,rpm$ to $-1000\,rpm$. Following this, at $t = 0.5\,s$, a load of $10\,N.m$ is introduced. Figures 6.10 to 6.13 depict the rotor speed, electromagnetic torque, stator phase current, and flux components, respectively.

Firstly, Figure 6.10 illustrates the speed response. The results indicate that the back-stepping SVM achieves a rapid response when the reference speed is reversed, surpassing the classical DTC method. In Figure 6.11, the obtained electromagnetic torque is shown. The classical DTC technique exhibits significant torque fluctuations ($\pm 2\,N.m$), whereas the back-stepping SVM approach demonstrates reduced torque fluctuations ($\pm 0.5\,N.m$). Moving on to Figure 6.12, the stator phase current is displayed with a zoomed-in view. The conventional DTC method exhibits a chopped sinusoidal current waveform, indicating a high level of harmonics. In contrast, the back-stepping SVM method produces a smoother sinusoidal waveform. Finally, Figure 6.13 presents the flux components. Both techniques exhibit favorable waveforms, but a closer look reveals lower flux fluctuations for the back-stepping SVM technique.

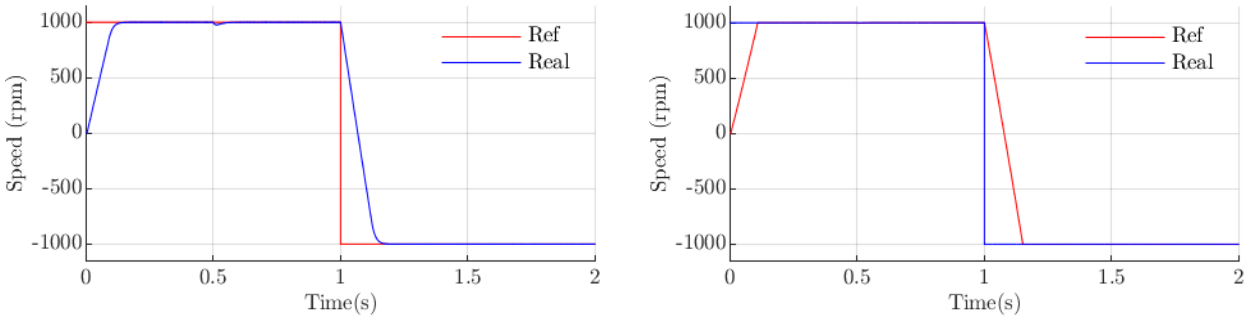

Figure 6.10. Rotor speed at speed reversing with load application.

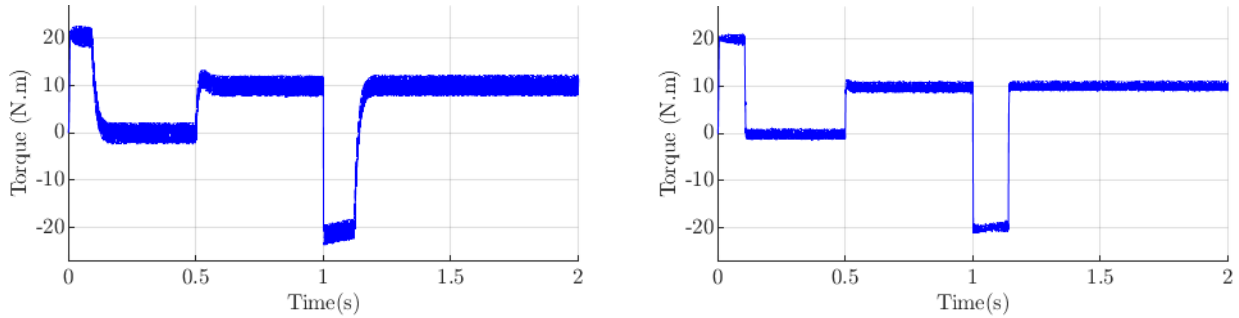

Figure 6.11. Electromagnetic torque at speed reversing with load application.

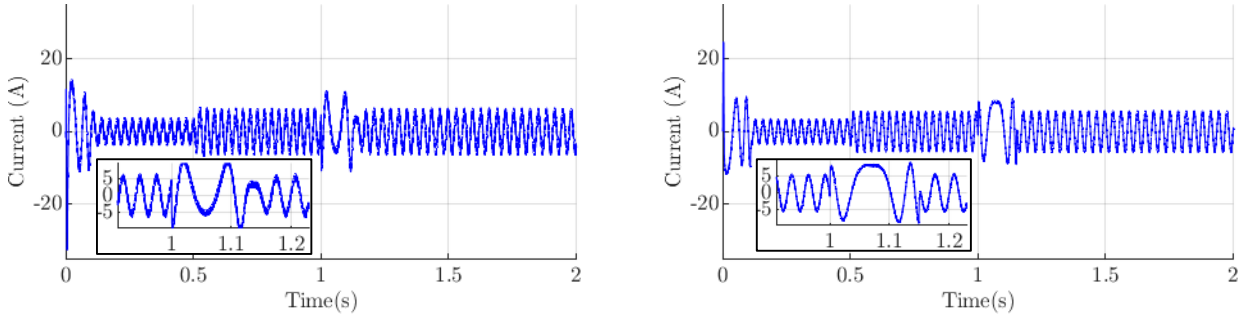

Figure 6.12. Stator current at speed reversing with load application.

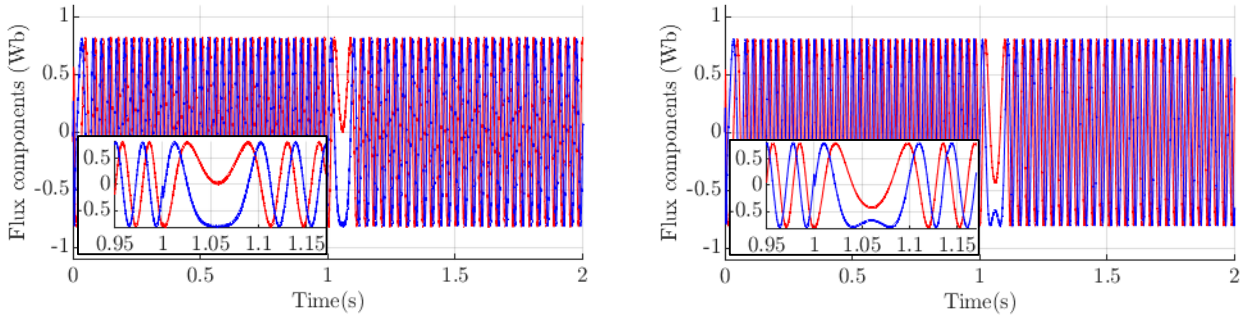

Figure 6.13. Flux components at speed reversing with load application.

6.4.3. Low speed operation

In this part, we analyze the performance of the induction motor in the low-speed range, specifically ranging from $200\,rpm$ to $400\,rpm$. Figures 6.14 to 6.17 illustrate the rotor speed, electromagnetic torque, stator phase current, and flux components, respectively.

Figure 6.14 displays the response of the rotor speed. The back-stepping SVM technique demonstrates a fast and stable response in the low-speed range, without any overshoot or significant fluctuations around the desired speed. In contrast, the classical DTC shows overshoot and some oscillations around the reference speed. Additionally, Figure 6.15 also presents the electromagnetic torque response for both control algorithms. It is evident that the back-stepping SVM exhibits rapid and smooth dynamic response with minimal ripples. Moving on, Figure 6.16 depicts the stator phase current, which demonstrates a desirable sinusoidal waveform with reduced harmonics, thanks to the SVM strategy. Finally, Figure 6.17 illustrates the flux components to indicate the speed variation. Both techniques showcase favorable waveforms, but a closer examination reveals that the back-stepping SVM technique exhibits lower flux fluctuations.

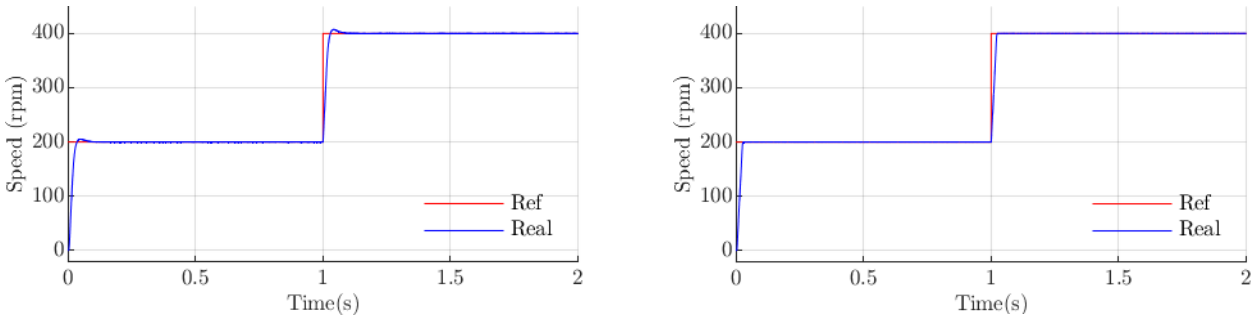

Figure 6.14. Rotor speed at low speed operation.

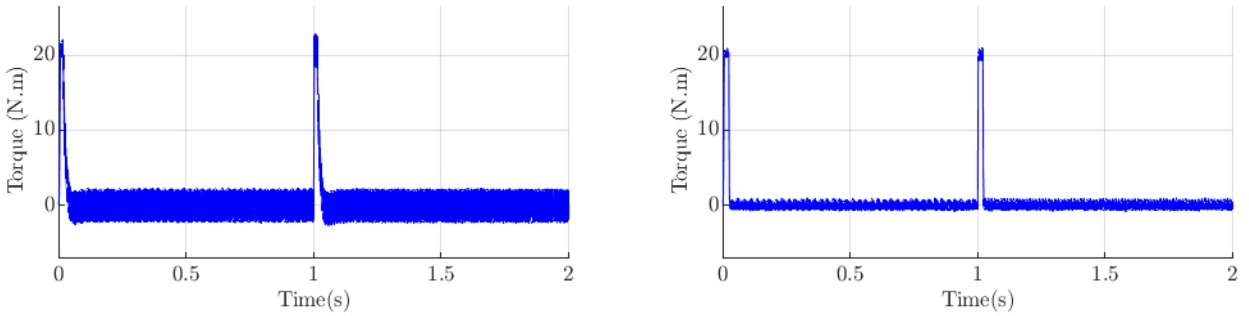

Figure 6.15. Electromagnetic torque at low speed operation.

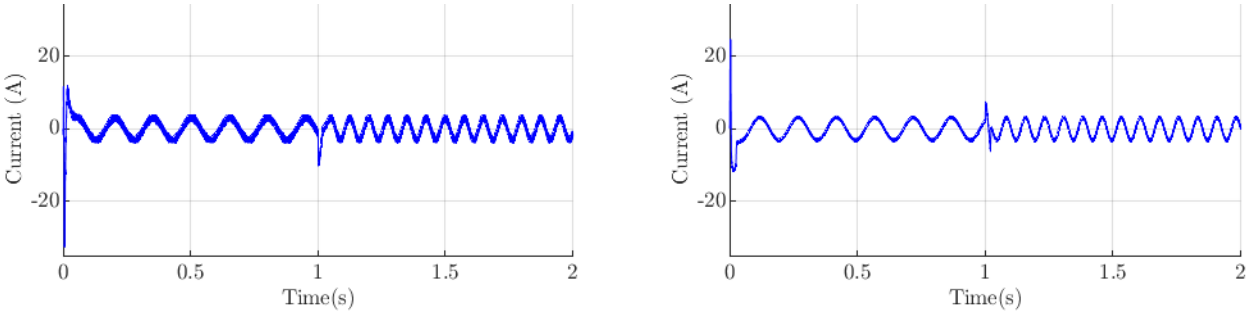

Figure 6.16. Stator current at low speed operation.

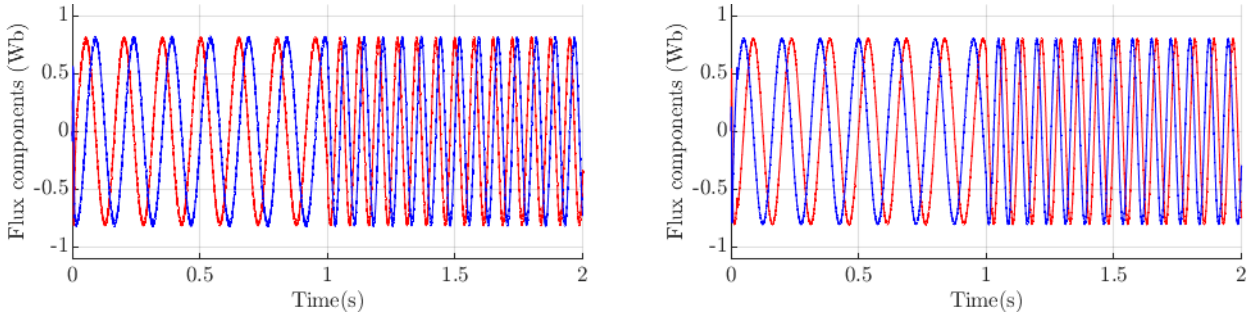

Figure 6.17. Flux components at low speed operation.

6.4.4. Comparison summary

Based on the provided comparative analysis, the subsequent table outlines the characteristics of the back-stepping SVM control method in comparison to the conventional DTC approach.

Table 6.2. Comparative analysis of classical DTC and back-stepping SVM.

Criteria	Classical DTC	Back – stepping SVM
Speed control accuracy	Good	Excellent
Torque ripple	High	Low
Dynamic response	Moderate	Fast
Robustness to Road	Moderate	High
Switching frequency	Variable	Constant
Computational complexity	Low	Moderate
Implementation difficulty	Easy	Moderate

6.5. Experimental results

In order to comprehensively analyze the ongoing performance of the autonomous electric vehicle, the extracted speed patterns from trajectories 1 and 2 in Chapter 5 are harnessed. These speed patterns serve as crucial input for determining the speed profiles of the induction motor (IM) and subsequently regulating its velocity. This process relies on considering the vehicle's speed alongside the knowledge of the gear ratio and wheel radius. By precisely selecting values for the gear ratio ($g_r = 1.5$) and wheel radius ($r_w = 0.2\ m$), the motor's speed profiles can be precisely calculated and visually represented in revolutions per minute (rpm), as illustrated in Figure 6.18.

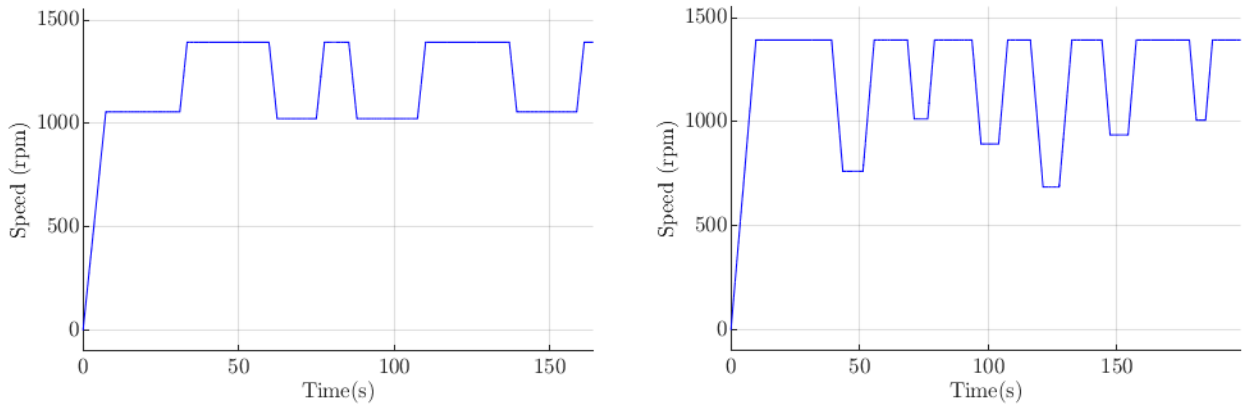

Figure 6.18. Induction motor speed profiles.

The extracted speed profiles play a crucial role in the real-time control of the electric vehicle induction motor, facilitated by the dSpace 1104 board. Acting as an intermediary between the power electronics converter and the software component (MATLAB/Simulink/Controldesk), dSpace enables seamless communication and integration. The successful implementation of the real-time control system is depicted in Figure 6.19, providing a visual representation of its functionality. it is essentially composed of: 1- supervision desktop with Matlab/Simulink software, 2- dSPACE 1104 card, 3- squirrel cage IM & DC machine, 4- resistive load, 5- incremental encoder, 6- current sensor, 7- power electronics Semikron converter, 8- voltage sensor, and 9- digital oscilloscope. For a comprehensive understanding of the experimental setup's components, readers can refer to Appendix A.2, which presents detailed information.

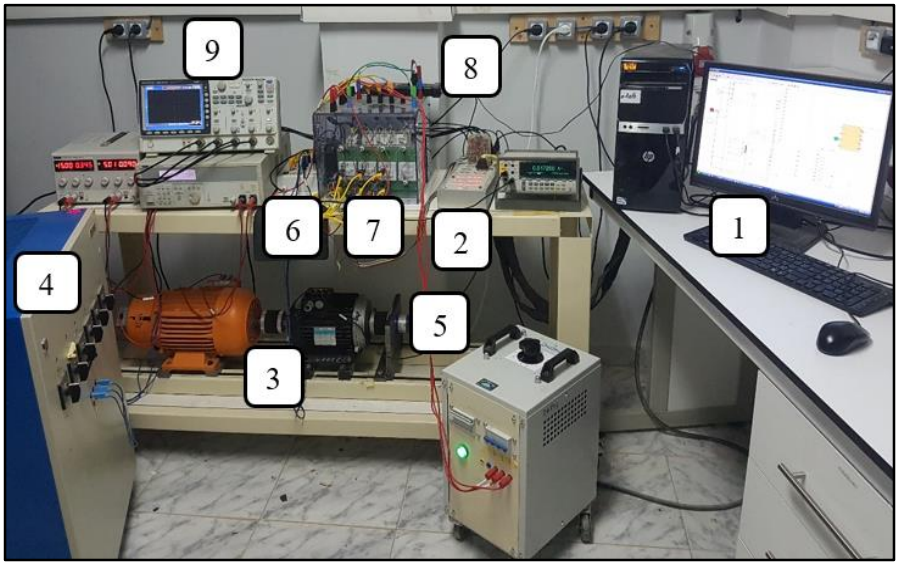

Figure 6.19. Experimental setup.

In Figures 6.20 to 6.25, a comprehensive representation of the system's performance is provided, covering various crucial aspects. These figures illustrate the response of the rotor speed, speed error, and electromagnetic torque, as well as the stator phase current, rotor flux components, rotor flux magnitude, and estimated load torque. The figures on the left pertain to the first trajectory speed profile, while the figures on the right correspond to the second trajectory speed profile. When it comes to vehicle navigation, meticulous consideration of the resistive forces that affect its motion is of utmost importance. These forces encompass the rolling force, aerodynamic drag force, and climbing force (Appendix A.1). Consequently, in order to accurately simulate real-life driving scenarios, we carefully select different load torque scenarios while taking into account an electric vehicle's speed (v), mass (m), and the inclination angle (φ) of an inclined plane.

The results presented in Figure 6.20 unequivocally reveal a strong alignment between the rotor speed and the desired speed patterns across the entirety of the trajectories, demonstrating exceptional dynamics. Notably, there is a complete absence of overshooting, and the response time is remarkably swift. Furthermore, Figure 6.21 visually demonstrates that the electromagnetic torque consistently adheres to its intended reference, adapting to fluctuations in speed. By closely examining specific intervals characterized by an increase in the applied load, it becomes strikingly apparent that the speed error is virtually negligible. This impressive outcome is accomplished by

effectively implementing the recommended back-stepping approach, which promptly and efficiently compensates for the speed error induced by the applied load torque.

Figure 6.22 offers detailed zoomed-in perspectives of the stator phase current, revealing a remarkably smooth waveform with negligible levels of harmonic distortion. This observation underscores the high quality and stability of the current. Notably, the integration of the SVM strategy in conjunction with the back-stepping technique plays a crucial role in effectively and substantially reducing the occurrence of chattering, an undesirable phenomenon that can introduce noise and disturbances in the system. Figures 6.23 and 6.24 visually represent the distinct components and magnitude of the flux. The magnitude demonstrates remarkable responsiveness, showcasing rapid reactions, minimal fluctuations, and outstanding monitoring capabilities specifically in close proximity to the reference value of 0.8 Wb. Moreover, the flux patterns exhibit a remarkably smooth and sleek appearance, characterized by exceptionally low levels of harmonic.

Figure 6.25 visually presents the load torque estimation, effectively highlighting the rapid and efficient response of the specifically designed back-stepping observer to variations in the load. The estimated load torque demonstrates a remarkable ability to make precise and accurate adjustments, exhibiting a notable absence of any discernible fluctuations. Notably, the observed time intervals of (14.5s to 24s), (93.5s to 103s), and (118s to 129.5s) for trajectory 1, as well as (18s to 28s), (98s to 102s), and (164s to 169.5s) for trajectory 2, are estimated to be directly attributed to an increase in the applied load during these specific temporal segments.

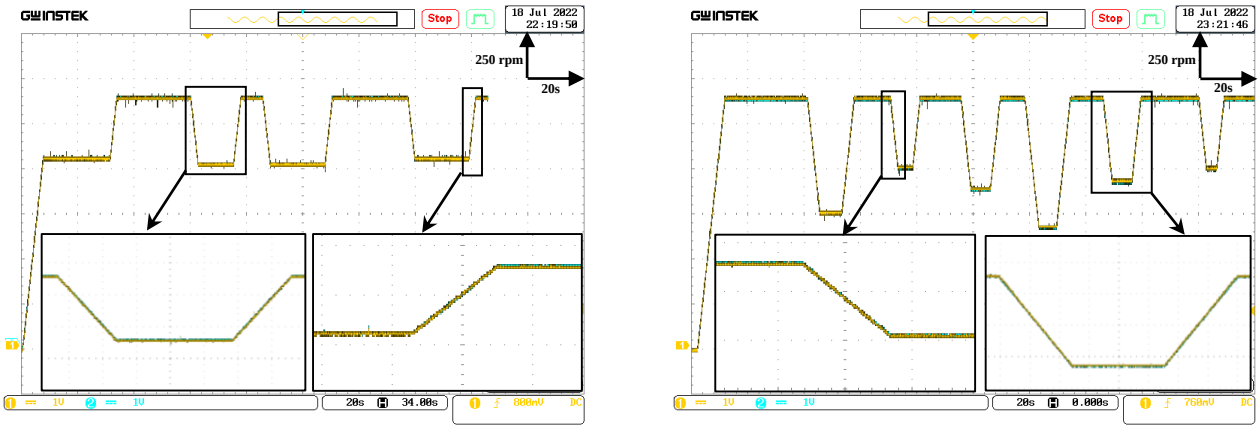

Figure 6.20. Speed response for trajectory 1&2.

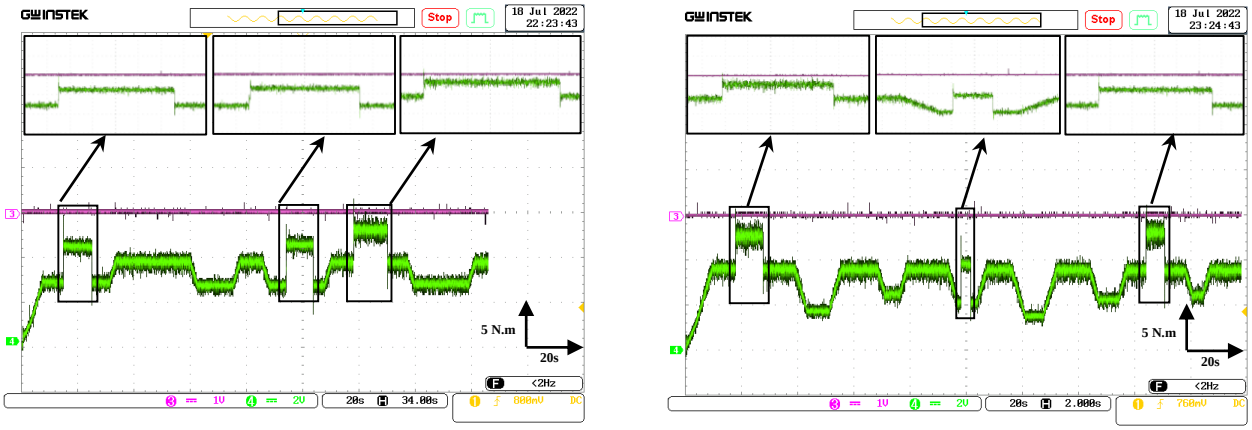

Figure 6.21. Speed error and electromagnetic torque for trajectory 1&2.

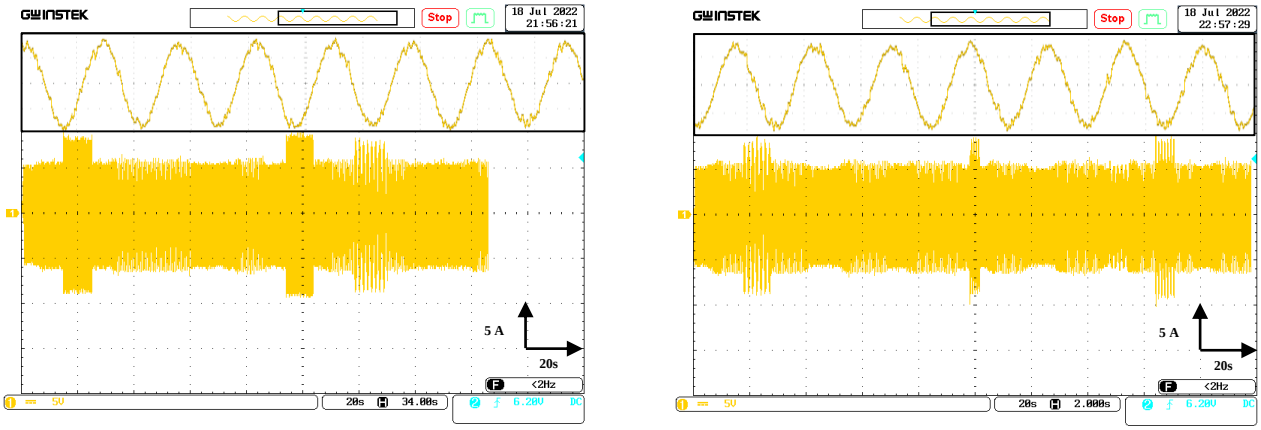

Figure 6.22. Stator current for trajectory 1&2.

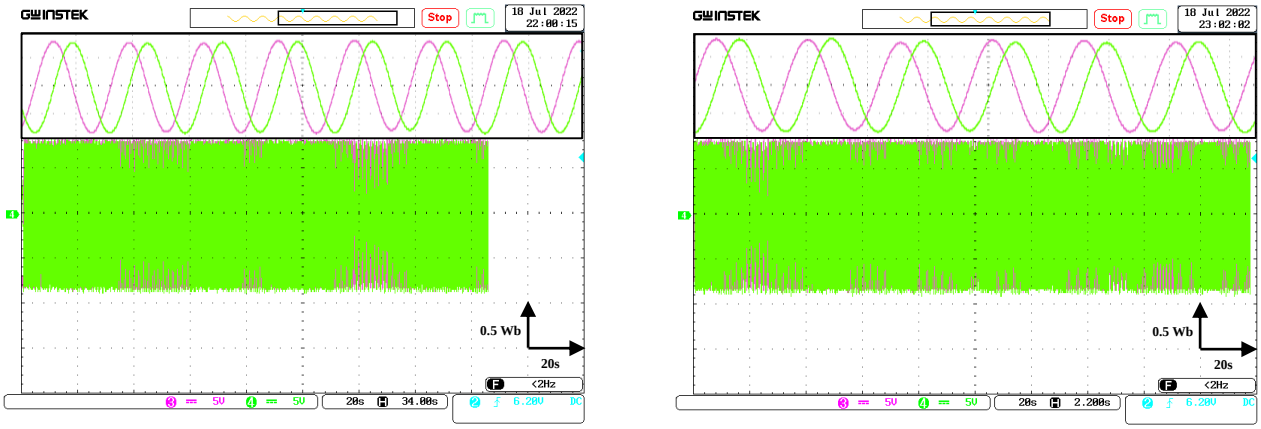

Figure 6.23. Flux components for trajectory 1&2.

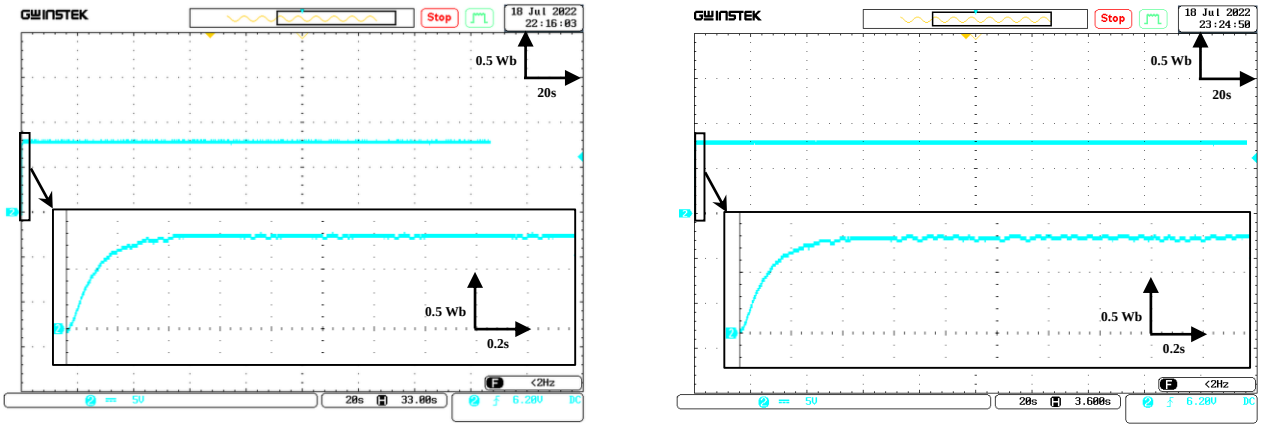

Figure 6.24. Flux magnitude for trajectory 1&2.

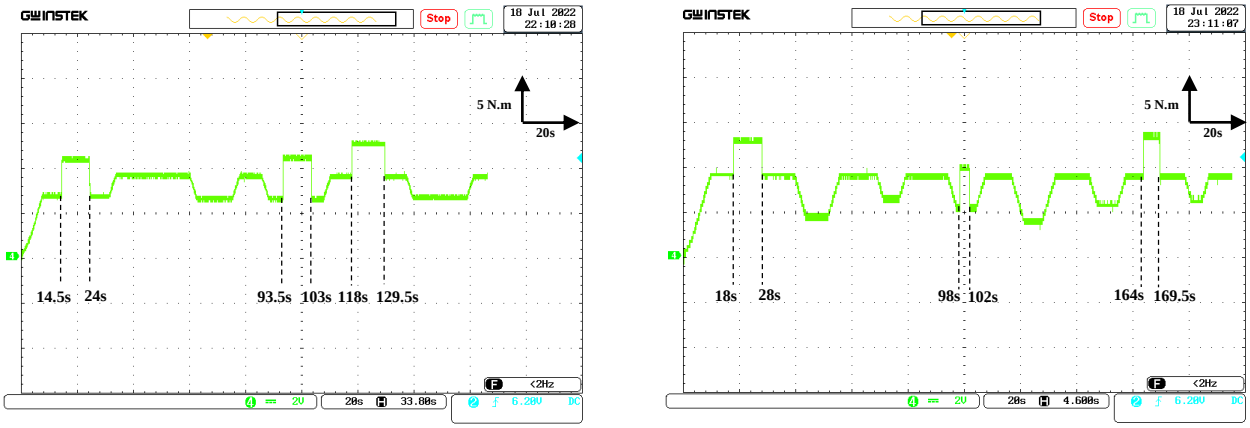

Figure 6.25. Estimated load torque for trajectory 1&2.

The use of the back-stepping SVM technique on the autonomous electric vehicle's induction motor has yielded truly remarkable results. With an unwavering commitment to precision, the motor flawlessly adheres to the speed profiles generated by the speed planning algorithm, effortlessly avoiding any overshoot. Even when confronted with a resistive load, the technique exhibits an exceptional level of robustness, seamlessly maintaining its stellar performance across varying load conditions. A particular highlight of this technique lies in its ability to produce smooth stator current and flux components, which exhibit an impressively low level of harmonic distortion. This distinctive attribute not only contributes to the overall excellence of the designed technique but also solidifies its position as a true embodiment of high-performance capabilities.

6.6. Conclusion

In conclusion, this study introduces a back-stepping SVM technique for precise speed control of an autonomous electric vehicle's induction motor. The primary objective was to develop a robust control system capable of accurately following speed profiles obtained from a speed planning algorithm. The effectiveness of the back-stepping SVM was thoroughly evaluated through both numerical simulations using MATLAB/Simulink and experimental implementation with the dSpace 1104 board.

The simulation results demonstrated that the designed back-stepping SVM technique outperformed the classical DTC technique. It exhibited exceptional precision in tracking the desired speed references, effectively eliminating any overshoot. Moreover, the technique showcased remarkable robustness, maintaining its performance even under varying load conditions.

The experimental results further validated the effectiveness of the back-stepping SVM technique in conjunction with the speed planning algorithm. The induction motor successfully achieved high-accuracy tracking of the extracted ideal speeds. Notably, the stator current and flux components exhibited smooth profiles with minimal harmonic distortion, underscoring the superior performance and robustness of the back-stepping SVM technique in autonomous electric vehicle speed control.

CHAPTER 7

GENERAL CONCLUSION

Contents **Page**

7.1. Conclusion

This thesis has contributed to the field of autonomous electric vehicles by addressing longitudinal and lateral control, speed planning, and electric drive control. This research has paved the way for enhancing the efficiency, safety, and maneuverability of autonomous electric vehicles. The findings and methodologies presented in this thesis provide valuable insights for researchers and practitioners working towards the advancement and implementation of autonomous electric vehicles in the future.

The thesis has been started in the first chapter with a detailed introduction that gives a broad view of autonomous electric vehicles. This helpful beginning didn’t only explain the research problems but also showed the objectives of the research and how they are important to explore the important details of this innovative study.

In the second chapter, a comprehensive overview of the latest advancements in longitudinal and lateral control techniques was presented, with a special focus on speed planning techniques specifically designed for autonomous electric vehicles. Additionally, the chapter thoroughly examined the various electrical drives commonly utilized in electric vehicles, placing significant emphasis on the control techniques implemented in induction motors for traction purposes. This comprehensive analysis equips readers with a deep understanding of the cutting-edge developments in control strategies and electric propulsion systems within the context of autonomous electric fields.

The third chapter diligently centered its attention on the meticulous mathematical modeling of the system under study, encompassing not only the autonomous vehicle but also the voltage inverter and electrical motor. By constructing a precise and comprehensive mathematical model, this chapter paved the way for the subsequent derivation of suitable control laws that effectively govern the behavior of the vehicle. This pivotal step establishes a solid foundation for the development of robust and reliable control strategies, ensuring optimal performance and safety in autonomous vehicle operations.

The fourth chapter was dedicated to the meticulous design of a cutting-edge lateral control law, leveraging the autonomous vehicle's dynamic model. To achieve superior tracking performance along the desired trajectory, the innovative super-twisting control technique was employed. This chapter was driven by the objective of enhancing the vehicle maneuverability and

stability during lateral movements. The outcome of this endeavor was substantiated through rigorous simulation using the renowned Matlab/Simulink software, showcasing the exceptional robustness of the designed super-twisting controller in accurately tracking desired trajectories with utmost precision and minimal error.

The fifth chapter delved deeply into the intricacies of designing a comprehensive speed planning algorithm, harnessing the power of path geometry and trajectory curvatures. This algorithm was meticulously crafted to generate an optimal speed profile for the vehicle, taking into account the dynamic variations in velocity during navigation. The primary objective of this endeavor was to enhance efficiency and safety in autonomous driving scenarios by precisely optimizing the speed profile. The simulation results obtained by seamlessly integrating this meticulously designed algorithm with the super-twisting controller exhibited remarkable performance in terms of significantly reducing tracking errors and ensuring safe motion that prioritizes human comfort.

Lastly, in chapter six, a careful implementation of a back-stepping approach was introduced. This approach was found to be exceptionally effective in controlling the induction motor. It allowed the motor to accurately follow the speed profile generated by the speed planning algorithm without any errors. This chapter emphasized the importance of precise motor control for the autonomous vehicle to perform well and respond quickly. Through hardware experiments using the real-time interface connected to the dSpace 1104 signal card, the results clearly showed that the back-stepping approach performed outstandingly. It closely followed the desired speed profiles with remarkable accuracy, proving its reliability and ability to maintain precise motor control in autonomous vehicle applications.

7.2. Future works

To ensure the ongoing progress of the research, future efforts can be directed towards exploring broader aspects within this field. Some potential areas of focus include:

- **Integration of Perception Systems:** Future research can focus on integrating advanced perception systems, such as computer vision and sensor fusion techniques, into the autonomous electric vehicle framework. This can improve the vehicle's ability to precisely

perceive and understand the surrounding environment, leading to enhancement in safety and decision making capabilities.

- **Autonomous Vehicle Communication:** Investigate communication protocols and strategies for enabling efficient and reliable communication between autonomous electric vehicles. This can facilitate cooperative behavior, such as platooning and coordinated navigation, resulting in improved traffic flow and energy efficiency.
- **Energy Management and Optimization:** Explore energy management strategies that consider dynamic variables, such as traffic conditions, road topology, and battery health, to optimize the energy consumption of autonomous electric vehicles. This can lead to improved range, charging efficiency, and overall energy utilization.
- **Human-Machine Interaction:** Research can be conducted to develop intuitive and user-friendly interfaces for human-machine interaction in autonomous electric vehicles. This includes designing effective displays, controls, and communication systems that ensure passenger comfort, trust, and acceptance of autonomous technology.
- **Real-world Testing and Validation:** Conduct extensive field trials and validation experiments to evaluate the performance, robustness, and safety of autonomous electric vehicles under various real-world scenarios. This includes testing the developed control strategies, speed planning algorithms, and motor control techniques in diverse environments and road conditions.
- **Regulatory and Legal Framework:** Investigate the legal and regulatory challenges associated with the deployment of autonomous electric vehicles. This involves addressing issues related to liability, privacy, cybersecurity, and the development of standardized protocols to ensure safe and ethical operation of these vehicles.

By exploring these prospective areas, researchers can further contribute to the advancement and implementation of autonomous electric vehicles, ultimately paving the way for a more sustainable and intelligent transportation system.

APPENDICES

Contents **Page**

A.1. Autonomous vehicle dynamics

A.1.1. Autonomous vehicle dynamic model parameters

The parameters encompassing the autonomous vehicle, crucial for simulating the trajectory tracking task, have been meticulously compiled and documented within Table A.1. This comprehensive compilation provides valuable insights into the essential characteristics and specifications of the vehicle, enabling accurate simulation and effective analysis of its trajectory tracking performance.

Table A.1. Autonomous vehicle dynamic model parameters.

Parameters	Value
Vehicle mass	$m = 2000\ kg$
Front axle-center of gravity distance	$L_f = 1.4\ m$
Rear axle-center of gravity distance	$L_r = 1.6$ m
Axle plane-center of gravity distance	$L_z = 0.35$ m
Moment of inertia	$I_z = 4000\ kg \cdot m^2$
Drift stiffness of the front tire	$C_f = 12000\ N/rad$
Drift stiffness of the rear tire	$C_r = 11000\ N/rad$

A.1.2. Autonomous vehicle dynamic forces

The way a vehicle moves up a slope is influenced by different forces working together. Figure A.1 shows the various forces at play during this uphill movement. When the vehicle moves forward, it faces a strong force that tries to stop it. This force includes rolling resistance, aerodynamic resistance, and gradient resistance. Together, these resistances diligently work to decelerate the vehicle's forward momentum, presenting significant challenges for its uphill advancement.

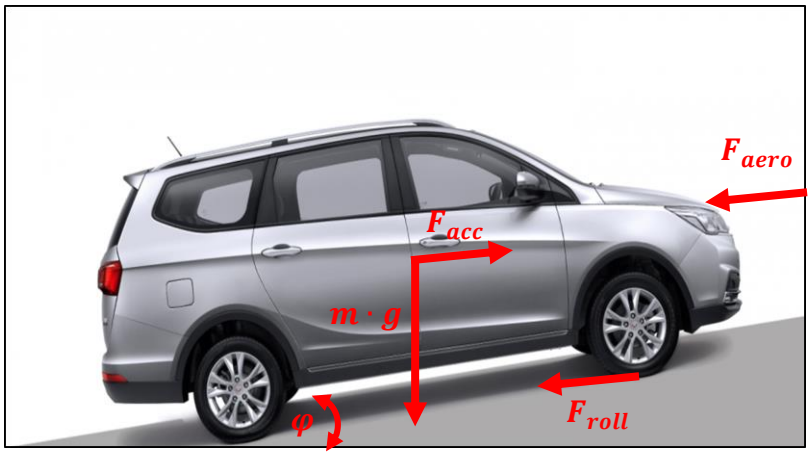

Figure A.1. Forces acting on an uphill vehicle.

The rolling force acting on a vehicle is the force that opposes its motion and is generated due to the friction between the tires and the surface on which it is moving. This force is called rolling resistance. It arises from the deformation of the tires and the interaction between the tire and the road surface. The rolling force acts in the opposite direction to the vehicle's motion and must be overcome by the engine or motor to keep the vehicle moving. Factors that affect rolling resistance include tire design, tire pressure, road surface conditions, and vehicle weight. The rolling force expression is given by the following equation:

$$F_{roll} = m \cdot g \cdot \mu \cdot \cos \varphi \tag{A.1}$$

The aerodynamic force acting on a vehicle is the force exerted by the air as the vehicle moves through it. When a vehicle is in motion, it encounters resistance from the air, which creates aerodynamic drag. This drag force acts in the opposite direction to the vehicle's motion and opposes its forward movement. The magnitude of the aerodynamic force depends on various factors such as the shape and design of the vehicle, its speed, the density of the air, and the aerodynamic properties of its components. The equation that describes the aerodynamic force is depicted as follow:

$$F_{aero} = \frac{1}{2} \cdot \rho_a \cdot A_a \cdot c_d \cdot v^2 \tag{A.2}$$

where c_d is gradient coefficient, ρ_a is the density of the air, and A_a is the frontal vehicle area.

The gradient force, also known as the grade force or slope force, is the force that acts on a vehicle when it is moving on an incline or gradient. It is caused by the gravitational pull of the earth and the angle of the slope. When a vehicle goes uphill, the gradient force acts in the opposite direction to its motion, making it more difficult for the vehicle to move forward. The steeper the slope, the greater the gradient force that needs to be overcome by the vehicle's engine or motor to maintain or increase its speed. The expression of the gradient force is expressed by the following equation:

$$F_{grad} = m \cdot g \cdot \sin \varphi \tag{A.3}$$

Obviously, all these resistance forces add up to oppose the movement:

$$F_{res} = F_{roll} + F_{aero} + F_{grad} \tag{A.4}$$

A.2. Practical application of induction motor control in real time

A.2.1. Experimental setup presentation:

A specially designed and constructed experimental setup was created to regulate the induction motor electrical drive, with the intention of emulating the traction system of an autonomous electric vehicle. The real-time control was carried out at the LGEB laboratory in Biskra, utilizing the dSpace 1104 board. The comprehensive depiction of the implementation environment for the induction motor drive is visually depicted in Figure A.2. It is essentially composed of:

1- Supervision desktop with Matlab/Simulink software.
2- dSPACE 1104 control board.
3- Squirrel cage IM & DC machine.
4- Resistive load.
5- Incremental encoder.
6- Current sensor.
7- Power electronics Semikron converter.
8- Voltage sensor.
9- Digital oscilloscope.

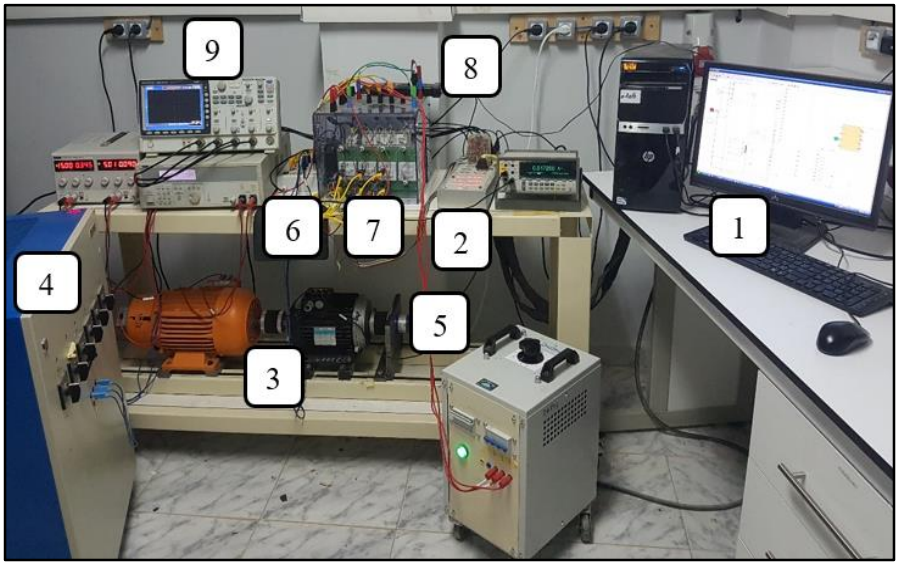

Figure A.2. Experimental setup.

A.2.2. dSpace DS1104 control board

By integrating the dSpace DS1104 Board into a computer, one can transform it into a rapid control prototyping development system. This versatile board is compatible with a wide range of PCs, as it can be effortlessly installed into any PC that has an available PCI or PCIe slot.

The dSpace DS1104 control board is equipped with an MPC8240 processor featuring a PPC 603e core and on-chip peripherals. It has a 64-bit floating-point processor and operates at a CPU clock speed of 250 MHz. The board offers 32 MB of SDRAM as global memory and 8MB of flash memory. It includes various timers, including four general-purpose timers with 32-bit down counters and 80-ns resolution, a sampling rate timer with 32-bit down counter and 40-ns resolution, and a time base counter with 64-bit up counter and 40-ns resolution. The board also features an interrupt controller with multiple interrupt options. It provides analog-to-digital conversion with multiplexed channels and parallel channels, offering 16-bit and 12-bit resolution, respectively. The board supports eight channels of digital-to-analog conversion with 16-bit resolution. It also includes 20-bit parallel I/O for digital input and output operations. It includes a digital incremental encoder interface with two independent channels, supporting single-ended (TTL) or differential (RS422) inputs. In terms of the serial interface, it features a single UART with FIFO, supporting accurate baud rate selection through a PLL-driven UART. The board is compatible with RS232,

RS422, and RS485 communication. The slave DSP on the board is a Texas Instruments TMS320F240 with a clock rate of 20 MHz. The dSpace DS1104 board is shown in Figure A.3.

Figure A.3. dSpace DS1104 control board.

To establish a seamless connection between the dSPACE board and the power converter, an interface board is employed to meticulously fine-tune the control signal levels. During each sampling period, the highly capable dS1104 board effortlessly captures input signals from an array of sensors, encompassing currents and voltages from ADC ports, as well as speed data from the encoder via INC ports. Leveraging this information, the dS1104 board promptly generates the essential digital control signals. Facilitated by a MATLAB/Simulink program with a real-time interface (RTI), these control signals are precisely derived, granting convenient accessibility to the dS1104 board's I/O ports through Simulink's extensive library.

A.1.3. Induction motor characteristics

The parameters of the three-phase induction motor used in both simulation and real-time implementation were meticulously obtained through experimental identification employing well-established conventional methods. To provide a comprehensive understanding, the nameplate of the motor is visually depicted in Figure A.4, showcasing vital information. Additionally, for ease of reference and precise comprehension, the corresponding parameters are meticulously tabulated in SI units within Table A.2. This meticulous documentation ensures accurate representation and

facilitates effective analysis and implementation of the motor system.

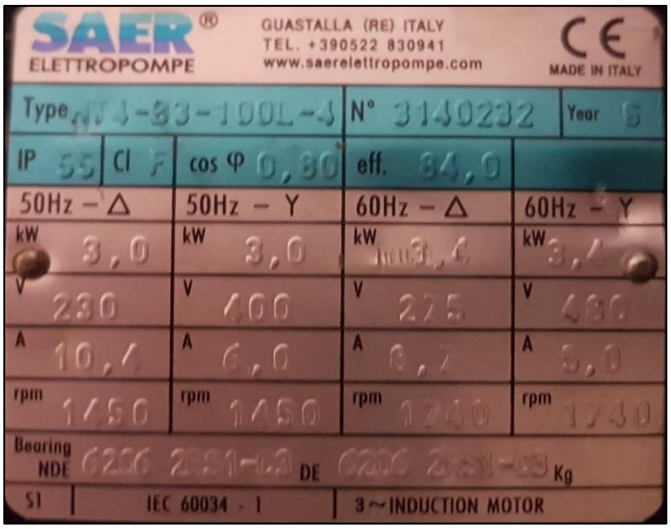

Figure A.4. Induction motor nameplate.

Table A.2. Induction motor parameters.

Parameters	Value
Power	$P = 3\ kW$
Frequency	$F = 50\ Hz$
Stator resistance	$R_s = 1.8\ \Omega$
Rotor resistance	$R_r = 2.45\ \Omega$
Stator inductance	$L_s = 0.268\ H$
Rotor inductance	$L_r = 0.268\ H$
Mutual inductance	$L_m = 0.257\ H$
Friction coefficient	$f = 0.00014\ N.m.s/rad$
Total inertia	$J = 0.02\ kg.m^2$
Pole pairs	$p = 2$

BIBLIOGRAPHY

[1] R. S. Wallace, A. Stentz, C. E. Thorpe, H. Maravec, W. Whittaker, and T. Kanade, "First results in robot road-following," *Proceedings of the 9th international joint conference on artificial intelligence*, pp. 1089-1095, 1985.

[2] T. Kanade, C. E. Thorpe and W. Whittaker, "Autonomous land vehicle project at CMU," *Proceedings of the 1986 ACM fourteenth annual conference on Computer science*, pp. 71-80, 1986.

[3] *40+ Corporations Working on Autonomous Vehicles*, 2020, [online] Available: https://www.cbinsights.com/research/autonomous-driverless-vehicles-corp%orations-list/.

[4] "Taxonomy and Definitions for Terms Related to On-Road Motor Vehicle Automated Driving Systems", *SAE Standard J3016*, pp. 01-16, 2014.

[5] O. Amidi and C. E. Thorpe, "Integrated mobile robot control," *Proceedings of SPIE*, vol. 1388, 1991.

[6] H. Ardiny, S. Witwicki, and F. Mondada, "Construction automation with autonomous mobile robots: A review," *2015 3rd RSI International Conference on Robotics and Mechatronics (ICROM)*, 2015.

[7] C. Katrakazas, M. Quddus, W.-H. Chen and L. Deka, "Real-time motion planning methods for autonomous on-road driving: State-of-the-art and future research directions," *Transportation Research Part C: Emerging Technologies*, vol. 60, pp. 416-442, 2015.

[8] L. Claussmann, M. Revilloud, D. Gruyer and S. Glaser, "A Review of motion planning for highway autonomous driving," *IEEE Transactions on Intelligent Transportation Systems*, vol. 21, no. 5, pp. 1826-1848, 2020.

[9] S. Dixit et al., "Trajectory planning and tracking for autonomous overtaking: State-of-the-art and future prospects," *Annual Reviews in Control*, vol. 45, pp. 76-86, 2018.

[10] R. Marino, S. Scalzi, and M. Netto, "Nested PID steering control for lane keeping in autonomous vehicles," *Control Engineering Practice*, vol. 19, no. 12, pp. 1459-1467, 2011.

[11] C. J. Taylor, J. Kosecka, R. Blasi, and J. Malik, "A comparative study of vision-based lateral control strategies for autonomous highway driving," *The International Journal of Robotics Research*, vol. 18, no. 5, pp. 442-453, 1999.

[12] C. Chen and H.-S. Tan, "Experimental study of dynamic look-ahead scheme for vehicle steering control," *Proceedings of the 1999 American Control Conference (Cat. No. 99CH36251),* San Diego, CA, USA, 1999, pp. 3163-3167 vol.5.

[13] N. H. Amer, H. Zamzuri, K. Hudha, V. R. Aparow, Z. A. Kadir and A. F. Zainal Abidin, "Modelling and trajectory following of an armoured vehicle," *2016 SICE International Symposium on Control Systems (ISCS),* Nagoya, Japan, 2016, pp. 1-6,

[14] E. P. Ping, K. Hudha, and H. Jamaluddin, "Hardware-in-the-loop simulation of automatic steering control for lanekeeping manoeuvre: outer-loop and inner-loop control design," *International Journal of Vehicle Safety,* vol. 5, no. 1, pp. 35-59, 2010.

[15] M. Park, S. Lee, and W. Han, "Development of steering control system for autonomous vehicle using geometry-based path tracking algorithm," *ETRI Journal,* vol. 37, no. 3, pp. 617-625, 2015.

[16] N. Matsumoto, H. Kuraoka and M. Ohba, "An experimental study on vehicle lateral and yaw motion control," *Proceedings IECON '91: 1991 International Conference on Industrial Electronics, Control and Instrumentation,* Kobe, Japan, 1991, pp. 113-118 vol.1.

[17] H. Mouri and H. Furusho, "Automatic path tracking using linear quadratic control theory," *Proceedings of Conference on Intelligent Transportation Systems,* Boston, MA, USA, 1997, pp. 948-953,

[18] K. Lee, S. Jeon, H. Kim and D. Kum, "Optimal Path Tracking Control of Autonomous Vehicle: Adaptive Full-State Linear Quadratic Gaussian (LQG) Control," *IEEE Access,* vol. 7, pp. 109120-109133, 2019,

[19] T. Hsiao and M. Tomizuka, "Design of position feedback controllers for vehicle lateral motion," *2006 American Control Conference,* Minneapolis, MN, USA, 2006.

[20] Y. S. Son, W. Kim, S.-H. Lee, and C. C. Chung, "Robust multirate control scheme with predictive virtual lanes for lane-keeping system of autonomous highway driving," *IEEE Transactions on Vehicular Technology,* vol. 64, no. 8, pp. 3378-3391, 2015.

[21] D. A. Pomerleau, "ALVINN: An autonomous land vehicle in a neural network," *Advances in neural information processing systems,* pp. 305-313, 1989.

[22] M. Kuderer, S. Gulati and W. Burgard, "Learning driving styles for autonomous vehicles from demonstration," *2015 IEEE International Conference on Robotics and Automation (ICRA),*

Seattle, WA, USA, 2015, pp. 2641-2646.

[23] T. Hessburg and M. Tomizuka, "Fuzzy logic control for lateral vehicle guidance," *IEEE Control Systems Magazine,* vol. 14, no. 4, pp. 55-63, 1994.

[24] L. Cai, A. B. Rad, W. L. Chan and K. Y. Cai, "A robust fuzzy PD controller for automatic steering control of autonomous vehicles," *The 12th IEEE International Conference on Fuzzy Systems, 2003. FUZZ '03.,* St Louis, MO, USA, 2003, pp. 549-554 vol.1.

[25] J. Pérez, V. Milanés and E. Onieva, "Cascade architecture for lateral control in autonomous vehicles," *IEEE Transactions on Intelligent Transportation Systems,* vol. 12, no. 1, pp. 73-82, 2011.

[26] E. Onieva, J. E. Naranjo, V. Milanés, J. Alonso, R. García, and J. Pérez, "Automatic lateral control for unmanned vehicles via genetic algorithms," *Applied Soft Computing,* vol. 11, no. 1, pp. 1303-1309, 2011.

[27] J. Wang, J. Steiber, and B. Surampudi, "Autonomous ground vehicle control system for high-speed and safe operation," *International Journal of Vehicle Autonomous Systems,* vol. 7, no. 1/2, pp. 18-35, 2009.

[28] L. Guo, P. -s. Ge, X. I. Yang and B. Li, "Intelligent vehicle trajectory tracking based on neural networks sliding mode control," *Proceedings 2014 International Conference on Informative and Cybernetics for Computational Social Systems (ICCSS),* Qingdao, China, 2014, pp. 57-62.

[29] P. Hingwe and M. Tomizuka, "Experimental evaluation of a chatter free sliding mode control for lateral control in AHS," *Proceedings of the 1997 American Control Conference (Cat. No.97CH36041),* Albuquerque, NM, USA, 1997, pp. 3365-3369 vol.5.

[30] R. Solea and U. Nunes, "Trajectory planning with velocity planner for fully-automated passenger vehicles," *2006 IEEE Intelligent Transportation Systems Conference,* Toronto, ON, Canada, 2006, pp. 474-480.

[31] G. Tagne, R. Talj and A. Charara, "Higher-order sliding mode control for lateral dynamics of autonomous vehicles, with experimental validation," *2013 IEEE Intelligent Vehicles Symposium (IV),* Gold Coast, QLD, Australia, 2013, pp. 678-683.

[32] H. Imine and T. Madani, "Sliding-mode control for automated lane guidance of heavy vehicle," *International Journal of Robust and Nonlinear Control,* vol. 23, no. 1, pp. 67–76, 2011.

[33] R. Solea and D. Cernega, "Super twisting sliding mode controller applied to a nonholonomic mobile robot," *2015 19th International Conference on System Theory, Control and Computing (ICSTCC),* Cheile Gradistei, Romania, 2015, pp. 87-92.

[34] L. Nehaoua and L. Nouvelière, "Backstepping based approach for the combined longitudinal-lateral vehicle control," *2012 IEEE Intelligent Vehicles Symposium,* Madrid, Spain, 2012, pp. 395-400.

[35] A. Norouzi, M. Masoumi, A. Barari, and S. Farrokhpour Sani, "Lateral control of an autonomous vehicle using integrated backstepping and sliding mode controller," *Proceedings of the Institution of Mechanical Engineers, Part K: Journal of Multi-body Dynamics,* vol. 233, no. 1, pp. 141-151, 2018.

[36] J. Jiang and A. Astolfi, "Lateral control of an autonomous vehicle," *IEEE Transactions on Intelligent Vehicles,* vol. 3, no. 2, pp. 228-237, 2018.

[37] M. S. Netto, S. Chaib and S. Mammar, "Lateral adaptive control for vehicle lane keeping," *Proceedings of the 2004 American Control Conference,* Boston, MA, USA, 2004, pp. 2693-2698 vol.3.

[38] J. Ahmadi, A. K. Sedigh, and M. Kabganian, "Adaptive vehicle lateral-plane motion control using optimal tire friction forces with saturation limits consideration," *IEEE Transactions on Vehicular Technology,* vol. 58, no. 8, pp. 4098-4107, 2009.

[39] S. Hima, S. Glaser, A. Chaibet and B. Vanholme, "Controller design for trajectory tracking of autonomous passenger vehicles," *2011 14th International IEEE Conference on Intelligent Transportation Systems (ITSC),* Washington, DC, USA, 2011, pp. 1459-1464.

[40] M. M. Shirazi and A. B. Rad, "$\mathcal{L}_1$ Adaptive Control of Vehicle Lateral Dynamics," vol. 3, no. 1, pp. 92-101, 2018.

[41] F. L. Lewis, "$\mathcal{L}_1$ Adaptive Control Theory: Guaranteed Robustness with Fast Adaptation (Hovakimyan, N. and Cao, C.; 2010 [Bookshelf]," *IEEE Control Systems Magazine,* vol. 31, no. 5, pp. 112-114, 2011.

[42] P. Falcone, F. Borrelli, J. Asgari, H. E. Tseng, and D. Hrovat, "Predictive active steering control for autonomous vehicle systems," *IEEE Transactions on Control Systems Technology,* vol. 15, no. 3, pp. 566-580, 2007.

[43] H. Merabti, K. Belarbi and B. Bouchemal,"Nonlinear predictive control of a mobile robot: a

solution using metaheuristcs," *Journal of the Chinese Institute of Engineers,* vol. 39, no. 3, pp. 282-290, 2016.

[44] I. Ballesteros-Tolosana, S. Olaru, P. Rodriguez-Ayerbe, G. Pita-Gil and R. Deborne, "Comparison of optimization-based strategies for constrained control of auto-steering systems," *2016 European Control Conference (ECC),* Aalborg, Denmark, 2016, pp. 1592-1597.

[45] D. Kim, J. Kang and K. Yi, "Control strategy for high-speed autonomous driving in structured road," *2011 14th International IEEE Conference on Intelligent Transportation Systems (ITSC),* Washington, DC, USA, 2011, pp. 186-191.

[46] G. M. Hoffmann, C. J. Tomlin, M. Montemerlo and S. Thrun, "Autonomous automobile trajectory tracking for off-road driving: controller design, experimental validation and racing," *2007 American Control Conference,* New York, NY, USA, 2007, pp. 2296-2301.

[47] S. Hima, B. Lusseti, B. Vanholme, S. Glaser, and S. Mammar, "Trajectory tracking for highly automated passenger vehicles," *IFAC Proceedings Volumes,* vol. 44, no. 1, pp. 12958-12963, 2011.

[48] P. Shakouri, A. Ordys, D. S. Laila, and M. Askari, "Adaptive cruise control system: comparing gain-scheduling PI and LQ controllers," *IFAC Proceedings Volumes,* vol. 44, no. 1, pp. 12964-12969, 2011.

[49] M. Eilers and C. Möbus, "Learning the human longitudinal control behavior with a modular hierarchical Bayesian Mixture-of-Behaviors model," *2011 IEEE Intelligent Vehicles Symposium (IV),* Baden-Baden, Germany, 2011, pp. 540-545.

[50] J. E. Naranjo, C. Gonzalez, J. Reviejo, R. Garcia and T. de Pedro, "Adaptive fuzzy control for inter-vehicle gap keeping," *IEEE Transactions on Intelligent Transportation Systems,* vol. 4, no. 3, pp. 132-142, 2003.

[51] J. Zhao and A. El Kamel, "Coordinated throttle and brake fuzzy controller design for vehicle following," *13th International IEEE Conference on Intelligent Transportation Systems,* Funchal, Portugal, 2010, pp. 659-664.

[52] L. Nouvelière and S. Mammar, "Experimental vehicle longitudinal control using a second order sliding mode technique," *Control Engineering Practice,* vol. 15, no. 8, pp. 943-954, 2007.

[53] A. Ferrara and C. Vecchio, "Second order sliding mode control of vehicles with distributed collision avoidance capabilities," *Mechatronics,* vol. 19, no. 4, pp. 471-477, 2009.

[54] S. Glaser, L. Nouveliere and B. Lusetti, "Speed Limitation Based on an Advanced Curve Warning System," *2007 IEEE Intelligent Vehicles Symposium,* Istanbul, Turkey, 2007, pp. 686-691.

[55] J. A. Bonneson, M. Pratt, and J. D. Miles, "Evaluation of Alternative Procedures for Setting Curve Advisory Speed," vol. 2122, no. 1, pp. 9-16, 2009.

[56] A. Várhelyi, "DYNAMIC SPEED ADAPTATION IN ADVERSE CONDITIONS," *IATSS Research,* vol. 26, no. 2, pp. 52-59, 2002.

[57] V. Huth, F. Biral, Ó. Martín, and R. Lot, "Comparison of two warning concepts of an intelligent curve warning system for motorcyclists in a simulator study," *Accident Analysis & Prevention,* vol. 44, no. 1, pp. 118-125, 2012.

[58] R. Solea and U. Nunes, "Trajectory planning and sliding-mode control based trajectory-tracking for cybercars," *Integrated Computer-Aided Engineering,* vol. 14, no. 1, pp. 33-47, 2007.

[59] Y. Chen, C. Lu, and W. Chu, "A Cooperative Driving Strategy Based on Velocity Prediction for Connected Vehicles With Robust Path-Following Control," *IEEE Internet of Things Journal,* vol. 7, no. 5, pp. 3822-3832, 2020.

[60] Q. Xian, Y. Feng, Z. Jinlong and X. Jun, "Study on the safety speed of vehicle turning with considering the driving safety evaluation," *Proceedings of the Institution of Mechanical Engineers, Part D: Journal of Automobile Engineering,* vol. 236, no. 12, pp.2544-2556, 2022.

[61] Z. Deng, D. Chu, C. Wu, Y. He, and J. Cui, "Curve safe speed model considering driving style based on driver behaviour questionnaire," *Transportation Research Part F: Traffic Psychology and Behaviour,* vol. 65, pp. 536-547, 2019.

[62] A. Eidehall, J. Pohl, and F. Gustafsson, "Joint road geometry estimation and vehicle tracking," *Control Engineering Practice,* vol. 15, no. 12, pp. 1484-1494, 2007.

[63] C. Lundquist and T. B. Schon, "Road geometry estimation and vehicle tracking using a single track model," *2008 IEEE Intelligent Vehicles Symposium,* Eindhoven, Netherlands, 2008, pp. 144-149.

[64] B. Bartin, S. Demiroluk, K. Ozbay, and M. Jami, "Automatic Identification of Roadway Horizontal Alignment Information Using Geographic Information System Data: CurvS Tool," *Transportation Research Record: Journal of the Transportation Research Board,* vol. 2676, no. 1, pp. 532–543, 2021.

[65] B. Bartin, K. Ozbay, and C. Xu, "Extracting Horizontal Curvature Data from GIS Maps: Clustering Method," *Transportation Research Record: Journal of the Transportation Research Board,* vol. 2673, no. 11, pp. 264-275, 2019.

[66] I. Bejleri, X. Xu, D. Brown, S. Srinivasan, and N. Agarwal, "Automatic Horizontal Curve Identification for Large Areas from Geographic Information System Roadway Centerlines," *Transportation Research Record: Journal of the Transportation Research Board,* vol. 2675, no. 12, pp. 1088-1105, 2021.

[67] C. Gámez Serna and Y. Ruichek, "Dynamic Speed Adaptation for Path Tracking Based on Curvature Information and Speed Limits," *Sensors,* vol. 17, no. 6, p. 1383, 2017.

[68] N. El Ouanjli et al., "Modern improvement techniques of direct torque control for induction motor drives - a review," *Protection and Control of Modern Power Systems,* vol. 4, no. 1, 2019.

[69] P. H. Camargos and R. E. Caetano, "A performance study of a high-torque induction motor designed for light electric vehicles applications," *Electrical Engineering,* vol. 104, pp.797-805, 2022.

[70] X. Xu, X. Qiao, N. Zhang, J. Feng, and X. Wang, "Review of intelligent fault diagnosis for permanent magnet synchronous motors in electric vehicles," *Advances in Mechanical Engineering,* vol. 12, no. 7, p. 168781402094432, 2020.

[71] K. Kakouche, A. Oubelaid, S. Mezani, D. Rekioua, and T. Rekioua, "Different Control Techniques of Permanent Magnet Synchronous Motor with Fuzzy Logic for Electric Vehicles: Analysis, Modelling, and Comparison," *Energies,* vol. 16, no. 7, p. 3116, 2023.

[72] Y. Zhu, H. Wu, and C. Zhen, "Regenerative braking control under sliding braking condition of electric vehicles with switched reluctance motor drive system," *Energy,* vol. 230, p. 120901, 2021.

[73] N. D. Irimia, M. Luchian, F. I. Lazar and A. Ipatiov, "Performant Fault Tolerant Control by Using Space Vector Modulation (SVM) Technique of a Five Phases BLDC Motor for Autonomous Driving Applications," *2022 10th International Conference on Systems and Control (ICSC),* Marseille, France, 2022, pp. 317-322.

[74] H. Lee, D. Ko, and J. Nam, "A Study on Optimization of Noise Reduction of Powered Vehicle Seat Movement Using Brushless Direct-Current Motor," *Sensors,* vol. 23, no. 5, p. 2483, 2023.

[75] M. Ehsani, Y. Gao, and J. M. Miller, "Hybrid Electric Vehicles: Architecture and Motor Drives," *Proceedings of the IEEE,* vol. 95, no. 4, pp. 719-728, 2007.

[76] Z. Q. Zhu and D. Howe, "Electrical Machines and Drives for Electric, Hybrid, and Fuel Cell Vehicles," *Proceedings of the IEEE,* vol. 95, no. 4, pp. 746-765, 2007.

[77] M. L. De Klerk and A. K. Saha, "A Comprehensive Review of Advanced Traction Motor Control Techniques Suitable for Electric Vehicle Applications," *IEEE Access,* vol. 9, pp. 125080-125108, 2021.

[78] X. Men, Y. Guo, G. Wu, S. Chen, and C. Shi, "Implementation of an Improved Motor Control for Electric Vehicles," *Energies,* vol. 15, no. 13, p. 4833, 2022.

[79] S. Roy, R. Pandey, A.K. Bohre, P. Chaturvedi, M.L. Kolhe and S.N. Singh, "A Review on Motor and Drive System for Electric Vehicle," Planning of Hybrid Renewable Energy Systems Electric Vehicles and Microgrid. *Energy Systems in Electrical Engineering,* Singapore: Springer, 2022.

[80] G. Sieklucki, "An Investigation into the Induction Motor of Tesla Model S Vehicle," *2018 International Symposium on Electrical Machines (SME),* Andrychow, Poland, 2018, pp. 1-6.

[81] R. Thomas, L. Garbuio, L. Gerbaud and H. Chazal, "Modeling and design analysis of the Tesla Model S induction motor," *2020 International Conference on Electrical Machines (ICEM),* Gothenburg, Sweden, 2020, pp. 495-501.

[82] Z. Zhang and A. M. Bazzi, "Robust Sensorless Scalar Control of Induction Motor Drives with Torque Capability Enhancement at Low Speeds," *2019 IEEE International Electric Machines & Drives Conference (IEMDC),* San Diego, CA, USA, 2019, pp. 1706-1710.

[83] G. S. Buja and M. P. Kazmierkowski, "Direct torque control of PWM inverter-fed AC motors - a survey," *IEEE Transactions on Industrial Electronics,* vol. 51, no. 4, pp. 744-757, 2004.

[84] K. Hasse, "Drehzahlgelverfahren für schnelle umkehrantriebe mit stromrichtergespeisten asynchron-kurzschlusslaufer-motoren," Reglungstechnik, vol. 20, pp. 60–66, 1972.

[85] F. Blaschke, "The principle of field orientation as applied to the new transvector closed-loop system for rotating-field machines," Siemens Review, vol. 34, no. 3, pp. 217-220, 1972.

[86] I. Takahashi and T. Noguchi, "A New Quick-Response and High-Efficiency Control Strategy of an Induction Motor," *IEEE Transactions on Industry Applications,* vol. IA-22, no. 5, pp. 820-827, 1986.

[87] X. Q. Wu and A. Steimel, "Direct self-control of induction machines fed by a double three-level inverter," *IEEE Transactions on Industrial Electronics*, vol. 44, no. 4, pp. 519-527, 1997.

[88] J. C. Travieso-Torres, C. Contreras-Jara, M. Diaz, N. Aguila-Camacho and M. A. Duarte-Mermoud, "New Adaptive Starting Scalar Control Scheme for Induction Motor Variable Speed Drives," *IEEE Transactions on Energy Conversion,* vol. 37, no. 1, pp. 729-736, 2022.

[89] F. Wang, Z. Zhang, X. Mei, J. Rodríguez, and R. Kennel, "Advanced Control Strategies of Induction Machine: Field Oriented Control, Direct Torque Control and Model Predictive Control," *Energies*, vol. 11, no. 1, p. 120, 2018.

[90] A. Kumar and T. Ramesh, "Direct Field Oriented Control of Induction Motor Drive," *2015 Second International Conference on Advances in Computing and Communication Engineering*, Dehradun, India, 2015, pp. 219-223,

[91] R. S. Hiware and J. G. Chaudhari, "Indirect Field Oriented Control for Induction Motor," *2011 Fourth International Conference on Emerging Trends in Engineering & Technology*, Port Louis, Mauritius, 2011, pp. 191-194.

[92] Y. Farajpour, M. Alzayed, H. Chaoui, and S. Kelouwani, "A Novel Switching Table for a Modified Three-Level Inverter-Fed DTC Drive with Torque and Flux Ripple Minimiza-tion," *Energies*, vol. 13, no. 18, p. 4646, 2020.

[93] N. Taïb, B. Metidji, and T. Rekioua, "A fixed switching frequency direct torque control strategy for induction motor drives using indirect matrix converter," *Arabian Journal for Science and Engineering*, vol. 39, no. 3, pp. 2001-2011, 2014.

[94] B. L. G. Costa, C. L. Graciola, B. A. Angélico, A. Goedtel, M. F. Castoldi, and W. C. de A. Pereira, "A practical framework for tuning DTC-SVM drive of three-phase induction motors," *Control Engineering Practice,* vol. 88, pp. 119-127, 2019

[95] Y. Zahraoui, M. Akherraz, C. Fahassa, and S. Elbadaoui, "Induction Motor DTC Performance Improvement by Reducing Flux and Torque Ripples in Low Speed," *Journal of Robotics and Control (JRC),* vol. 3, no. 1, pp. 93-100, 2022.

[96] A. Ammar, "Improvement of Direct Torque Control Performances for Asynchronous Machine Using Non-Linear Techniques," *Ph.D. Thesis,* University Mohamed Khider–Biskra, 2017.

[97] F. F. M. El-Sousy, M. M. Amin and O. A. Mohammed, "Robust Adaptive Neural Network

Tracking Control with Optimized Super-Twisting Sliding-Mode Technique for Induction Motor Drive System," *IEEE Transactions on Industry Applications*, vol. 58, no. 3, pp. 4134-4157, 2022,

[98] A. Ammar, "Performance improvement of direct torque control for induction motor drive via fuzzy logic-feedback linearization: Simulation and experimental assessment," *COMPEL-The international journal for computation and mathematics in electrical and electronic engineering,* vol. 38, no. 2, pp. 672-692, 2019.

[99] A. Ammar, B. Talbi, T. Ameid, Y. Azzoug, and A. Kerrache, "Predictive direct torque control with reduced ripples for induction motor drive based on T-S fuzzy speed controller," *Asian Journal of Control,* vol. 21, no. 4, pp. 2155–-166, 2019.

[100] H. Dan, P. Zeng, W. Xiong, M. Wen, M. Su, and M. Rivera, "Model predictive control-based direct torque control for matrix converter-fed induction motor with reduced torque ripple," *CES Transactions on Electrical Machines and Systems,* vol. 5, no. 2, pp. 90-99, 2021.

[101] P. Maidana, C. Medina, J. Rodas, E. Maqueda, R. Gregor, and P. Wheeler, "Sliding-Mode Current Control with Exponential Reaching Law for a Three-Phase Induction Machine Fed by a Direct Matrix Converter," *Energies,* vol. 15, no. 22, p. 8379, 2022.

[102] C. Lascu, A. Argeseanu, and F. Blaabjerg, "Super-twisting sliding-mode direct torque and flux control of induction machine drives," *IEEE Transactions on Power Electronics,* vol. 35, no. 5, pp. 5057-5065, 2019.

[103] A. Ammar, A. Kheldoun, B. Metidji, T. Ameid, and Y. Azzoug, "Feedback linearization based sensorless direct torque control using stator flux MRAS-sliding mode observer for induction motor drive," *ISA Transactions,* vol. 98, pp. 382-392, 2020.

[104] C. Chen and H. Yu, "Back-stepping sliding mode control of induction motor based on disturbance observer," IET Electric Power Applications, vol. 14, no. 12, pp. 2537-2546, 2020.

[105] L. Gomes, "When will Google's self-driving car really be ready? It depends on where you live and what you mean by "ready" [News]," *IEEE Spectrum,* vol. 53, no. 5, pp. 13-14, 2016.

[106] K. Tomzcak *et al.*, "Let Tesla Park Your Tesla: Driver Trust in a Semi-Automated Car," *2019 Systems and Information Engineering Design Symposium (SIEDS),* Charlottesville, VA, USA, 2019, pp. 1-6, doi: 10.1109/SIEDS.2019.8735647.

[108] B. Thuilot, "Contribution à la modélisation et à la commande de robots mobiles à roues," *PhD Thesis,* Ecole Nationale Supérieure des Mines de Paris, 1995.

[109] R. Rajamani, "Vehicle Dynamics and Control," New York, NY, USA: Springer Science & Business Media, 2011.

[110] A. De Luca, G. Oriolo and M. Vendittelli, "Control of wheeled mobile robots: An experimental overview," in Ramsete, New York, NY, USA: Springer, pp. 181-226, 2001.

[111] B. Thuilot, J. Bom, F. Marmoiton and P. Martinet, "Accurate automatic guidance of an urban electric vehicle relying on a kinematic GPS sensor," *IFAC Proceedings Volumes,* vol. 37, no. 8, pp. 155-160, 2004.

[112] L. Menhour. "Synthèse de commandes au volant d'une automobile pour le diagnostic de rupture d'un itinéraire : développement et validation expérimentale," *PhD Thesis,* Compiègne, 2010.

[113] F. Ben Amar, "Modèles de Comportement Des Véhicules Tout Terrain Pour la planification Géométrico-Physique de Trajectoires, " *Phd Thesis,* Université de Paris, 1994.

[114] H. Dugoff, P. Fancher and L. Segel, "An analysis of tire traction properties and their influence on vehicle dynamic performance," *SAE Transactions,* vol. 79, pp. 1219-1223, 1970.

[115] G. Gim and P. Nikravesh, "An analytical model of pneumatic tyres for vehicle dynamics simulations. Part 1: Pure slips," *International Journal of Vehicle Design,* vol. 11, no. 6, pp. 589-618, 1990.

[116] G. Gim and P. E. Nikravesh, "An analytical model of pneumatic tyres for vehicle dynamics simulations part 2: Comprehensive slips," *International Journal of Vehicle Design,* vol. 12, no. 1, pp. 19-39, 1991.

[117] U. Kiencke and L. Nielsen, "Automotive Control Systems for Engine Driveline and Vehicle," New York, NY, USA: Springer-Verlag, 2005.

[118] P. R. Dahl, "Solid friction damping of mechanical vibrations," *AIAA Journal*, vol. 14, no 12, pp. 1675-1682, 1976.

[119] C. Canudas de Wit, H. Olsson, K. J. Astrom and P. Lischinsky, "A new model for control of systems with friction," *IEEE Transaction on Automatic Control*, vol. 40, no. 3, pp. 419-425, 1995.

[120] H. Pacejka, "Tire and Vehicle Dynamics," Amsterdam, The Netherlands: Elsevier, 2005.

[121] D. Lechner, " Analyse du comportement dynamique des vehicules routiers legers: developpement d'une methodologie appliquee a la securite primaire," *Ph.D. Thesis,* Ecole Centrale de Lyon, 2002.

[122] S. Bacha, R. Saadi, M. Y. Ayad, A. Aboubou and M. Bahri, "A review on vehicle modeling and control technics used for autonomous vehicle path following," *2017 International Conference on Green Energy Conversion Systems (GECS),* Hammamet, Tunisia, 2017, pp. 1-6.

[123] S. Bacha, M. Y. Ayad, R. Saadi, A. Aboubou, M. Bahri and M. Becherif, "Modeling and control technics for autonomous electric and hybrid vehicles path following," *2017 5th International Conference on Electrical Engineering - Boumerdes (ICEE-B),* Boumerdes, Algeria, 2017, pp. 1-12.

[124] S. Bacha, M. Y. Ayad, R. Saadi, O. Kraa, A. Aboubou and M. Y. Hammoudi, "Autonomous Vehicle Path Tracking Using Nonlinear Steering Control and Input-Output State Feedback Linearization," *2018 International Conference on Electrical Sciences and Technologies in Maghreb (CISTEM),* Algiers, Algeria, 2018, pp. 1-6.

[125] S. Thrun et al., "Stanley: The robot that won the DARPA Grand Challenge," *Journal of Field Robotics,* vol. 23, no. 9, pp. 661-692, 2006,

[126] L. Li, "Modélisation et Contrôle d'un Véhicule Tout-Terrain à deux Trains Directeurs, " *Ph.D. Thesis,* Université Paris Sciences et Lettres, 2021.

[127] G. Baffet, "Développement et validation expérimentale d'observateurs des forces du contact pneumatique/chaussée d'une automobile," *PhD Thesis,* Université de Technologie de Compiègne, 2007.

[128] A. Guillet, "Commande locale décentralisée de robots mobiles en formation en milieu naturel," *Phd Thesis, Université Blaise PASCAL-CLERMONT 2,* 2015.

[129] R. Lenain, "Contribution à la modélisation et à la commande de robots mobiles en présence de glissement," *Phd Thesis, Université Blaise PASCAL-CLERMONT 2,* 2005.

[130] R. Lenain, B. Thuilot, C. Cariou and P. Martinet, "Mixed kinematic and dynamic sideslip angle observer for accurate control of fast off-road mobile robots," *Journal of Field Robotics,* vol. 27, no. 2, pp. 181-196, 2010.

[131] P. Wójcik, "Direct Torque and Flux Control of Inverter–Fed Induction Motor Drive Including Field Weakening Region," *Ph.D. Thesis,* Warsaw University of Technology, 2009.

[132] I. Harzelli, "Contrôle non linéaire de la machine asynchrone en vue du diagnostic des défauts en utilisant des techniques avancées," *Ph.D. Thesis,* University Mohamed Khider–Biskra, 2020.

[133] F. Tazerart, "Étude, Commande et Optimisation des Pertes d'Énergie d'une Machine à Induction Alimentée par un Convertisseur Matriciel," *Ph.D. Thesis,* Bejaia University, 2016.

[134] M.E. El-Hawary, "Induction Motors and Their Control," *Principles of Electric Machines with Power Electronic Applications*, IEEE, 2002, pp.323-395,

[135] B. Francois, B. Robyns, P. Degobert, and J.P. Hautier, "Vector Control of Induction Machines, Desensitisation and Optimisation Through Fuzzy Logic," Springer-Verlag, London, 2012.

[136] F. Giri, "AC Electric Motors Control: Advanced Design Techniques and Applications," Hoboken, NJ, USA: John Wiley & Sons, 2013.

[137] J. Ackermann, J. Guldner, W. Sienel, R. Steinhauser and V. I. Utkin, "Linear and nonlinear controller design for robust automatic steering," *IEEE Transaction on Control Systems Technology*, vol. 3, no. 1, pp. 132-143, 1995.

[138] J. Zhang et al., "Adaptive Sliding Mode-Based Lateral Stability Control of Steer-by-Wire Vehicles With Experimental Validations," *IEEE Transactions on Vehicular Technology*, vol. 69, no. 9, pp. 9589-9600, 2020.

[139] J. He, D. A. Crolla, M. C. Levesley, and W. J. Manning, "Coordination of active steering, driveline, and braking for integrated vehicle dynamics control," *Proceedings of the Institution of Mechanical Engineers, Part D: Journal of Automobile Engineering,* vol. 220, no. 10, pp. 1401-1420, 2006.

[140] J. Li, J. Wang, H. Peng, Y. Hu and H. Su, "Fuzzy-Torque Approximation-Enhanced Sliding Mode Control for Lateral Stability of Mobile Robot," *IEEE Transactions on Systems, Man, and Cybernetics: Systems,* vol. 52, no. 4, pp. 2491-2500, 2022.

[141] S. Bacha, R. Saadi, M.-Y. Ayad, and A. Aboubou, "Speed-planning algorithm and super twisting control for autonomous vehicle steering system," *Bulletin of Electrical Engineering and Informatics,* vol. 12, no. 1, pp. 109-120, 2023.

[142] J. J. Slotine and S. S. Sastry, "Tracking control of nonlinear systems using sliding surface with application to robot manipulator," *International Journal of Control,* vol. 38, no. 2, pp. 931-938, 1983.

[143] J. J. E. Slotine and W. Li, "Applied Nonlinear Control," Upper Saddle River, NJ, USA: Prentice-Hall, vol. 199, no. 1, 1991.

[144] V. Utkin, "Variable structure systems with sliding modes," *IEEE Transaction on Automatic Control*, vol. 22, no. 2, pp. 212-222, 1977.

[145] V. I. Utkin, "Sliding Modes in Control and Optimization," New York, NY, USA: Springer, 2013.

[146] K. D. Young, V. I. Utkin and U. Ozguner, "A control engineer's guide to sliding mode control," *IEEE Transaction on Control Systems Technology,* vol. 7, no. 3, pp. 328-342, 1999.

[147] V. Utkin, "Sliding Modes in Control and Optimization," Berlin, Germany: Springer-Verlag, 1992.

[148] G. Bartolini and P. Pidynowsky, "An improved chattering free VSC scheme for uncertain dynamic systems," *IEEE Transaction on Automatic Control,* vol. 41, no 8, pp. 1220-1226, Aug. 1996.

[149] G. Bartolini, A. Ferrara and E. Usai, "Chattering avoidance by second order sliding mode control," *IEEE Transaction on Automatic Control,* vol. 43, no. 2, pp. 241-246, 1998.

[150] A. Levant, "Sliding order and sliding accuracy in sliding mode control," *International Journal of Control,* vol. 58, no. 6, pp. 1247-1263, 1993.

[151] A. Levant, "Higher-order sliding modes, differentiation and output-feedback control," *International Journal of Control,* vol. 76, no. 9-10, pp. 924-941, 2003.

[152] G. T. Fokam, "Commande et planification de trajectoires pour la navigation de véhicules autonomes, " *Ph.D. Thesis,* Université de Technologie de Compiègne, 2014.

[153] A. Akhmet, W. Hare and Y. Lucet, A Policy on Geometric Design of Highways and Streets, Washington, DC, USA: American Association of State Highway and Transportation Officials, 2013.

[154] Z. Li, M. V. Chitturi, A. R. Bill, and D. A. Noyce, "Automated Identification and Extraction of Horizontal Curve Information from Geographic Information System Roadway Maps," *Transportation Research Record: Journal of the Transportation Research Board,* vol. 2291, no. 1, pp. 80-92, 2012.

[155] W. Luo and L. Li, "Automatic geometry measurement for curved ramps using inertial measurement unit and 3D LiDAR system," *Automation in Construction,* vol. 94, pp. 214-232, 2018.

[156] Z. Li, M. V. Chitturi, A. R. Bill, D. Zheng, and D. A. Noyce, "Automated Extraction of Horizontal Curve Information for Low-Volume Roads," *Transportation Research Record: Journal of the Transportation Research Board,* vol. 2472, no. 1, pp. 172-184, 2015.

[157] S. Gargoum, K. El-Basyouny, and J. Sabbagh, "Automated Extraction of Horizontal Curve Attributes Using LiDAR Data," *Transportation Research Record: Journal of the Transportation Research Board,* vol. 2672, no. 39, pp. 98-106, 2018.

[158] S. Bacha, R. Saadi, M. Y. Ayad, M. Sahraoui, K. Laadjal, and A. J. M. Cardoso, "Autonomous Electric-Vehicle Control Using Speed Planning Algorithm and Back-Stepping Approach," *Energies,* vol. 16, no. 5, p. 2459, 2023,

[159] J. Zhou and C. Wen, "Adaptive Backstepping Control of Uncertain Systems", Springer Science & Business Media, 2008.

[160] S. Vaidyanathan and A. T. Azar, "Backstepping Control of Nonlinear Dynamical Systems," Academic Press, 2020.

[161] H. K. Khalil, "Nonlinear Systems," Upper Saddle River, NJ, USA: Prentice-Hall, 2002.

[162] M. Żelechowski, "Space Vector Modulated – Direct Torque Controlled (DTC – SVM) Inverter – Fed Induction Motor Drive," *Ph.D. Thesis,* Warsaw University of Technology, 2005.

[163] T. G. Habetler, F. Profumo, M. Pastorelli, and L. M. Tolbert, "Direct torque control of induction machines using space vector modulation," *IEEE Transactions on Industry Applications,* vol. 28, no. 5, pp. 1045-1053.

[164] A. Ammar, A. Bourek, and A. Benakcha, "Sensorless SVM-Direct Torque Control for Induction Motor Drive Using Sliding Mode Observers," *Journal of Control, Automation and Electrical Systems,* vol. 28, no. 2, pp. 189-202, 2016.